2010

Characterization of Stabilized Palladium Nanocatalysts

Meghann Broderick
Virginia Commonwealth University

Characterization of Stabilized Palladium Nanocatalysts

A thesis submitted in partial fulfillment of the requirements for the degree of Master of Science in Chemistry at Virginia Commonwealth University

by

Meghann E. Broderick

B.S. in Chemistry

Aquinas College, 2007

M.S. in Chemistry

Virginia Commonwealth University, 2010

Director: Everett Carpenter

Professor, Department of Chemistry

Virginia Commonwealth University

Richmond, Virginia

May, 2010

Acknowledgements

I would like to acknowledge the many people who made this research possible. First and foremost I thank my advisor Dr. Everett Carpenter and Virginia Commonwealth University's Chemistry Department for giving me the opportunity to pursue graduate studies. I would like to thank Dr. Frank Gupton and Dr. Ali Siamaki, our collaborators in the Department of Chemical Engineering. Also, a very special thanks goes to Vince Ong and my group members for all their support and great input throughout this process.

Dedicated to my father.

Contents

List of Figures

Appendix Figures

List of Schemes

List of Abbreviations

THF	Tetrahydrofuran
ACAC	Acetyl Acetonate
MAOS	Microwave-Assisted Organic Synthesis
Oleyl	Sample Synthesized By Oleylamine Method
HM	Sample Synthesized By Polyol Method Heated Conventionally
MW	Sample Synthesized By Polyol Method Irradiated By Microwave
PVP	Sample Coated With Polyvinylpyrrolidone
PVA	Sample Coated With Polyvinyl Alcohol
Sorbitol	Sample Coated With Sorbitol
Citrate	Sample Coated With Citrate
XRD	X-Ray Diffractometry
SEM	Scanning Electron Microscope
EDS	Energy-Dispersive X-Ray Spectroscopy
XPS	X-Ray Photoelectron Spectroscopy
ICP-MS	Inductively Coupled Plasma- Mass spectrometry
PTFE	Polytetrafluoroethylene
JCPDS	Joint Committee On Powder Diffraction Standards
AMCSD	American Mineralogist Crystal Structure Database

Abstract

Metal nanoparticles have received much interest for their application in catalysis due to high surface-to-volume ratios resulting in more available active sites. Ideally these catalysts are heterogeneous and allow for facile separation from the catalytic reaction mixture making them ideal for industrial application. Dispersed metal nanoparticles are explored due to their high reactivity in solution and are stabilized by surfactants and polymers. However, it is difficult to determine whether or not a catalyst is truly heterogeneous as a certain degree of leaching from the metal nanoparticle is inevitable. Determining the mechanisms involved in nanocatalysis is also a challenge. In this study, a series of dispersed palladium nanocatalysts in the Suzuki reaction with phenylboronic acid and bromobenzene were characterized before and after catalysis to determine what changes occur. Samples where characterized before and after the catalytic reaction by XPS, SEM, and EDS to monitor changes in particle size and composition. Reaction mixtures after catalysis were analyzed by ICP-MS for leached palladium species to determine if concentrations were high enough for homogeneous catalysis to take place. The dispersed palladium nanoparticles studied experienced growth during the catalytic process and a significant amount of leaching. XPS analysis indicates the presence of aromatic species on the particle surface after the catalytic reaction. The aromatic species is likely biphenyl, the product of the catalytic reaction, as the presence of boron and bromine was not found in XPS and EDS analysis.

1. Introduction

The development of catalysts in synthetic chemistry has led to very efficient and sophisticated transformations that would otherwise be unattainable. Transition metals are among chemists most powerful tools for catalyzing reactions[1,2]. Highlighting the significance of this field are two recent Nobel prizes given for transition metal catalysis: Sharpless, Noyori, and Knowles were cited for enantioselective catalysis in 2001 and Chauvin, Grubbs, and Schrock were honored for olefin metathesis in 2005[3].

The current trend governing research in this area is sustainability. Sustainable catalysts are efficient, easily recovered, and recyclable, which simplifies industrial processes and makes them more environmentally friendly. In order to attain this goal, researchers have begun to develop efficient heterogeneous catalysts that can function in aqueous solvents[1]. Organic solvents are often hazardous to the environment and require expensive waste treatment. Minimizing the amount of organic solvent that is needed in synthetic processes is an important step in greening chemistry on the industrial scale[4]. In general, water is the ideal solvent as water is inexpensive, readily available, and environmentally friendly[5–8]. Water also allows for facile separation and recovery of catalyst due to its limited miscibility in organic solvents[1]. The issues associated with utilizing water as a solvent in catalytic reactions are low solubility of substrates and poor stability of catalyst. These obstacles have been overcome in part by heterogeneous catalysis[9,10] and thus heterogeneous catalysts are sought after, which also have the advantage of being removed via filtration leaving the products virtually free of any metal residues from the catalyst[1].

Palladium has become a popular choice for numerous transition-metal catalyzed synthetic reactions and is used in many industrial processes such as the production of fine chemicals and pharmaceuticals[11,12]. This is particularly true for carbon bond forming reactions because high selectivity, activity, and efficiency can be ob-

tained[11,13]. Thus far, palladium has not posed any serious environmental or toxicity threats and a recent study found that palladium/magnetite catalysts used for wastewater treatment were not toxic, even in high concentrations[14]. Other advantages of palladium include its toleration of a wide variety of functional groups, which is a very important feature since synthetic versatility is so desirable. Additionally, many palladium reagents and catalysts are not very sensitive to oxygen, moisture, or acids. Palladium is also less expensive than other transition metals with similar chemistry such as rhodium, platinum, iridium and even gold, although prices are known to fluctuate dramatically,[11].

Much of the literature on palladium catalysis is focused on the development of heterogeneous catalysts. Although the use of heterogeneous palladium catalysts has existed for years, many details on the mechanisms behind their activity and selectivity remain elusive[1,15–17]. Isolation and characterization of catalytic material is highly desirable because the key to advancing the development and fundamental understanding of heterogeneous catalysis and improving catalytic systems is the ability to characterize their structure, composition, and properties[18,19].

1.1 Carbon-Carbon Couping Reactions

The development of heterogeneous transition-metal nanoparticles for carbon-carbon coupling reactions has been growing in recent years[20]. Palladium is perhaps the most notable transition metal for its utility in carbon-carbon coupling reactions. The well-controlled formation of carbon-carbon bonds enables the construction of complex architectures. Many carbon-carbon bond formation reactions have been developed for their use in synthetic chemistry and among the most popular are the Suzuki-Miyaura, Heck, Stille, and Sonogashira reactions.

The Suzuki reaction couples aryl halide with boronic acid shown in Scheme 1.1.

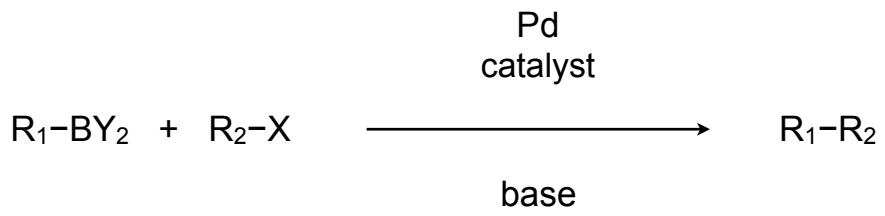

Scheme 1.1: Suzuki-Miyaura Reaction.

The Heck reaction involves coupling an aryl or vinyl halide with an alkene[3,21] shown in Scheme 1.2.

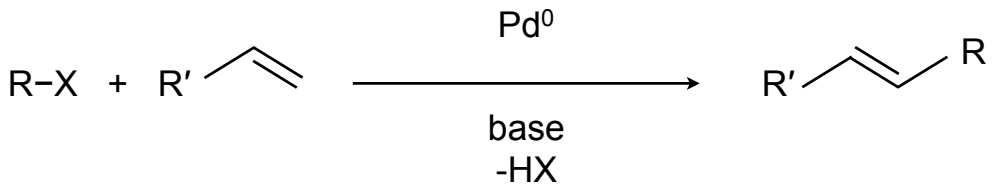

Scheme 1.2: Heck Reaction.

Stille couples aryl halides with tin reagents shown in Scheme 1.3.

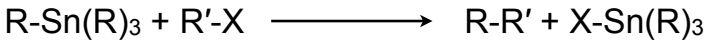

Scheme 1.3: Stille Reaction.

And Sonogashira couples aryl halides with acetlylenes[3] as shown in Scheme 1.4.

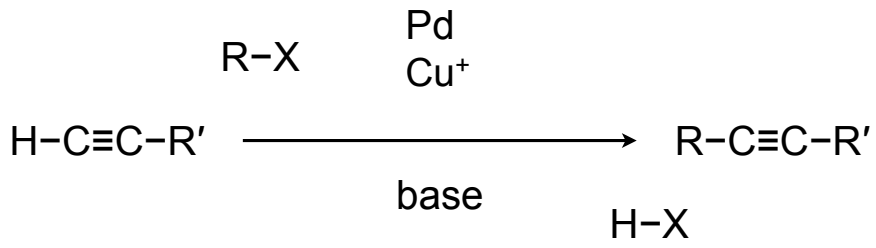

Scheme 1.4: Sonogashira Reaction.

Coupling products are found to have good applications as intermediates in the preparation of materials, natural products, and bioactive compounds, which are extremely important in the pharmaceutical industry[22–24]. The use of transition metal catalysts in cross-coupling reactions has become increasingly popular over the past few decades due to mild reaction conditions, high functional group tolerance, and broad availability of starting materials[25,26]. Despite the many qualities of these reactions, there are still challenges being faced in the development of new catalytic systems. Many catalysts are limited to expensive aryl bromides and iodides, which restricts their widespread industrial use[27]. The ideal catalyst would efficiently react with aryl chlorides while maintaining mild reaction conditions and low catalyst loading[28,29].

1.1.1 Suzuki-Mayuari Reaction

The Suzuki cross-coupling reaction is one of the most important for the production of these compounds[23]. It has become a main stay for the preparation of biaryls[30–33] and one of the major advantages of the Suzuki process is that it employs boronic acid. Organoboron compounds are inexpensive, readily available, and easy to handle, however the desired reactivity is limited due to weak nucleophilicity of the organic groups attached to boron[30].

Palladium is often used for the Suzuki-Miyaura reaction and the generally accepted

mechanism (see Figure 1.1) starts with an oxidative addition to the Pd(0) species, a transmetalation then occurs, followed by a reductive elimination[34]. The steps in the reaction mechanism will be described in greater detail in the experimental section.

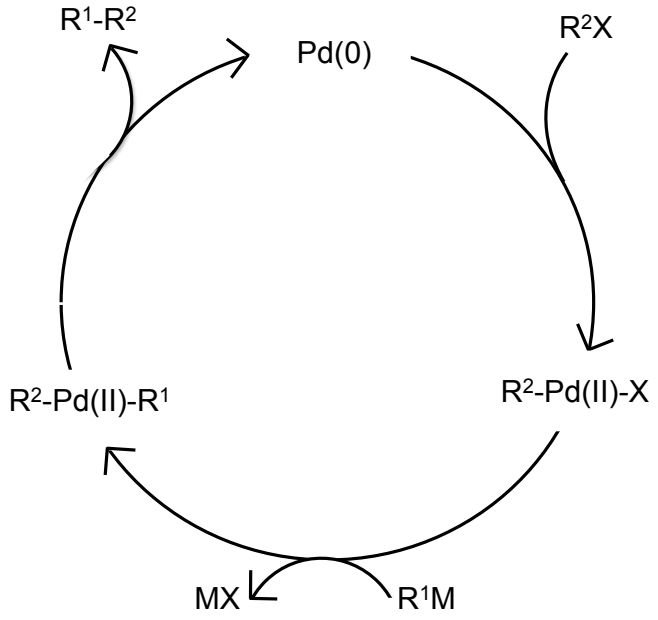

Figure 1.1: General mechanism for Suzuki reaction[34].

1.2 Determination of Heterogeneity

Heterogeneity is a much-desired quality in catalysts because they allow for facile separation and recovery from the product mixture, which would otherwise require expensive extractions and treatment. In addition, a catalysts activity, selectivity, stability, and lifetime are influenced greatly between the two types of species. Distinguishing homogeneous catalysis from heterogeneous has become an important question that researchers struggle to answer[19,35–37]. Determining whether a catalyst is truly heterogeneous is of great difficulty due to the inevitable partial dissolution of the solid phase[1]. The homogeneous component tends to be much more catalytically active than the parent metal surface. The difficulties are a result of the intricate equilibrium

between different sizes of palladium: small active and aggregated inactive clusters[38], and the fact that soluble species may re-deposit on the support[39]. Furthermore, only a trace amount of homogeneous catalyst is necessary for some reactions to occur[1,40].

There are several methods that exist for determining whether a catalyst is heterogeneous. Among the most popular are kinetic studies comparing reaction rates to concentrations of homogeneous palladium and filtration tests where the catalytic activity is monitored before and after filtration of the catalyst, both of which are limited when it comes to detecting re-deposition of the soluble species[41]. Other tests for heterogeneity include selective poisoning and the Redbeck-Collmand three-phase test. Selective poisoning is a test in which the addition of a reagent to the catalytic reaction selectively poisons either the homogeneous or heterogeneous component and has been achieved in certain cases. The Rebeck-Collmand three-phase test involves immobilizing the substrate on a solid support. This will significantly limit the activity of a heterogeneous catalyst due to its limited contact with the reactant. Therefore, high catalytic activity is indicative of a homogeneous catalyst[1]. This test can be useful but it is difficult to prevent the substrate from leaching off of the solid support[23].

1.3 Palladium Nanocatalysts

The field of nanoscience has grown exponentially over the past few decades due to the wide range of applications offered by this new science and has led to the development of nanocatalysis. Nanocatalysts have different catalytic properties depending on shape, size, and temperature of reaction, which makes them considerably versatile[15]. In principle, optimizing size, shape, and morphology can enhance catalytic performance[42–44]. It is possible to control size and particle shape by directing the nucleation, growth, and aggregation process of crystallites during synthesis[42]. Various morphologies of palladium nanoparticles have been prepared using polymers and

surfactants as capping agents, but the mechanism of controlling the morphology of metal nanoparticles is not yet well understood[45]. Despite this fact, interest in the formation of nanoparticles in the presence of surfactant and polymers has increased for the purpose of heterogeneous catalysis.[42,46].

Although many species of palladium can be employed in the Suzuki reaction, attention has turned to heterogeneous nanocatalysts. The greatest attraction of nanocatalysis is the decrease in required catalyst loading. Smaller particle size gives greater surface area (a greater surface-to-volume ratio) therefore increasing the number of available active sites for catalytic processes[47,48]. There is strong evidence for the usefulness of palladium nanoparticles in carbon bond formations. No other transition metal catalyst offers as much flexibility in carbon-carbon bond formation as palladium and improvements in substrate scope (e.g. using aryl chlorides in place of aryl bromides) have been made[11].

1.4 Parameters Affecting Nanocatalysis

The aggregation of nanomaterials is an obstacle faced by researchers in the field of catalysis because it lowers catalytic efficiency at the desired loading percent[5,16,23,49]. To overcome aggregation, stabilizing or capping agents (such as surfactants) have been introduced as a preventative measure[5]. The surfactants also allow the particles to better disperse in solution giving them greater access to reactants[47,50].

Coupling reactions catalyzed by surfactant stabilized palladium nanoparticles were first pioneered by Reetz in 1996[5,51]. Now surfactant stabilized palladium nanoparticles are being widely used in various cross-coupling reactions[52] and studies by El-Sayed et al. show that PVP-stabilized nanoparticles are efficient catalysts for the Suzuki reaction in aqueous media[16]. However, nanoparticles stabilized by surfactants face certain issues. Stabilizers that bind strongly to the nanoparticle surface

offer greater stability and therefore recyclability, but unfortunately strongly binding stabilizers also leave less active sites available for catalysis. This means that there must be a balance between high catalytic activity and stability of nanocatalysts capped with stabilizing agents and these factors are the basis for which the development of new and effective catalysts are designed[53].

Metal nanoparticles of different shapes have different crystallographic facets and different fractions of surface atoms on corners and edges. Surface atoms are very active, especially those atoms on the corners and edges of the particle. These atoms have the lowest degree of coordination and are thus the most reactive. Therefore, manipulating the shape and size of the nanoparticle can improve its effectiveness as a catalysts. However, these surface atoms are the first to leach into solution and may be responsible for Ostwald ripening. Ostwald ripening is a mechanism for cluster growth and is a process where atoms leach from smaller clusters and re-deposit on the surface of larger more stable clusters[16,54].

It has been observed that over the course of the catalytic reaction the corners and edges of the particles become distorted to form spheres and the activation energy increases in relation with this change[55]. The loss of surface atoms possessing the highest reactivity causes an elevation in activation energy of the catalytic reaction. Therefore the number of atoms on the corners and edges of the particle is related to the particle's catalytic activity. However, the most reactive atoms are also the least stable and the first to leach[43]. The leaching surface atoms cause growth and eventually aggregation[16,54].

It has been established by El-Sayed et al. that the nanoparticle preparation method and stabilizer play a role in the amount of growth that occurs over the course of the Suzuki reaction[56]. The amount of free metal present during the catalytic reaction governs the growth of the particles and varies depending on the preparation method. Another interesting observation made by El-Sayed et al. was that differ-

ent reactants could either promoted or inhibited growth. In the case of the Suzuki reaction with phenylboronic acid and iodobenzene, iodobenzene promoted particle growth while phenylboronic acid inhibited it[57]. The minimized growth observed with phenylboronic acid was attributed to it binding to the particle surface and acting as a capping agent, slowing the growth process[58].

Supported nanocatalysts are also very present in the literature and have been proposed as an alternative to dispersed particles. It is expected that the integrity of metal particles dispersed in solution undergoing catalysis is affected greater than gas-phase catalysis with supported nanoparticles[16]. However, in solution it has been observed that supported nanoparticles are less catalytically active than dispersed nanocatalysts. On the other-hand, supported nanoparticles have a much greater recycle potential, and although particles still grow in size during catalysis they do resist aggregation and precipitation[56].

1.5 Motivation

Among the many types of catalysts being researched (supported[59], surface modified, polymer protected, heterogeneous, homogeneous etc.[1]) the most important attribute is their ability to remain stable throughout the catalytic cycle. For example, an unstable catalyst that aggregates to form palladium black limits recyclability and hence its use in industrial application[5]. The assessment of a nanocatalyst requires a detailed study to determine its stability and to better understand the mechanisms involved[16].

Few studies have been done on the characterization of nanoparticles before and after catalysis. Most studies use imaging techniques to track changes in size distribution. There has not been a systematic study of reusable transition metal dispersed catalyst[49] and a good method of characterizing the changes that occur during catal-

ysis has not been well established. This study further assesses the stability of the nanoparticles and provides information about what is occurring to the particles during the catalytic process.

2. Experimental

2.1 Synthesis

Though metal nanocatalysts can be prepared by a number of different methods, chemical reduction syntheses are popular because they generate nanopaticles with uniform morphology[60]. Common chemical reduction methods for synthesizing metal nanoparticles include alcohol, hydrogen, and sodium borohydride reduction. Non-traditional reduction methods such as electrochemical, photochemical, and sonochemical exist but have been used to a lesser extent. Many of these chemical reduction syntheses involve stabilizers such as polymers and ligands that bind to the particle surface and also act as capping agents to control size and allow particles to disperse in solution[49]. Most chemical reduction methods involve a step of precipitation from a homogeneous solution conducted under kinetically controlled conditions[60].

The chemical reduction syntheses used to generate palladium nanoparticles in this study involved three steps. Step one is the dissolution of palladium precursor, step two is the reduction of dissolved palladium species, and step three is the nucleation and growth of palladium nanoparticles. The general mechanism of producing nanoparticles via chemical reduction is by reduction of a metal salt to give zero valent metal atoms. These atoms collide with other metal ions, atoms, or clusters and once a critical mass is reached, an irreversible seed is formed and growth can occur[61]. The formation of this seed is called nucleation and is the process of overcoming the interfacial energy barrier or in other words the energy cost of creating an interface between two phases[62].

In order for nucleation to occur supersaturation must be achieved. Supersaturation is the point at which formation of the solid phase is thermodynamically favorable and is driven by the difference in chemical potentials between two phases. For ex-

ample, if at a given temperature the solid phase has a lower chemical potential than the liquid phase, the solid phase is thermodynamically favorable[63] and energy will be released upon its formation. This process requires a critical concentration level of reduced metal atoms[60,63]. Once nucleation has started growth can occur. Separating these steps allows for the formation of particles with well-defined morphologies. If the reduced metal is generated slowly and the rate of nucleation is high, the nucleation step will be rapid due to the concentration of reduced metal atoms quickly dropping below the critical level. The nucleation step will be very fast and is thus separated from the growth step[60].

Particle growth may proceed by the addition of metal atoms or by the merging of primary particles to form a secondary particle[60]. The growth process is limited by either diffusion or the kinetic integration of metal atoms to the surface[64]. Protective or capping agents control particle growth by preferentially adsorbing to distinct surface regions that are known as growth centers and slow the kinetic incorporation of metal atoms on the particle surface[60,64]. This coating also provides stabilization and helps to prevent aggregation and agglomeration[61].

The nanoparticles in this study were synthesized by three different methods: the oleylamine synthesis, the polyol synthesis heated conventionally and heated by microwave irradiation. The oleylamine synthesis produced small particles but had a limited yield and required nitrogen flow. The polyol synthesis offered a greater yield, could be carried out in atmosphere, and requires inexpensive reagents. The synthesis was first heated conventionally; microwave irradiation was then explored as an alternative because it is known to offer better control over particle size and can produce different morphologies[65,66].

The development of well-controlled microwave instrumentation has allowed for this method of heating to grow in popularity as a synthetic route. In the synthesis of nanoparticles, microwave heating is faster and more efficient than conventional

heating methods, allowing for the production of more uniform particles. The simplicity of the method also makes it ideal to work with and there is continuing effort to develop the science of microwave synthesis[67]. Conventional methods heat by conduction and convection, resulting in non-homogeneous heating of the reaction mixture. Microwaves on the other hand, heat by the dielectric heating mechanism, which is both rapid and comparatively uniform. Dielectric heating is a result of the direct interaction between the electromagnetic radiation of microwaves and charged or polar species in the reaction mixture. This means the reaction mixture is being heated directly and results in more uniform heating[68]. Thus, microwaves are a solution to heating-inhomogeneity and may be scalable for industrial application[69], a very useful aspect in the development of a catalysts[65,66,70–72].

Stabilizing agents also have an effect on morphology and catalytic efficiency[42–44]. PVP is the most studied stabilizer for dispersed nanocatalysts[17,23] although many stabilizers are commercially available. Dependencies of surfactant on catalytic activity have been observed, but what governs the optimization of surfactant for catalytic purposes is not fully understood[53,73]. Four different stabilizers were studied herein: polyvinyl alcohol (PVA), polyvinylpyrrolidone (PVP), citrate and sorbitol. Coating of the particle with different stabilizers was achieved by adding them to the polyol synthesis and is described in more detail below.

2.1.1 Oleylamine Synthesis of Pd(0) Nanoparticles

Pd nanoparticles of approximately 5 nm in size were produced in the following way: Solution 1 was prepared by dissolving 0.15 g of $Pd(acac)_2$, palladium acetyl acetonate, in 20 ml of oleylamine . Solution 2 was prepared by mixing 18 ml of 1.0 M hydrazine in tetrahydrofuran (THF) and 16 ml of oleylamine. Solution 2 was added to solution 1 via addition funnel under N_2 flow. After a black product was formed, 30 ml of a 50:50 ethanol/chloroform mixture was added to precipitate the product. Particles were

collected by centrifugation, washed with methanol, and dried in a vacuum oven[74]. The sample was then refluxed in pyridine for one hour to exchange the oleylamine coating for pyridine. Reflux was done under N_2 flow. Samples were recovered by centrifugation and washed with methanol until solution was clear. The sample was again dried in a vacuum oven.

2.1.2 Polyol Synthesis of Pd(0) Nanoparticles

Conventional Heating

Pd nanoparticles were synthesized by mixing 25 ml of ethylene glycol, 1.50 g of sodium hydroxide and 0.50 g of palladium chloride in a 100 ml, one neck round bottom flask. The solution was refluxed until a black product was formed and then cooled in an ice bath. Particles were collected by centrifugation, washed with methanol until a clear solution was achieved, and dried in a vacuum oven[42,67].

Microwave Irradiation

Pd nanoparticles were synthesized by mixing 25 ml of ethylene glycol, 1.50 g of sodium hydroxide and 0.50 g of palladium chloride in a 100 ml beaker. The solution was heated by microwave for 2 minutes. As with the previous synthesis, articles were collected by centrifugation, washed with methanol until a clear solution was achieved, and dried in a vacuum oven[42,67].

Stabilizing agents

Different surfactants were used as stabilizing agents to prevent the particles from aggregating during the catalytic experiments. Particles with surfactants were synthesized using the microwave irradiated polyol synthesis. A 1:1 molar ratio of surfactant-to-palladium was added to the reaction mixture and allowed to mix via magnetic

stir bar before the solution was heated by microwave irradiation. The surfactants polyvinyl alcohol (PVA), polyvinylpyrrolidone (PVP), citrate and sorbitol were studied.

2.2 Catalytic Experiments

The use of microwave-assisted organic synthesis (MAOS) has significantly enhanced productivity and expanded the range of chemical transformations available in organic synthesis[33]. Since transition-metal-catalyzed cross-coupling reactions using heterogeneous catalysts often require high temperatures and/or extended reactions times, microwave heating methods have been employed to improve synthesis[25]. Rate enhancements are observed when using microwave heating due to the efficiency of the dielectric heating mechanism[75]. Reactions that would typically take hours or days to reach completion are much more rapid when irradiated by microwave. Water is used as a solvent in the catalytic reactions which has a high dielectric constant, making it ideal for microwave-mediated synthesis[76–78].

As in the synthesis of metal nanoparticles, the homogeneity of microwave heating is a great advantage. Heating conventionally by conduction and convection involves an external source that heats the walls of the reaction vessel. The vessel walls then heat the reaction mixture creating a gradient where the walls of the vessel are hotter than the desired temperature for the reaction[68]. The high temperatures of the vessel cause wall effects, degradation of the catalyst decreasing its efficiency and lifetime[32]. Microwaves however, heat inversely by interacting directly with the solvent and mitigate these wall effects[32].

The Suzuki reaction between bromobenzene and phenylboronic acid was studied and as mentioned previously there are three steps in the catalytic cycle: oxidative addition, transmetalation, and reductive elimination (see Figure 2.1).

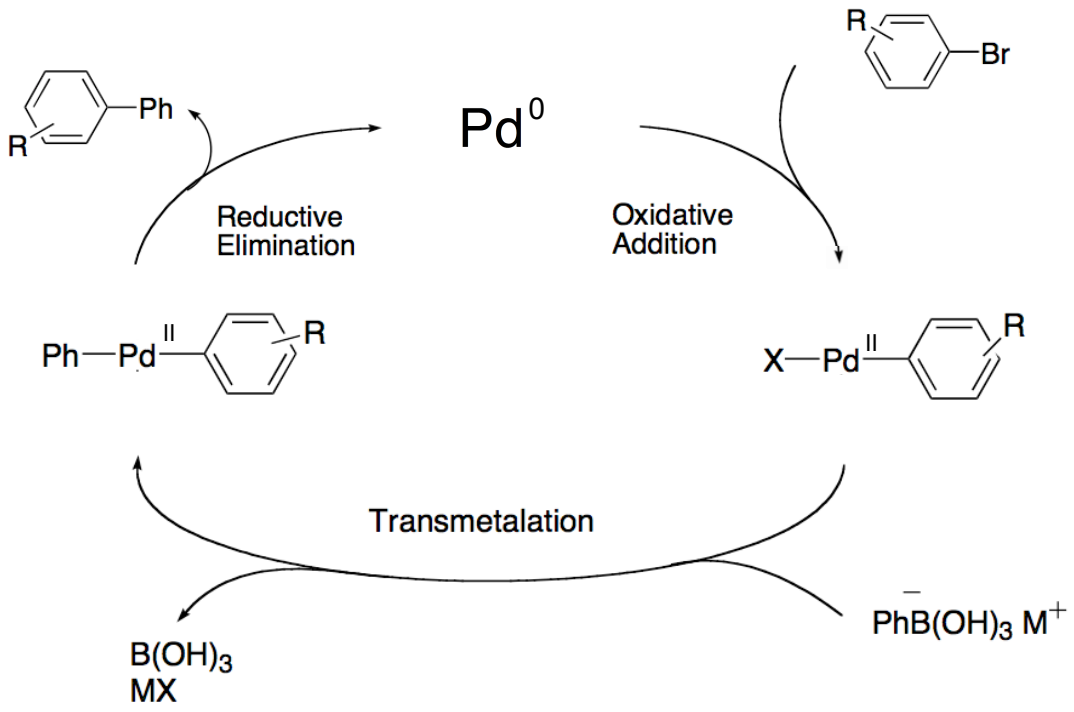

Figure 2.1: Suzuki Mechanism with Phenylboronic Acid and Bromobenzene.

Oxidative addition is the addition of a molecule, A-X to Pd(0), cleaving the A-X covalent bond and forming two new covalent bonds with palladium. Palladium increases its formal charge by two units so that Pd(0) becomes Pd(II). This process is facilitated by higher electron density of Pd so that in general electron donating ligands promote oxidative addition and electron withdrawing ligands suppress oxidative addition.

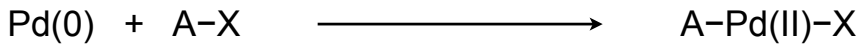

Scheme 2.1: Oxidative Addition.

Pd(0) complexes are stable when the sum of their d electrons and electrons from donating ligands equals 16 and is therefore an exception to the 18 electron rule. Pd(0) forms complexes with its d8 electrons ($5s^2$, $4d^8$) and will be saturated upon coordinating with four, two electron donating ligands. This means the coordination number of a stable Pd(0) complex is four and has a square planar geometry[79]. In many cases the oxidative addition will occur after the dissociation of ligands to supply vacant coordination sites and is the first step in many catalytic reactions.

Transmetalation is a process by which two metals exchange either an alkyl group or a hydride. The driving force of transmetalation is attributed to the difference in electronegativity of two metals. Palladium complexes (A-Pd-X) formed by oxidative addition react with organometallic compounds (M-R) and hydrides (M-H) of main group metals. The organic group or the hydride is transferred to the palladium through the substitution of X. So, the alkylation or hydride formation of palladium takes place, which is a process called transmetalation. In order for the transmetalation to occur, the main group metal M must be more electropositive than palladium.

Scheme 2.2: Transmetalation.

Reductive elimination is the opposite of oxidative addition where the formal oxidation state of palladium is reduced by two units, for example Pd(II) is reduced to Pd(0). It is a unimolecular decomposition that involves the loss of two ligands of cis configuration around the palladium center. The combination of these two ligands results in a single product. Reductive elimination is a common termination step in a catalytic cycles[11,80].

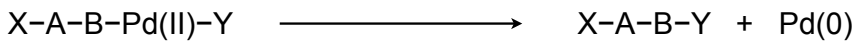

Scheme 2.3: Reductive Elimination.

Seven different samples were used in the catalytic experiments: a sample from the oleylamine synthesis that will be referred to as oleyl, a sample from the polyol synthesis heated conventionally that will be referred to as HM, a sample from the polyol synthesis heated by microwave that will be referred to as MW, and the four other samples coated with the stabilizing agents PVP, PVA, Citrate, and Sorbitol, which will be referred to by their coatings. Samples were characterized before and after catalysis via several different characterization techniques.

2.2.1 Suzuki-Miyaura Coupling Reactions

As mentioned above, phenylboronic acid was reacted with bromobenzene to give a biphenyl product (see Scheme 2.4). The reaction was done in a 1:1 solvent mixture of water and ethanol. 1.2 molar equivalents of substrate were added to a 4 mL solvent mixture in a 10 mL glass reaction vessel. The media was mixed with a magnetic stir bar and 3 mmol of phenylboronic acid was added to the mixture followed by 3 molar equivalents of K_2CO_3. Extra care was taken to ensure that nothing was left on the walls of the reaction vessel.

The reactions were carried out under microwave irradiation in a CEM Discover Microwave Reactor with pressure and temperature controls. The reactions were carried out at a pressure of 17.0 atm, 200 W power level, and temperature of 80°C with 3 mole percent catalyst loading. More catalyst could not be used for the characterization after catalysis because when the concentration of catalyst is too high,

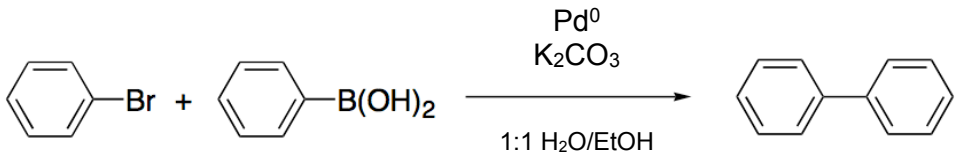

Scheme 2.4: Suzuki Reaction with Phenylboronic Acid and Bromobenzene.

aggregation of the nanoparticles occurs[49]. Percent conversion was measured by GC-MS and determined by comparing peak area of the product (biphenyl) to the reactant (phenylboronic acid).

Samples were used in the Suzuki-Miyaura coupling reaction and recovered for further characterization by the following process: The particles were precipitated out of the reaction mixture with 2 ml of ethanol. After particles had settled in the bottom of the reaction flask, the reaction mixture was decanted. Particles were rinsed with ethanol three-to-four times, or until the ethanol was clear upon addition. The samples were transferred to a glass vial and dried in a vacuum oven.

2.3 Characterization

Samples were characterized by XRD, SEM, EDS, XPS, and ICP-MS. X-ray diffraction measurements were taken of samples before catalytic experiments to confirm that palladium nanoparticles were formed and give an approximate particle size. SEM images, EDS spectra and XPS spectra were taken of the samples before and after catalytic experiments to track changes in size and composition that occur during catalysis, to gain understanding of the mechanisms involved in nanocatalysis. These techniques were selected because sample size was limited for characterization after catalysis and they could provide the most information with the smallest sample size. Finally, analysis of palladium concentration by ICP-MS of the reaction mixture after the removal of solid palladium species was done to give an indication of whether

the catalyst was heterogeneous or homogeneous in nature. Although analysis of the filtered reaction mixture by ICP-MS alone cannot prove that a catalyst is heterogeneous over homogeneous, it can give information on whether or not the catalyst is leaching. ICP studies must be done in conjunction with kinetic studies to determine if a catalyst is heterogeneous and are done on the basis that it requires a certain concentration of catalyst for a reaction to proceed at a given rate. If the measured concentration is too low for the observed rate then some heterogeneous catalysis must be taking place. This method cannot account for the re-deposition of homogeneous species onto the parent particle and it cannot give any clear picture of what the actual reaction mechanism may be. However, it is known that homogeneous species are much more catalytically active than their solid phase counterparts and can catalyze a reaction with concentrations as low as a few ppm[1,39]. Thus, ICP analysis was done to determine if there was enough palladium present for homogeneous catalysis to be possible.

2.3.1 XRD

XRD measurements were taken on a Panalytical X'Pert Pro with a Cu Kα radiation source (λ=1.4506 Å). A low background sample tray was used. Diffractograms were taken with the maximum sample capacity of the tray (or maximum amount of sample available) and smoothed with a glass slide. The instrument's current and tension settings were 40 mA and 45 kV respectively, and samples were scanned from 20 to 80 degrees on the 2Θ setting.

2.3.2 XPS

XPS data was measured with a Thermoscientific ESCAlab250 Microprobe with an Al Kα radiation source (E_b=1486.6 eV) and a 180° hemispherical analyzer with a 6 element multi-channel detector. The incident X-ray beam was 45° of normal with the

photoelectron detector normal to the sample. Charge compensation was employed during data collection by an internal flood gun (2 eV electrons) and a low energy ionic argon external flood gun. Binding energies of photoelectrons were corrected to an aliphatic hydrocarbon C1s peak at 285 eV. XPS data was processed with Advantaged Software using Gaussian-Lorentzian functions at 20 iterations.

2.3.3 ICP-MS

Samples were collected and prepared for ICP analysis in the following way. Particles were allowed to fall out of the reaction mixture after the catalytic experiment was performed and 2 ml of ethanol were added to help precipitate particles. The Solution was decanted and centrifuged at an RPM of 6,200 for one hour. A small amount of black precipitate was observed at the bottom of the centrifuge tube. Samples were also filtered with a 200 nm polytetrafluoroethylene (PTFE) Whatman filter to help ensure that all solid palladium was removed. The solution was decanted and used in the next step of ICP analysis.

Samples were digested with trace metal hydrochloric acid so that any organics present would not cause interference in ICP anlysis. A 100-1000 μl Rainin pipette was used to add 600 μl of trace metal HCl to 3 ml of sample. The solution was heated in a beaker to 90°C and stirred with a magnetic stir bar for 5 minutes. The solution was then left to cool to room temperature after which it was filtered with a PTFE Whatman filter. 250 μl of digested sample was diluted with 5 ml of 5% trace metal HCl solution. 2 L of this diluent solution was prepared for the dilution of both samples and standards. Standards were prepared in the following manner: A 1000 μg/ml palladium standard solution was used to make 100ml of a 5ppm stock solution using a 100-1000 μl Rainin pipette. Five standard solutions were prepared from the stock solution with the following concentrations: 10 ppb, 40 ppb, 100 ppb, 200 ppb, and 400 ppb.

Samples were analyzed on a Varian 820-MS, ICP Mass Spectrometer with a hydrogen sampler flow of 50 mL/min and the tune file 323. The auto sampler was used and a twenty-second delay between samples was employed to allow enough time for the sample to travel through the instrument. A 10% nitric solution was used to clean the instrument between samples.

2.3.4 SEM and EDS

Sample images were taken with a Hitach SU-70 scanning electron microscope and EDS spectra were taken with an EDAX Apollo 10 detector. An aluminum sample mount was used. The mount was cleaned in a 50/50 solution of ethanol and acetone to prevent contamination. The tray was allowed to soak in the solution for fifteen minutes and then dried in the vacuum oven. Graphite tape was used to adhere the sample to the sample tray. The sample was packed into the tip of a pasture pipette and blown onto the graphite tape with a rubber bulb. N_2 gas was blown over the sample to displace any loose particles.

3. Results and Discussion

Analysis of X-ray diffraction patterns (see Figure 3.1) confirm that nanosized palladium particles were formed with miller indices corresponding to the Joint Committee on Powder Diffraction Standards (JCPDS) reference file no. 01-087-0638.

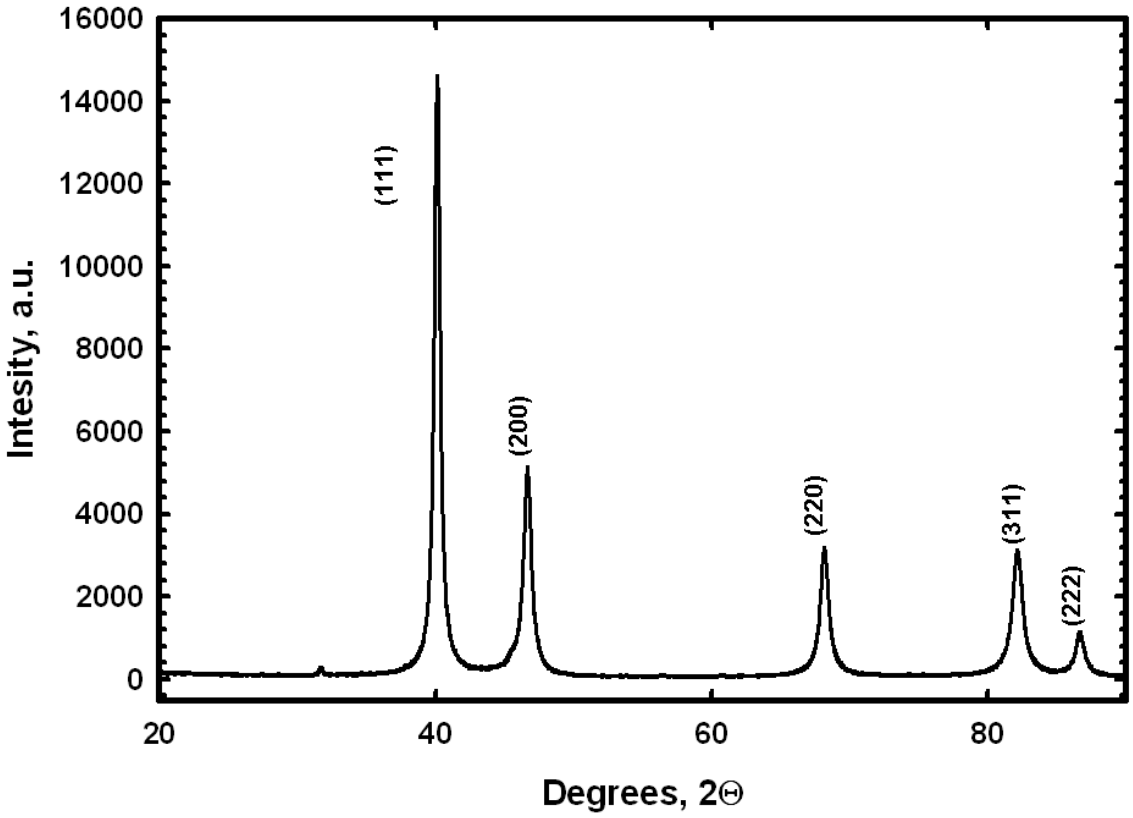

Figure 3.1: XRD Pattern Sample MW.

The Scherrer equation, d = $k\lambda/\beta_{1/2}Cos\theta$, was used to calculate particle sizes, where θ is the peak position, $\beta_{1/2}$ is the peak width at half maximum, k is a constant (0.89), and the wavelength of radiation is λ=1.5406 Å. Scherrer's equation approximates particle size by peak broadening that occurs as a function of decreasing crystallite size and is based on the assumption that particles are spherical[81]. Particle size was calculated by Scherrer's equation using each peak in the diffractogram and these values were averaged to estimate particle sizes for each sample (see Figure 3.2).

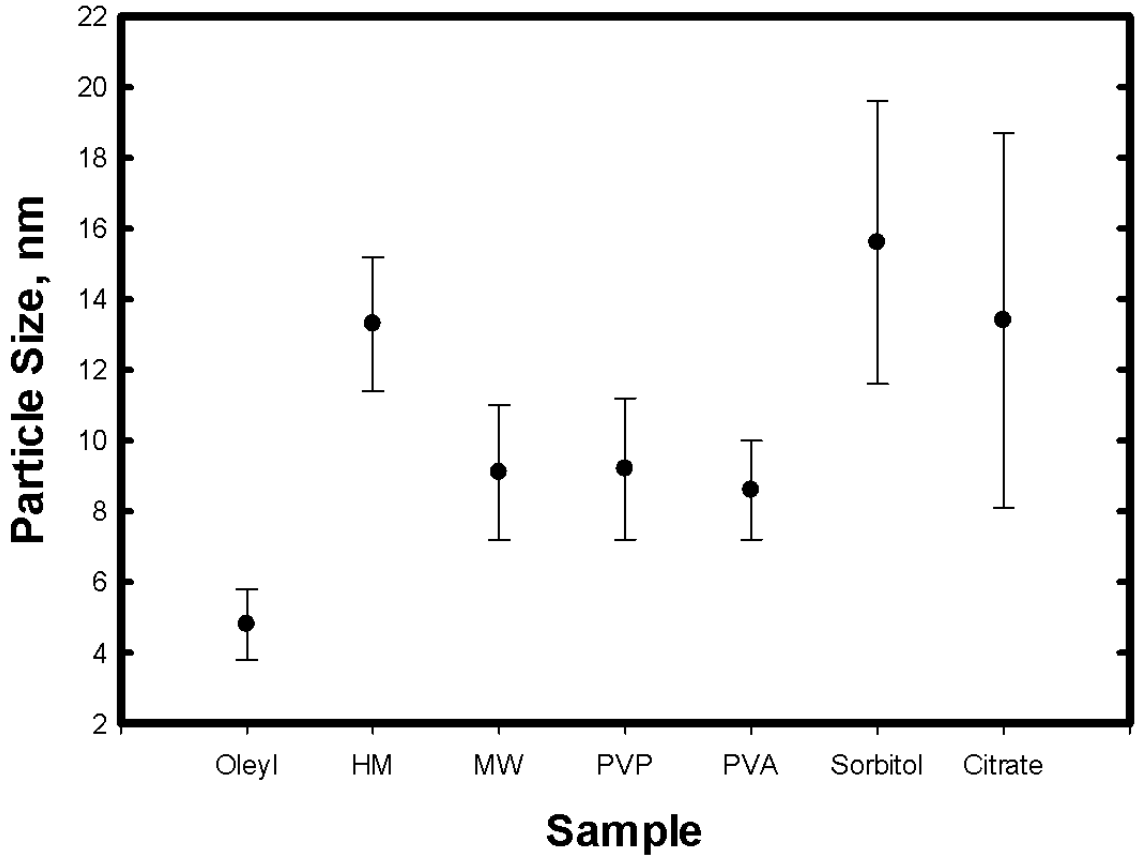

Figure 3.2: Particle Size by Scherrer's Equation.

Particle size increased when going from the oleylamine synthesis to the polyol synthesis. A decrease in particle size was observed when samples were synthesized by microwave irradiation in the polyol method over being heated conventionally. This can be rationalized by the argument that particle size depends on the length of the nucleation and growth period and therefore time of reaction[65]. Microwave synthesis is much more rapid (2 min) than conventional heating (1 hr). Particle size then increased in the microwave-irradiated polyol synthesis with the addition of sorbitol and citrate. These stabilizers are likely the cause of this increase in particle size, though the mechanism for which this occurs is not well known[42,46].

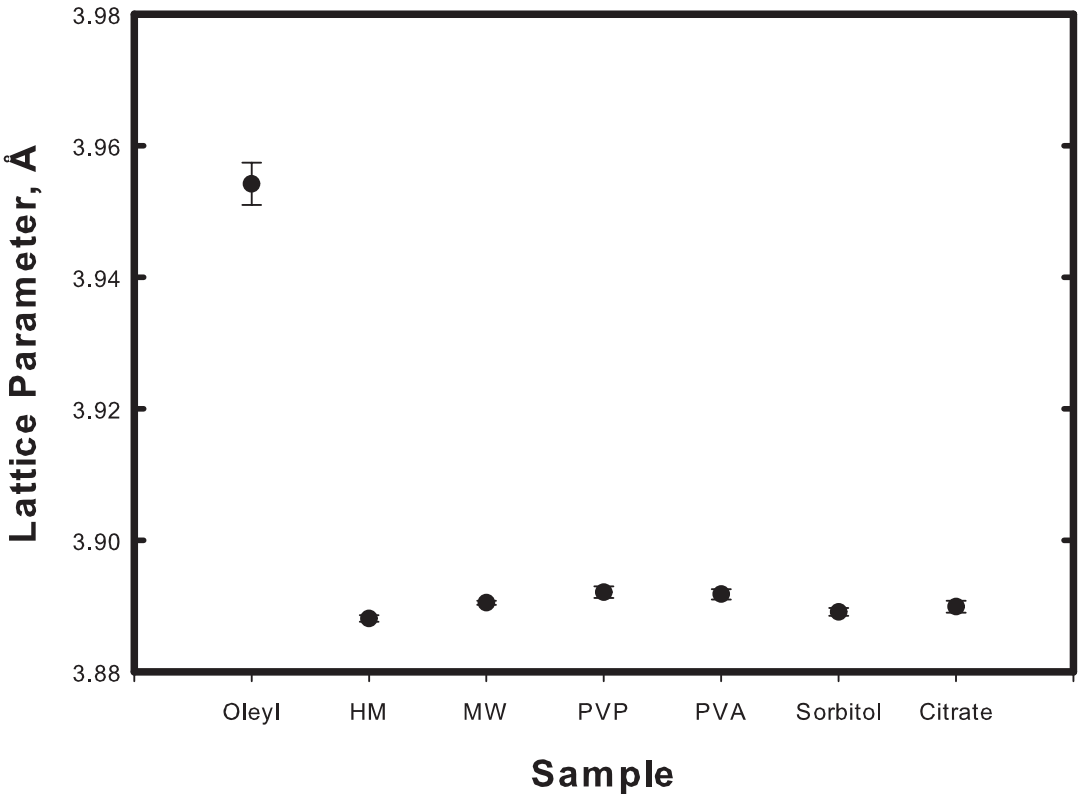

Figure 3.3: Lattice Parameters by Rietveld Refinement.

Lattice constants (see Figure 3.3) were calculated using Rietveld refinement with the American Mineralogist Crystal Structure Database (AMCSD) reference file no. 7-83 and are in good agreement with the reference lattice constant a=3.8898 Å for samples synthesized by the polyol method. It is interesting to point out that the lattice constant for the sample synthesized by the oleylamine method is significantly higher. This sample also has the smallest particle size. Generally, lattice constants contract for metal nanoparticles as particle size decreases[82,83]. Palladium is an exception to this rule experiencing an expansion in lattice constant as a function of decreasing particle size[83,84] and this correlation between lattice constant and particle size is observed here. This is of interest in catalysis because changes in morphology can have affects on reactivity[43,85]. The increased lattice constant of oleyl is also an indication of decreased stability[86] which is observed in analysis by ICP-MS as well as oleyl had the highest concentration of leached palladium.

Results from ICP-MS (see Figure 3.4) show that there is a significant amount of palladium leaching during the catalytic experiment. A study by Leadbeater et al. found that the Suzuki reaction with bromobenzene and phenylboronic acid only requires a soluble palladium catalyst concentration of 50 ppb for catalytic activity to be observed and a minimum concentration of 1 ppm is required to achieve complete conversion[40]. Concentrations of palladium found in the catalytic solution after filtration are above 1 ppm for oleyl, HM, PVP and PVA and all concentrations are above 50 ppb. The data indicates that there is enough palladium in solution to catalyze the reaction homogeneously.

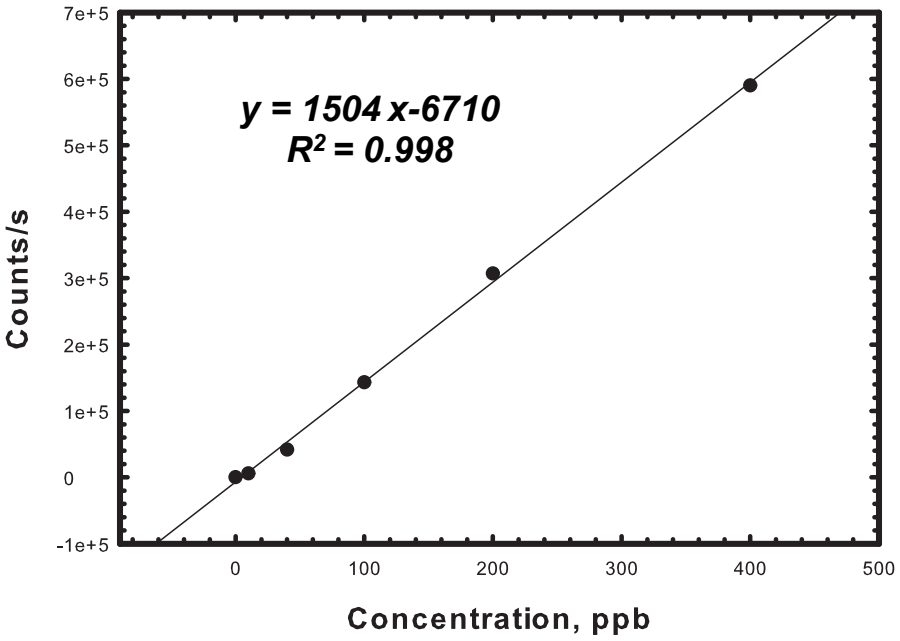

(a) Calibration Curve

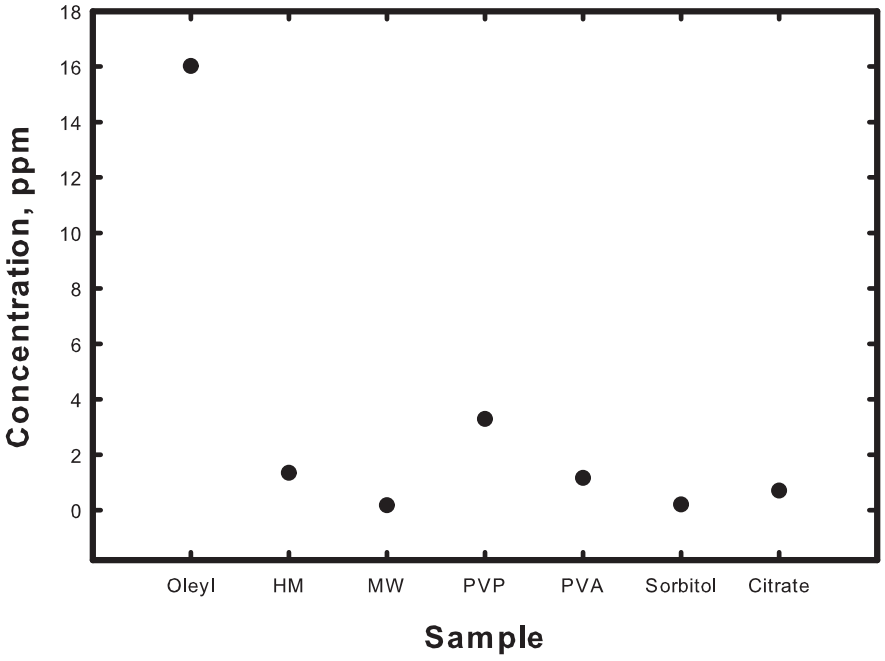

(b) Concentrations of leached palladium after catalysis

Figure 3.4: Palladium Leaching by ICP-MS Analysis

SEM images support particle size determination by Scherrers equation and a comparison of SEM images before and after the catalytic experiment shows that a change in morphology takes place (see Figure 3.5, also see Appendix B).

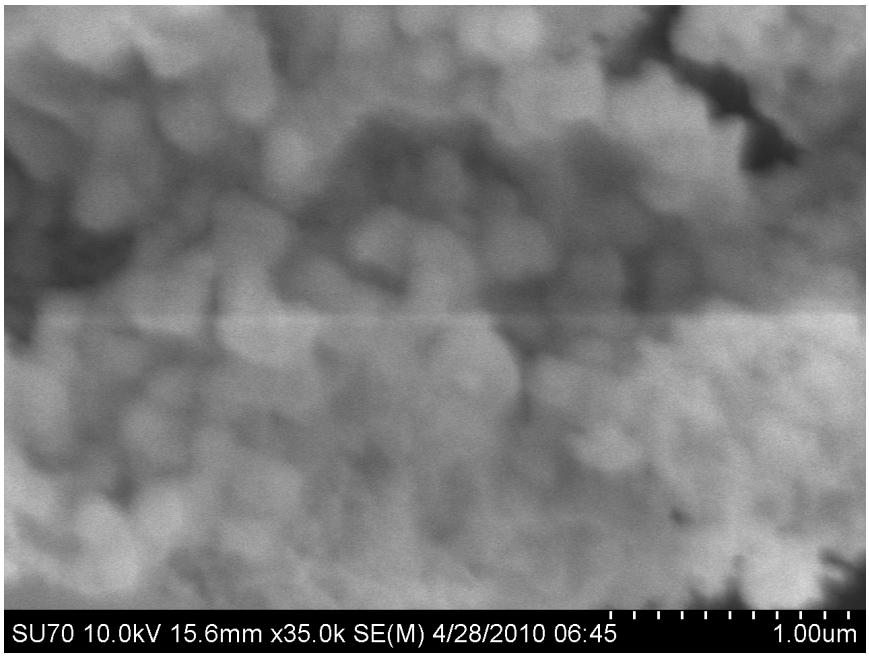

(a) Before

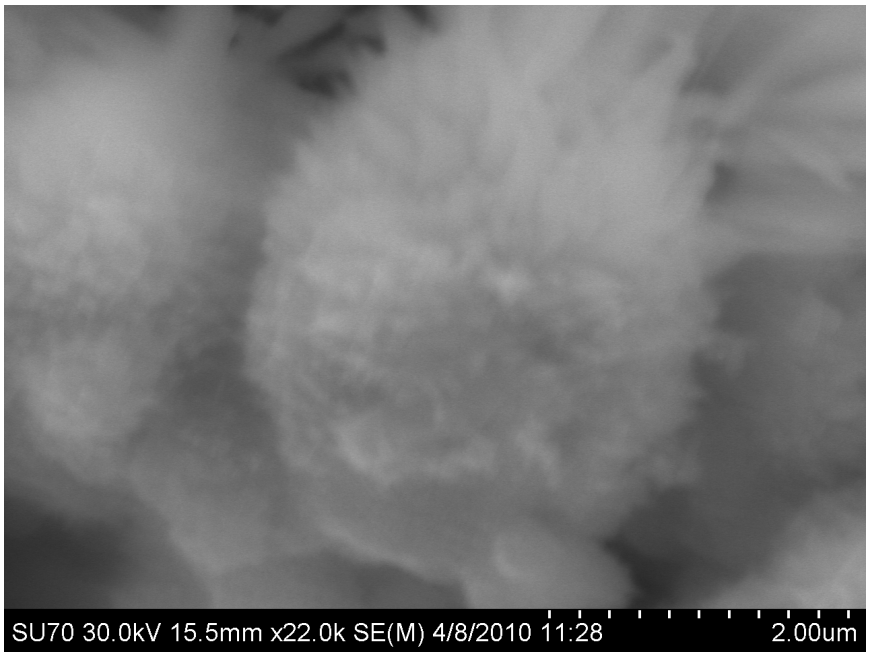

(b) After

Figure 3.5: Before and After Catalysis SEM Images of Sample HM

Particle sizes increase after catalysis. The observed increase in particle size is due to Ostwald ripening and aggregation[16,54]. The amount of free metal present during the catalytic reaction also governs particle growth during the catalytic experiment[57], and the dissolved palladium species observed by ICP-MS analysis likely contribute to growth in particle size via Ostwald ripening[16,54]. It is difficult to determine exact particle sizes by the SEM images taken, particularly after catalysis due to the presence of organics on the particle surface, which cause a build up of charge and lowers resolution[87]. Nonetheless, it appears that oleyl, citrate, and sorbitol experience the least amount of growth, while HM experiences the most growth (see Appendix B).

XPS spectra were measured before and after catalysis to monitor any changes in the surface chemical composition. Representative spectra for sample MW are given in Figure 3.6. Survey scans, C1s, O1s, and Pd3d region scans were taken for each sample (see Appendix C) and all peaks observed are presented in Table 3.1 with corresponding binding energies.

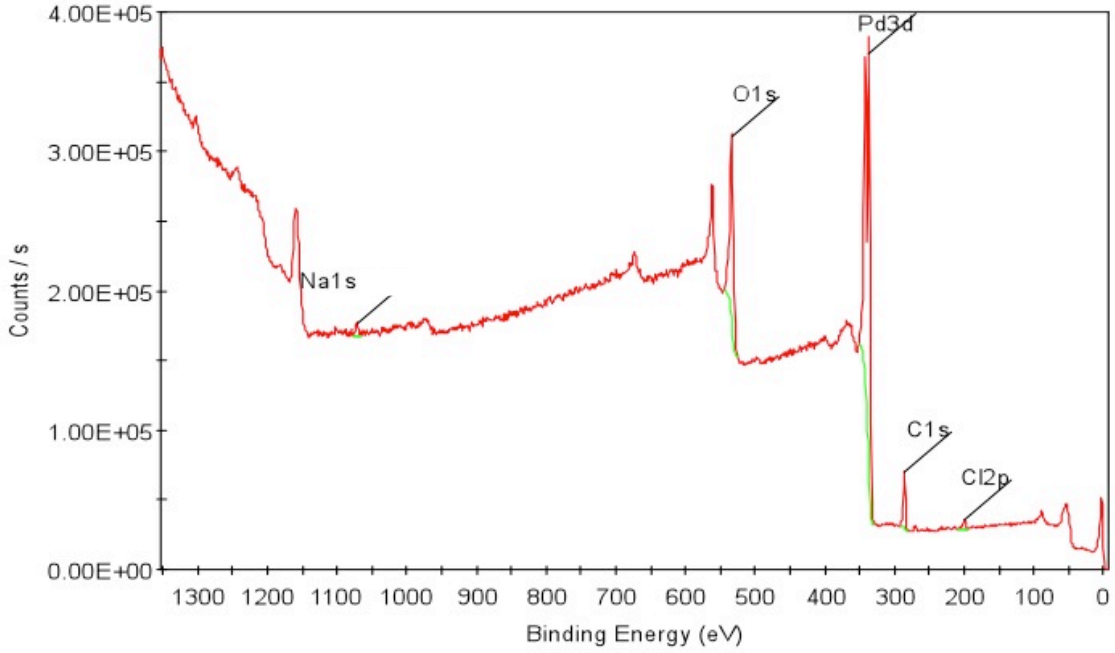

(a) Before

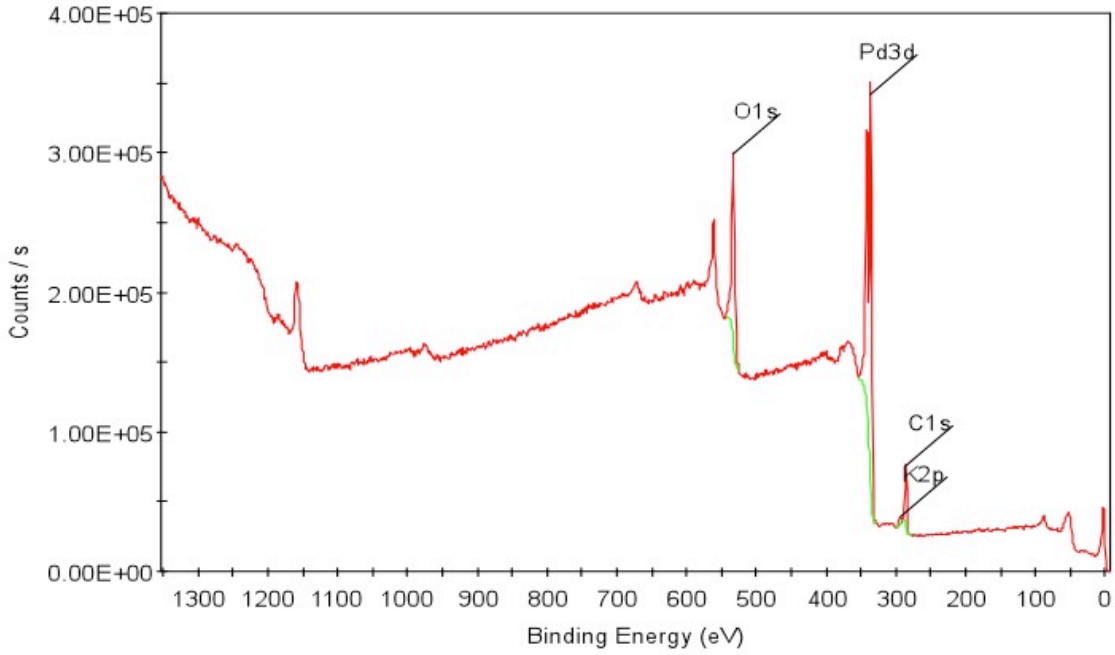

(b) After

Figure 3.6: XPS Survey Scan of Sample MW: Before and After Catalysis

The observation of most interest from XPS analysis is a peak occurring at 290 eV in samples after catalysis. This peak corresponds to a π-π^* transition[88]. A study published by Minkov also observed this peak for biphenyl in theoretical calculations and experimental data[89]. This peak was found in XPS spectra for all samples accept Sorbitol and HM, and is indicative of aromatics being present on the particle surface after catalysis. The absence of boron and bromide in both the XPS and EDS data (see Figure 3.6, also Appendix C and D) indicates that the aromatic species present is not due to bromobenzene or phenylboronic acid. This means that the aromatic species present on the surface of the particle is likely biphenyl, the product of the catalytic reaction and is evidence of catalyst poisoning by biphenyl. Other peaks observed in the C1s region include a C-C peak at 285 eV[90], a C-O peak at 287 eV and a C=O peak at 288 eV[91]. Two peaks arising from potassium were present as well, at binding energies of 293 eV and 296 eV corresponding to K2p3 and K2p1 respectively[92].

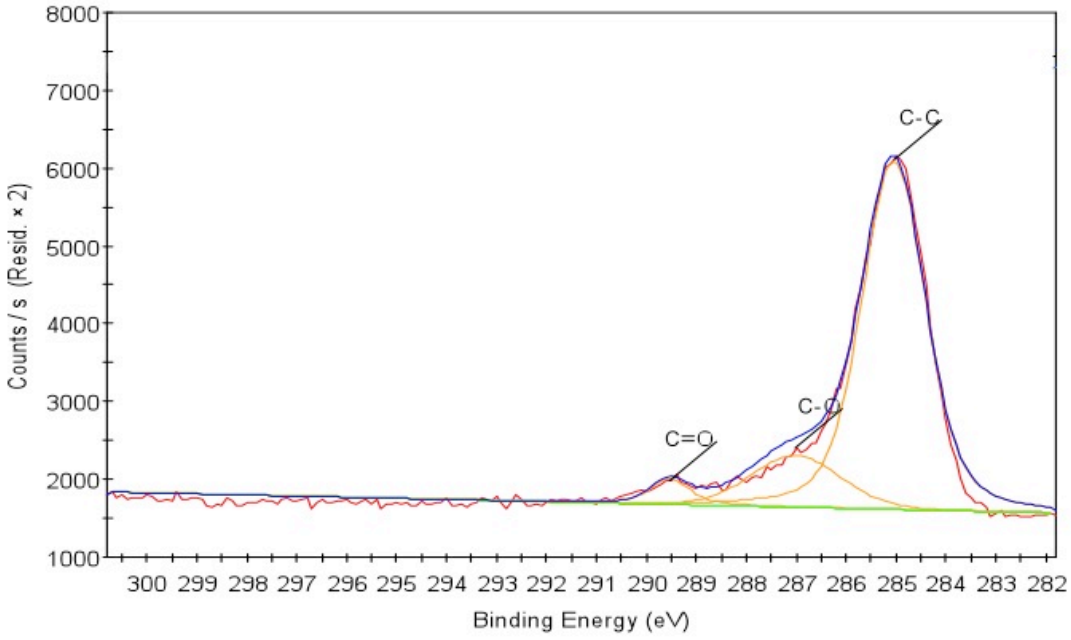

(a) Before

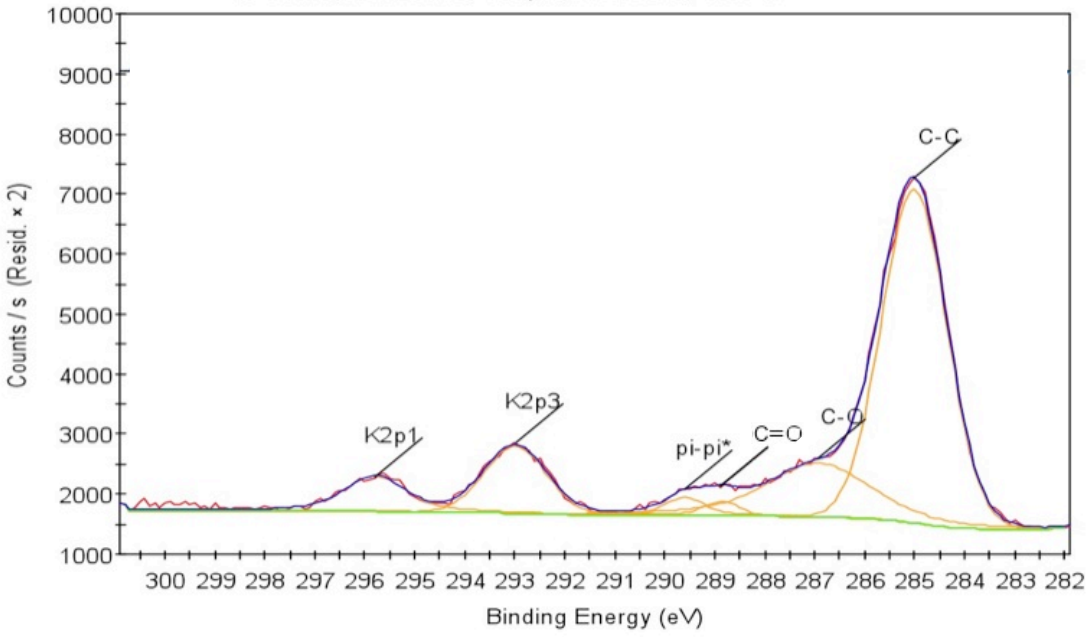

(b) After

Figure 3.7: XPS C1s Region Scan of Sample MW: Before and After Catalysis

Another interesting observation was made in the Pd3d region scan of the sorbitol and citrate samples. In all other samples only two peaks occur: a peak at 336 eV corresponding to Pd(0)[93] and a peak at 337 eV corresponding to PdO[94]. A third peak appears in the spectra of sorbitol and citrate at 338 eV and corresponds to Palladium (II) chloride[95].

Four peaks were found in the O1s region scan corresponding to PdO[96], C=O, C-O, and chemibsorbed H_2O with respective binding energies of 531 eV, 533 eV, 534 eV, and 536 eV[97,98]. Chemisorption is a very strong interaction between an adbsorbent and a substrate and can withstand ultra high vacuum[98].

Table 3.1: Peak Positions for XPS Spectra in C1s, Pd3d, and O1s Region Scans

Pd3d		O1s		C1s	
Peak	BE (eV)	Peak	BE (eV)	Peak	BE (eV)
Pd(0)	336	PdO	531	C-C	285
PdO	337	C=O	533	C-O	287
$PdCl_2$	338	C-O	534	C=O	288
		H_2O	536	K2p3	293
				K2p1	296

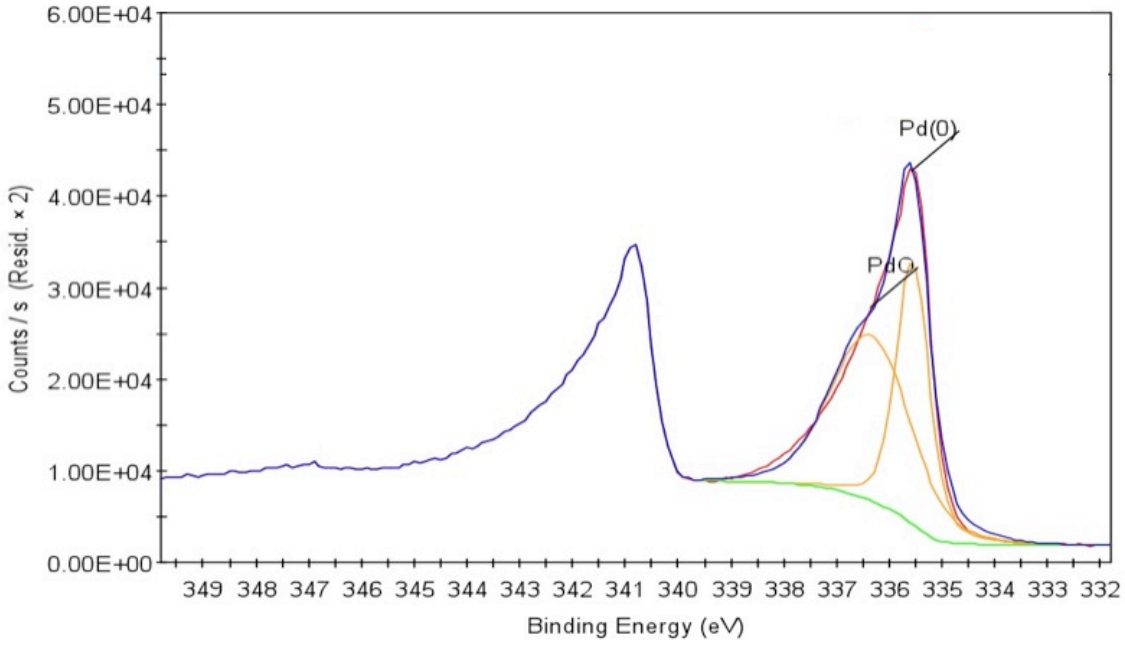

(a) Before

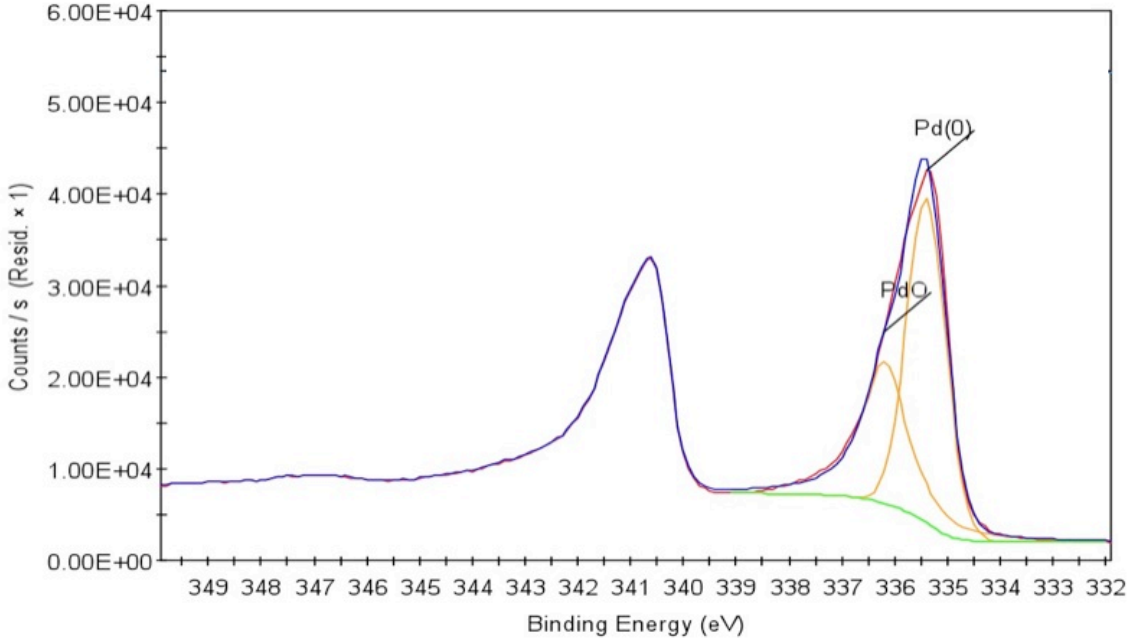

(b) After

Figure 3.8: XPS Pd3d Region Scan of Sample MW: Before and After Catalysis

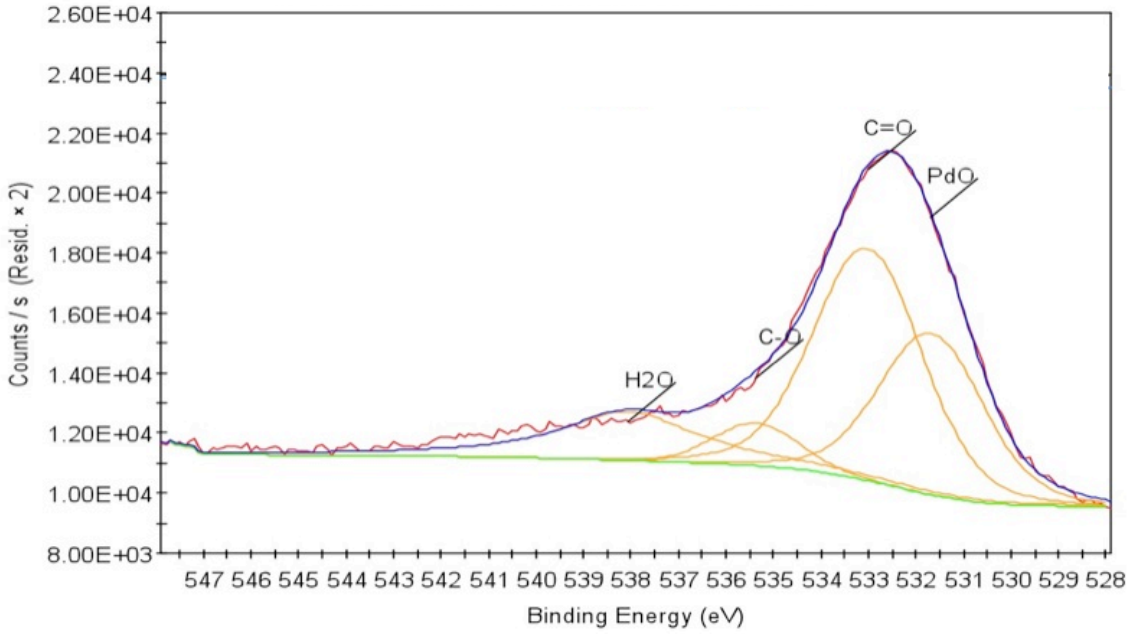

(a) Before

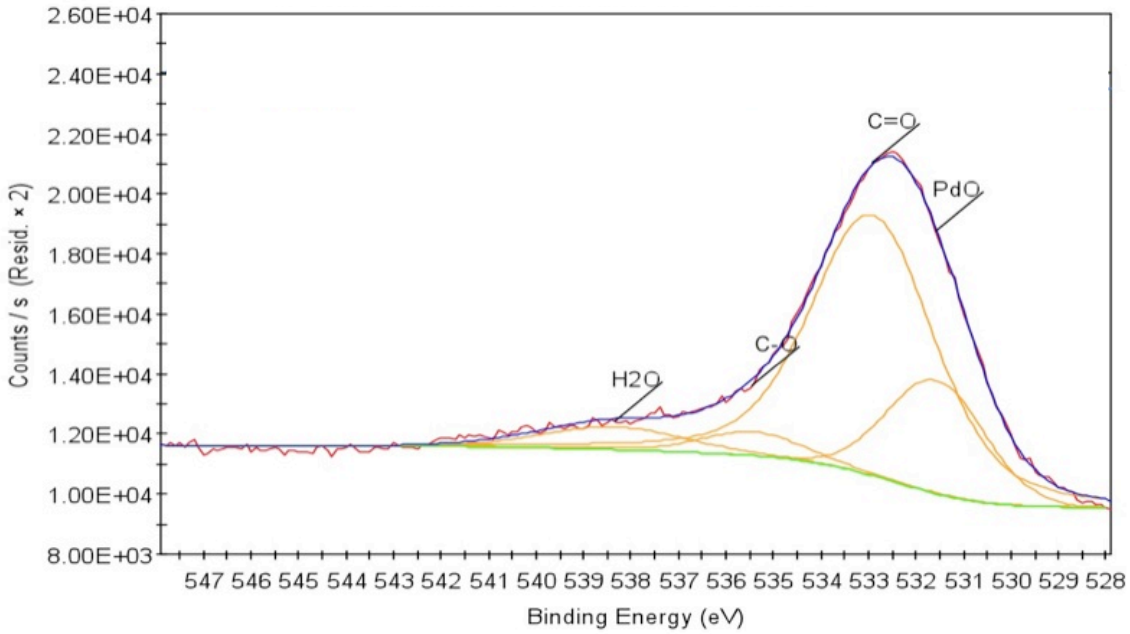

(b) After

Figure 3.9: XPS O1s Region Scan of Sample MW: Before and After Catalysis

4. Conclusions

Seven different types of nanocatalysts were investigated in the Suzuki carbon-carbon coupling reaction to determine what changes occur during the catalytic process and to gain a better understanding of the mechanisms involved. To achieve this, palladium nanoparticles were characterized before and after the catalytic reaction. XPS spectra for the after catalysis samples contain a peak corresponding to aromatic species. The absence of boron and bromine in both the XPS survey scan and EDS spectra indicate that the aromatic species present on the surface of the particle is due to biphenyl, the product of the catalytic reaction.

ICP-MS analysis of the filtered reaction mixture suggests that the catalysts studied may not be truly heterogeneous as the concentration of dissolved palladium in the catalytic reaction mixture was high enough for homogeneous catalysis to occur. The soluble palladium species is much more catalytically active than its heterogeneous counterpart[1] and concentrations as low as 50 ppb can catalyze the Suzuki reaction homogeneously[40]. This being said, heterogeneous catalysis may be taking place as well. A kinetic study correlating the reaction rates with soluble palladium concentrations would help to elucidate this answer[1,39]. SEM images show that particle size is increasing during the catalytic reaction, and the dissolved palladium found in ICP-MS analysis indicates that growth is due, in part, to Ostwald ripening.

Characterization of the different catalysts studied has provided important information about the mechanisms of the cross-coupling reaction. This study indicates that decreases in catalytic efficiency may not only be due to particle growth as was observed by El-sayed et al.[49,57,58] but also poisoning by biphenyl. The catalysts studied also experienced a significant amount of leaching, which indicates that some homogeneous catalysis is taking place.

5. Appendix

5.1 Appendix A: XRD Data

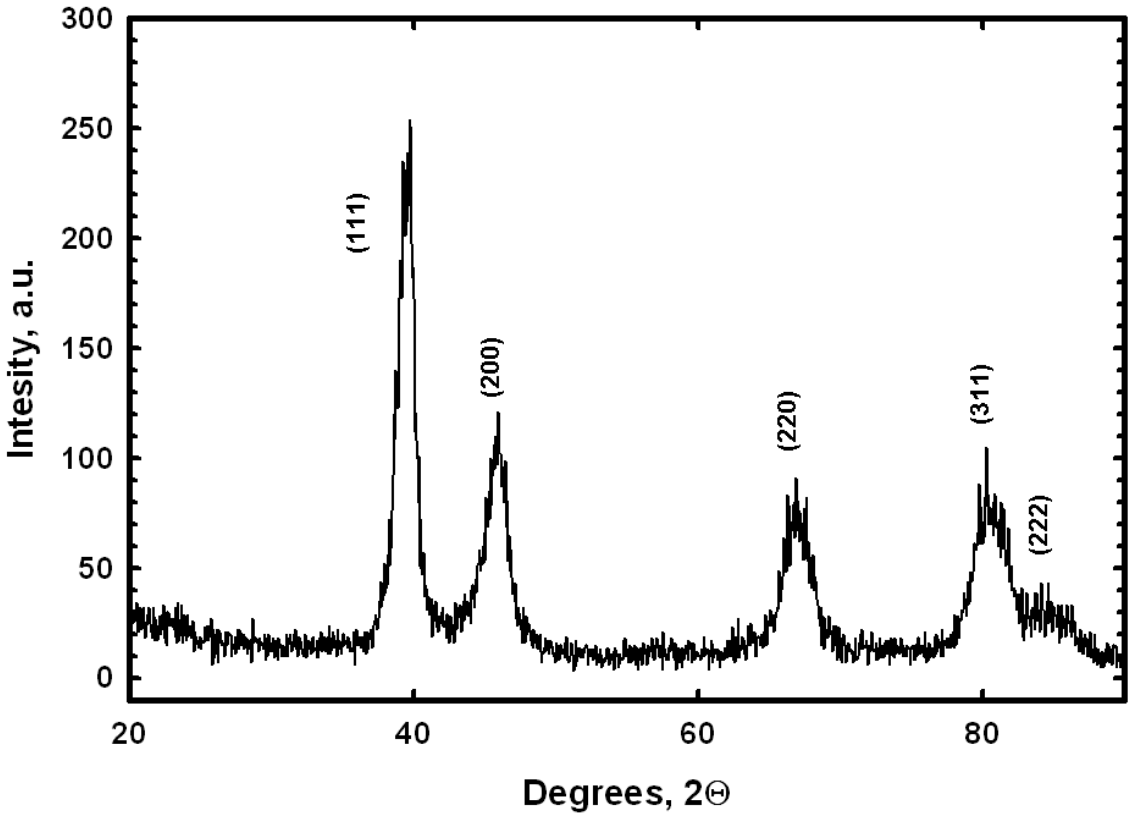

Figure 5.1: XRD Pattern Sample Oleyl

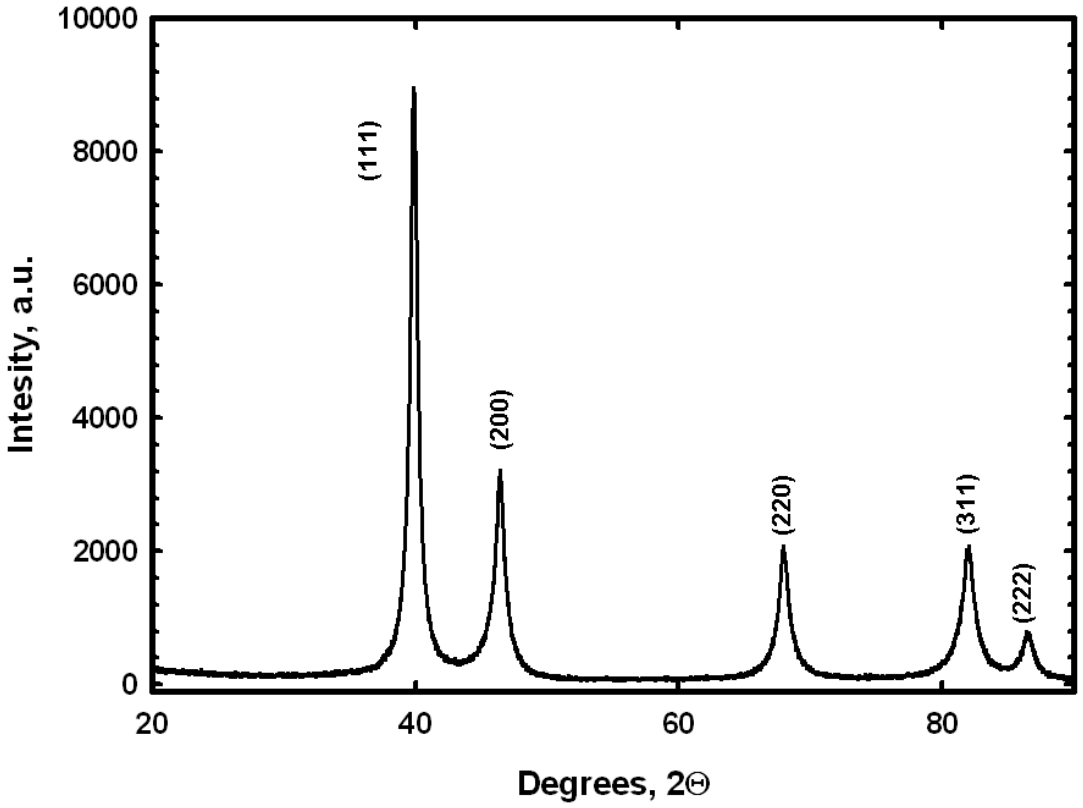

Figure 5.2: XRD Pattern Sample HM

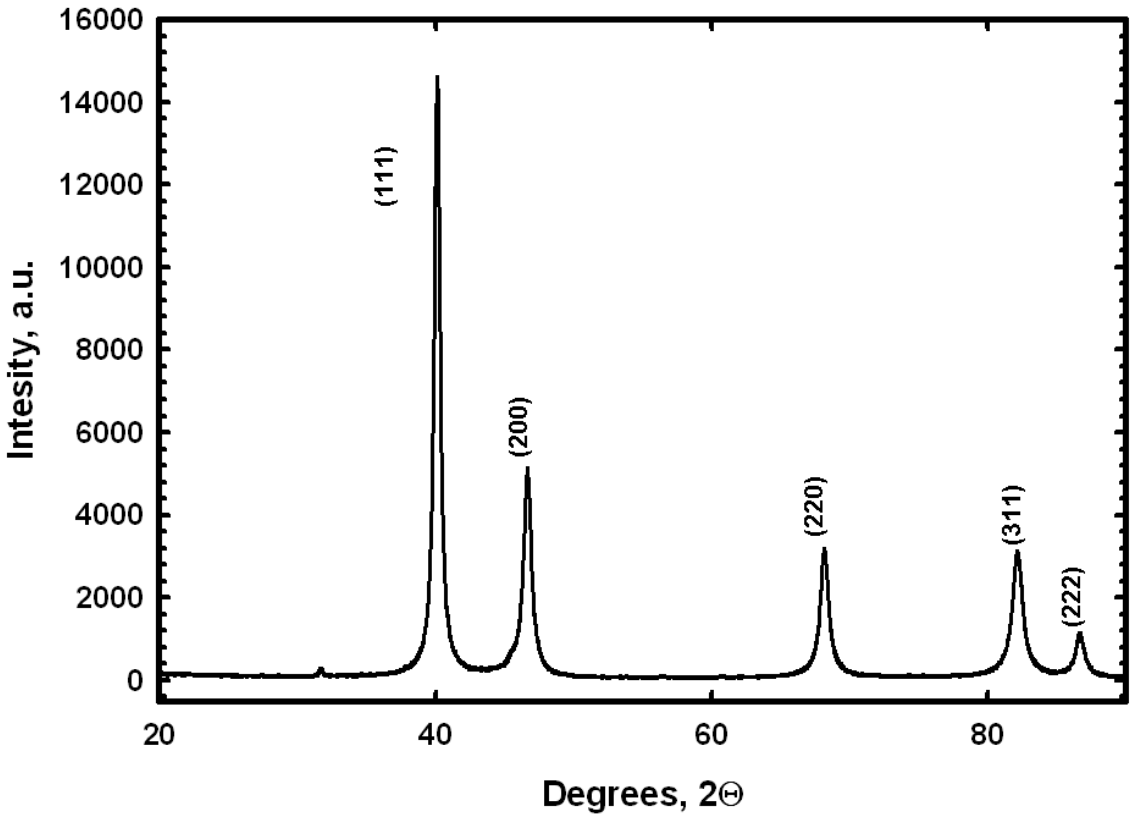

Figure 5.3: XRD Pattern Sample MW

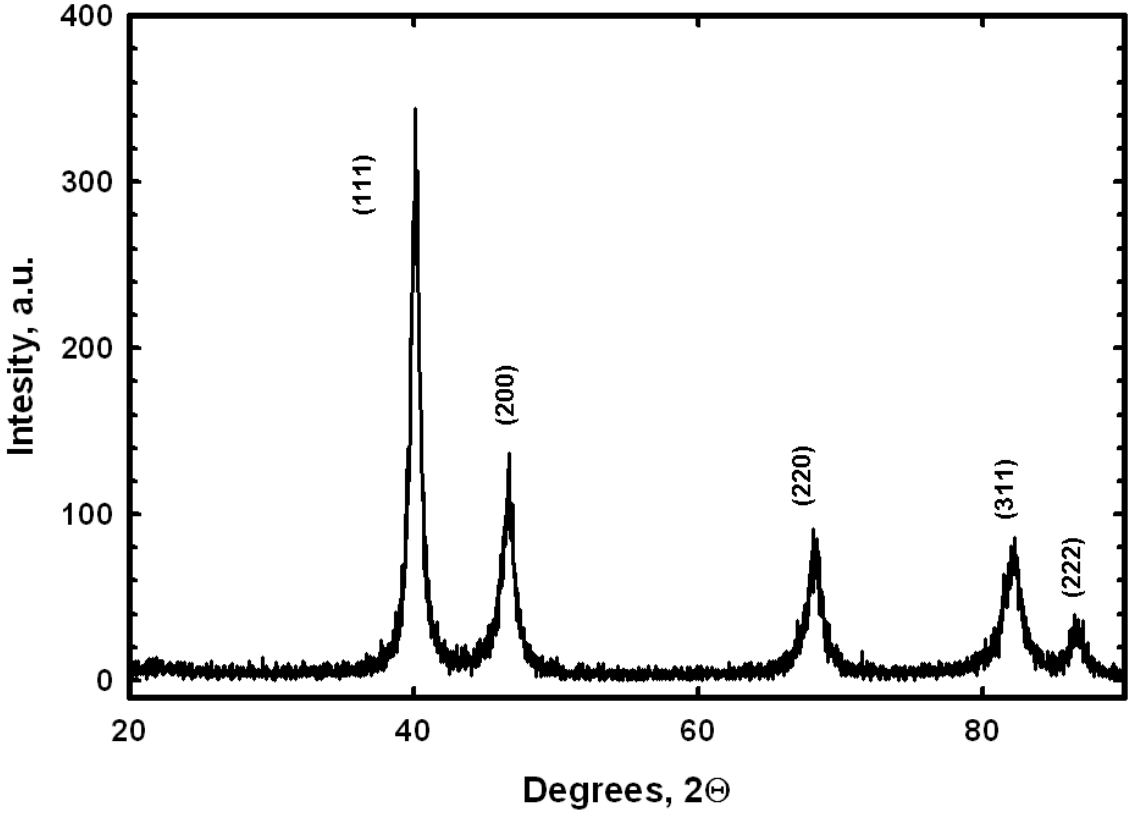

Figure 5.4: XRD Pattern Sample PVP

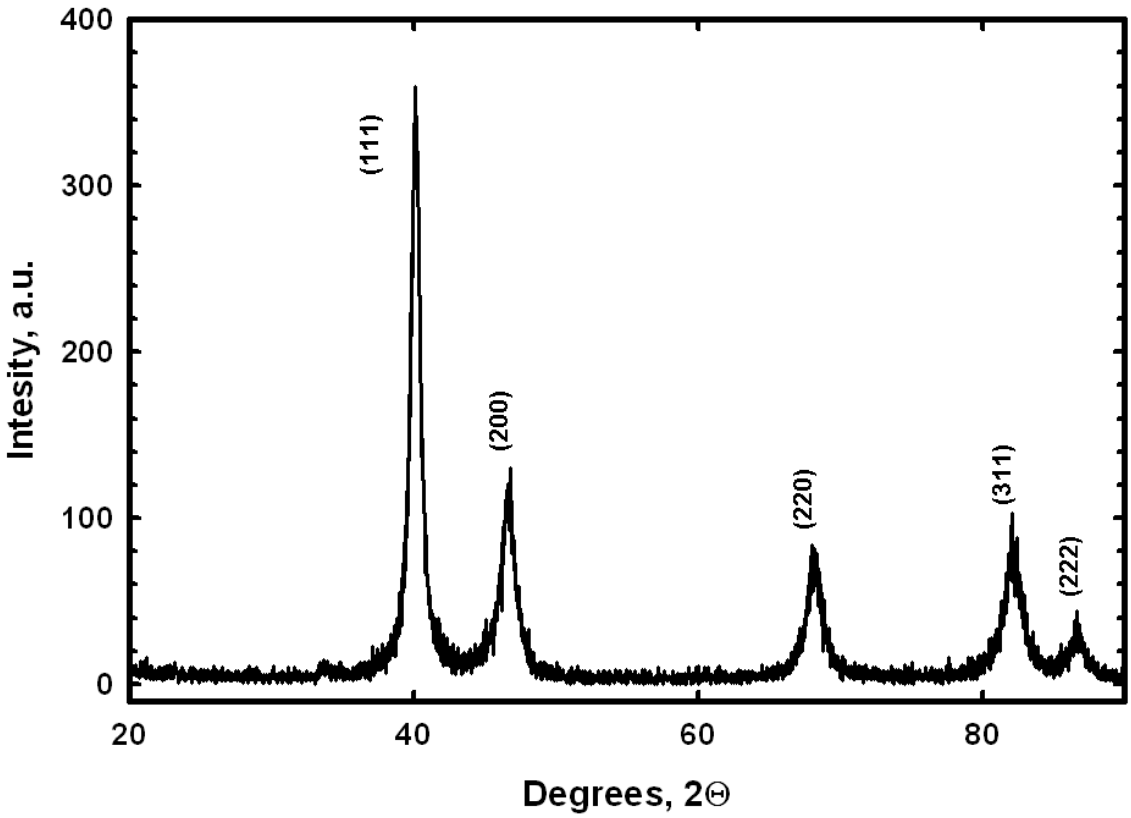

Figure 5.5: XRD Pattern Sample PVA

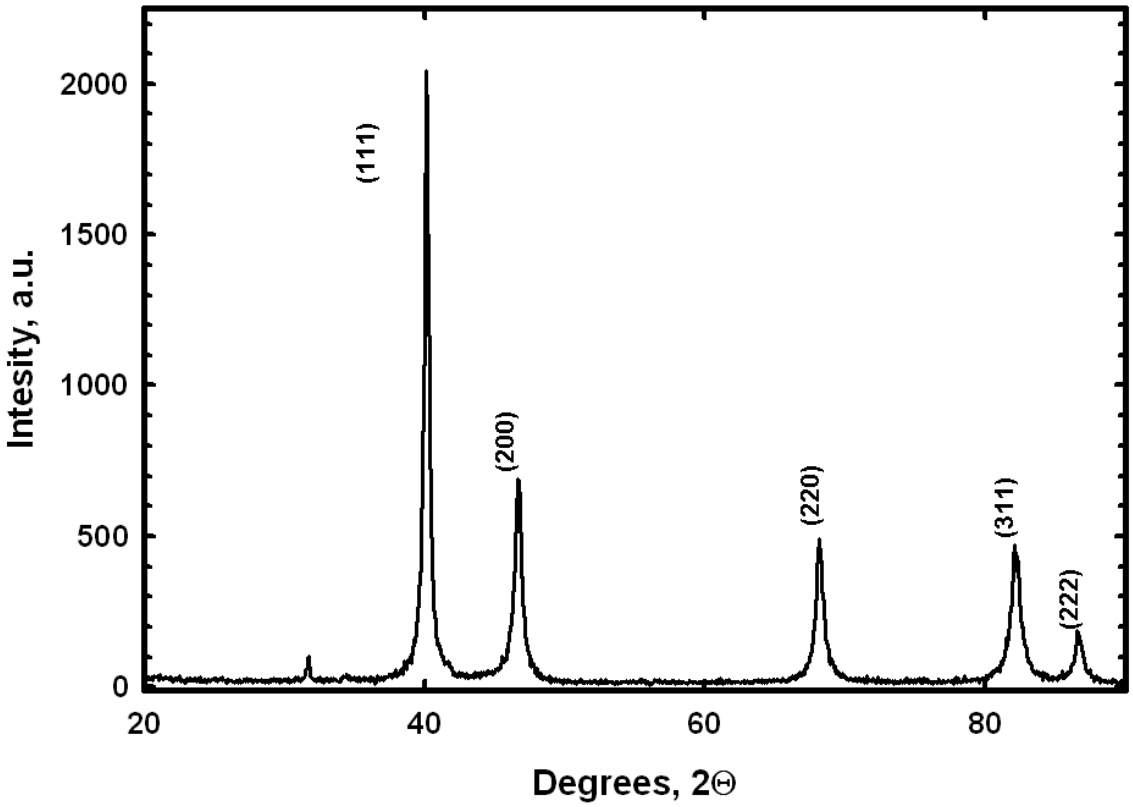

Figure 5.6: XRD Pattern Sample Sorbitol

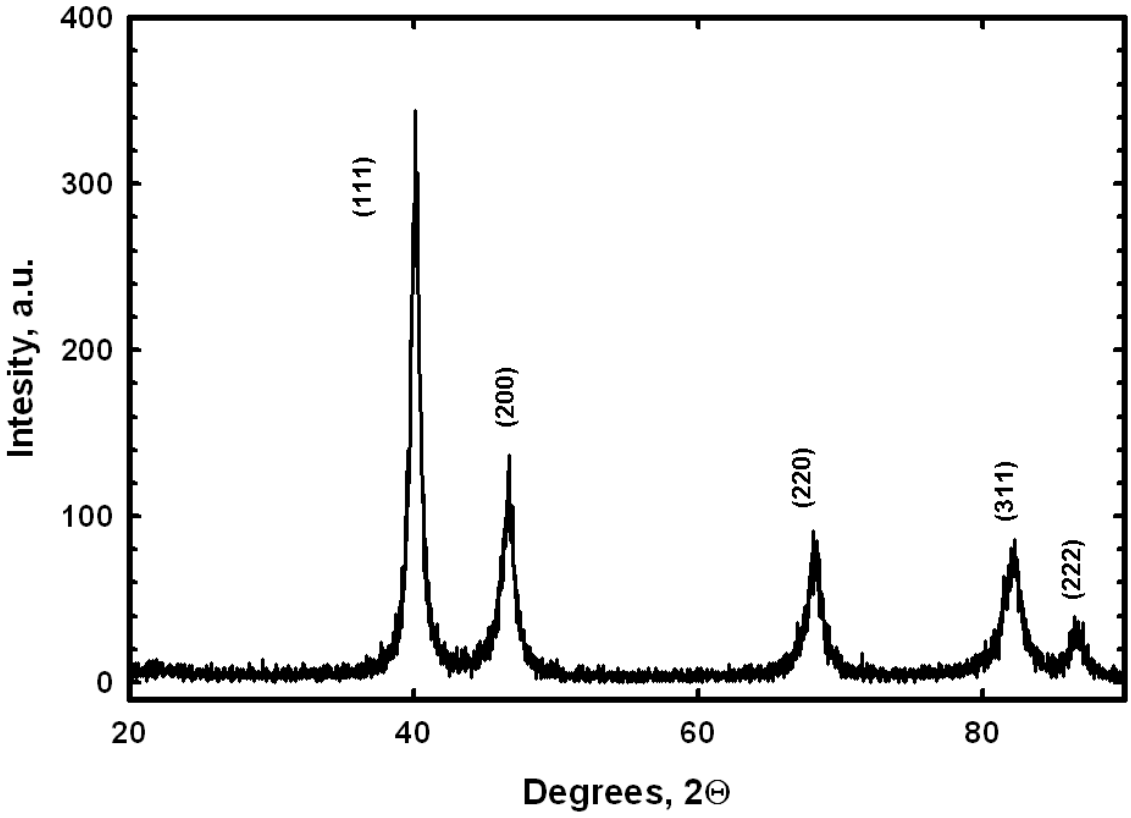

Figure 5.7: XRD Pattern Sample Citrate

5.2 Appendix B: SEM Images

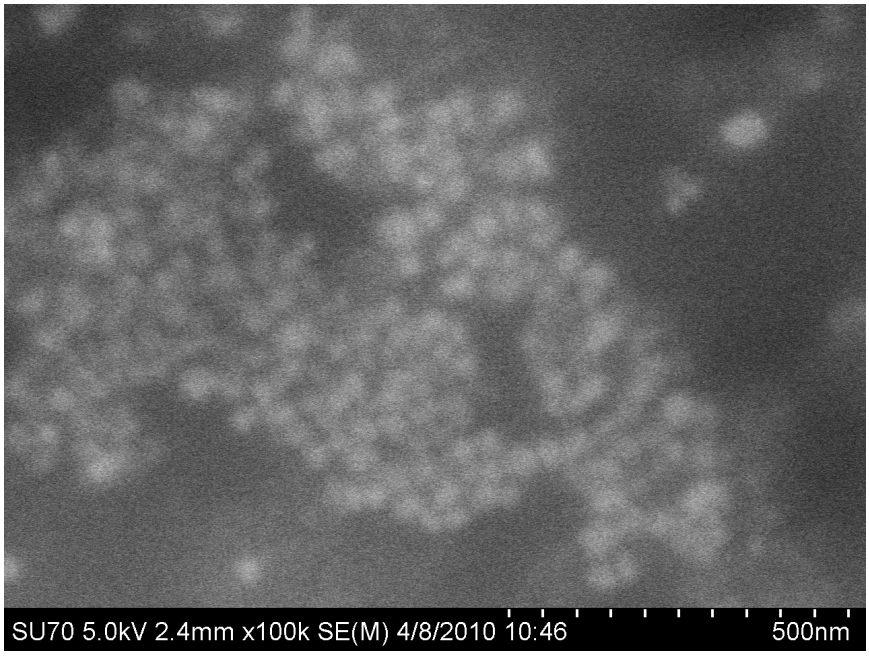

(a) Before

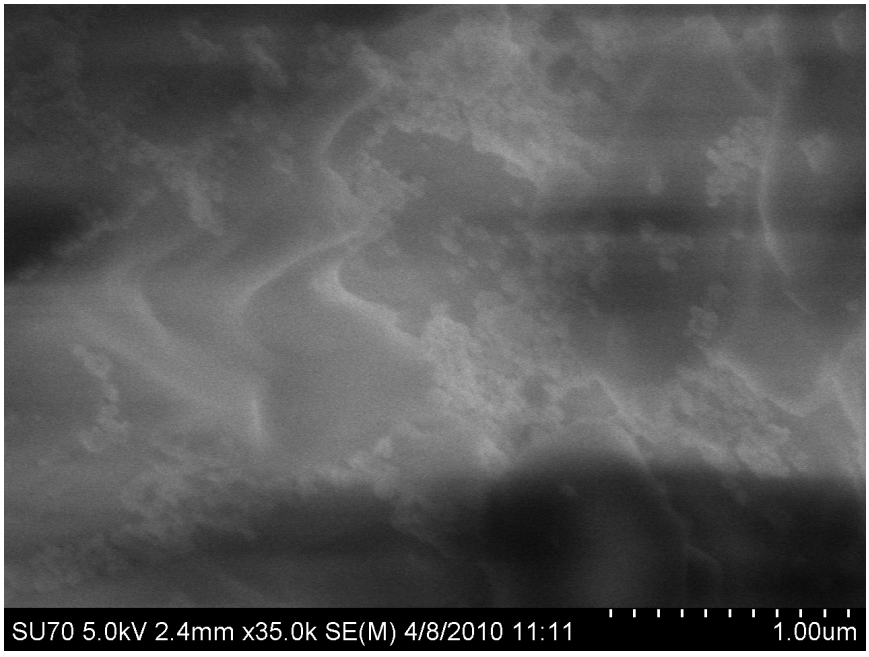

(b) After

Figure 5.8: SEM Images of Sample Oleyl: Before and After Catalysis

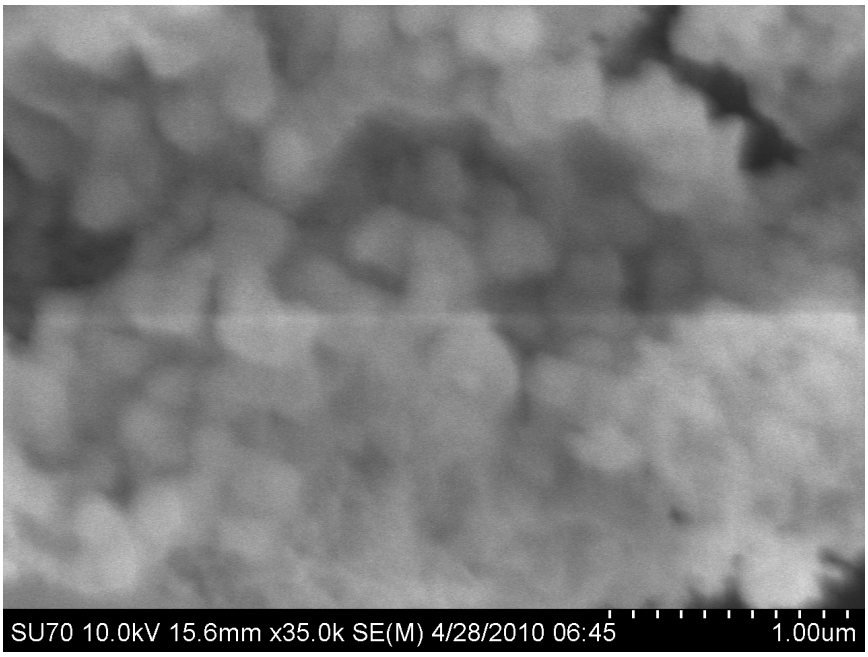

(a) Before

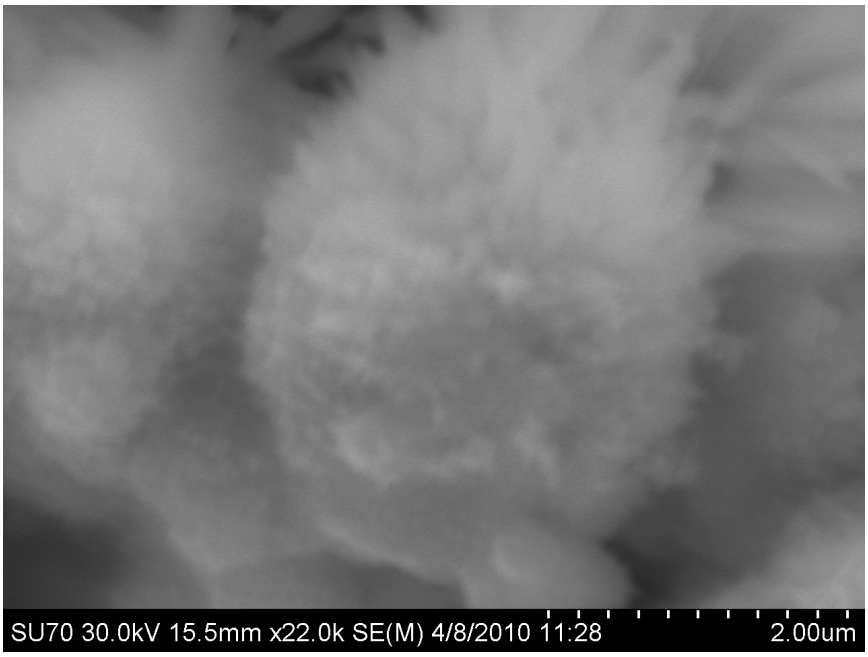

(b) After

Figure 5.9: SEM Images of Sample HM: Before and After Catalysis

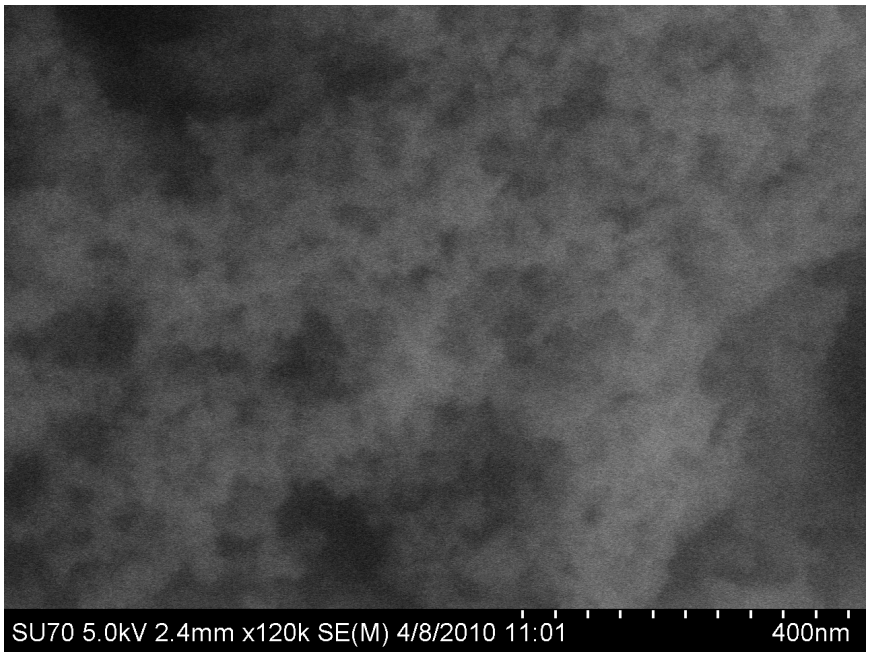

(a) Before

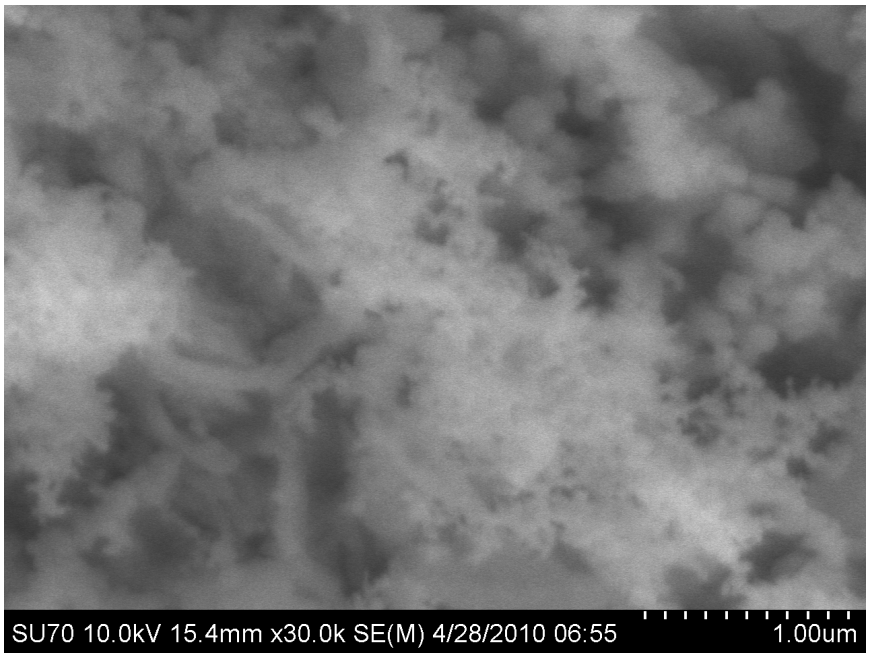

(b) After

Figure 5.10: SEM Images of Sample MW: Before and After Catalysis

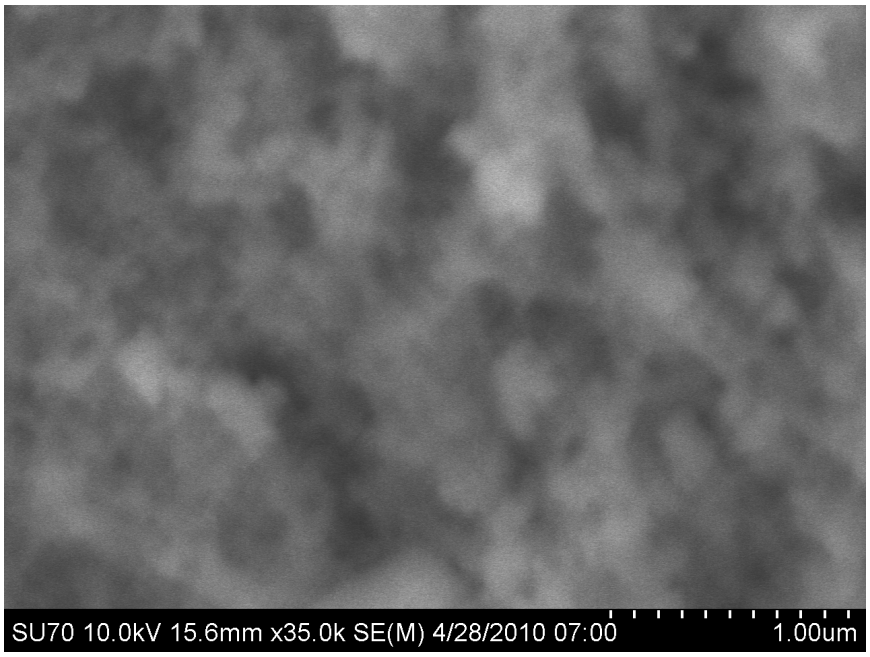

(a) Before

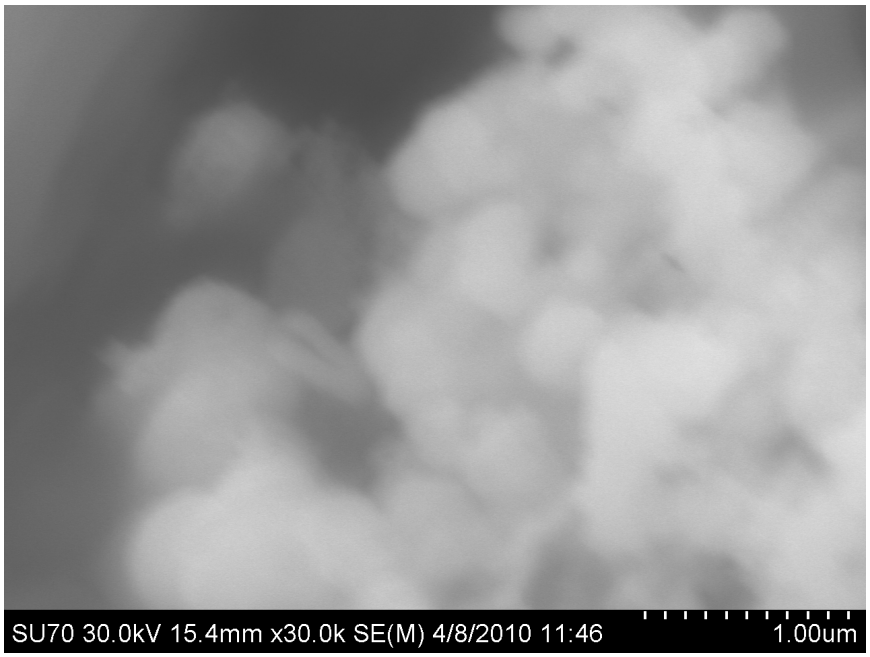

(b) After

Figure 5.11: SEM Images of Sample PVP: Before and After Catalysis

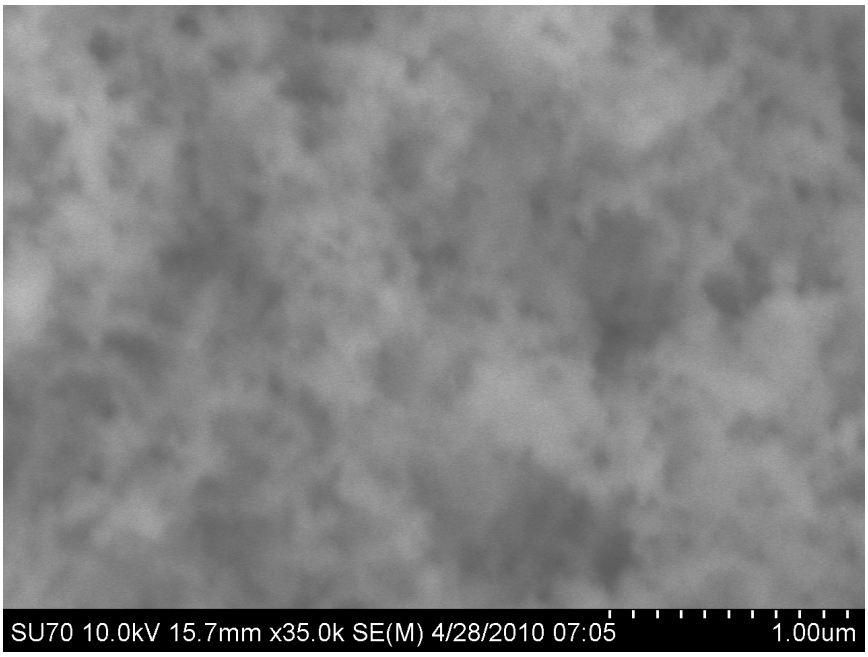

(a) Before

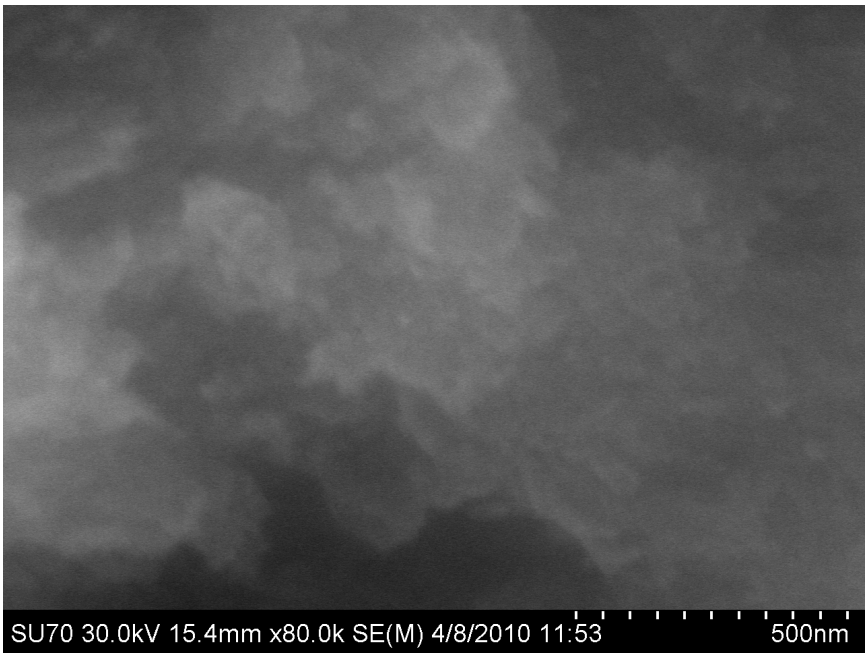

(b) After

Figure 5.12: SEM Images of Sample PVA: Before and After Catalysis

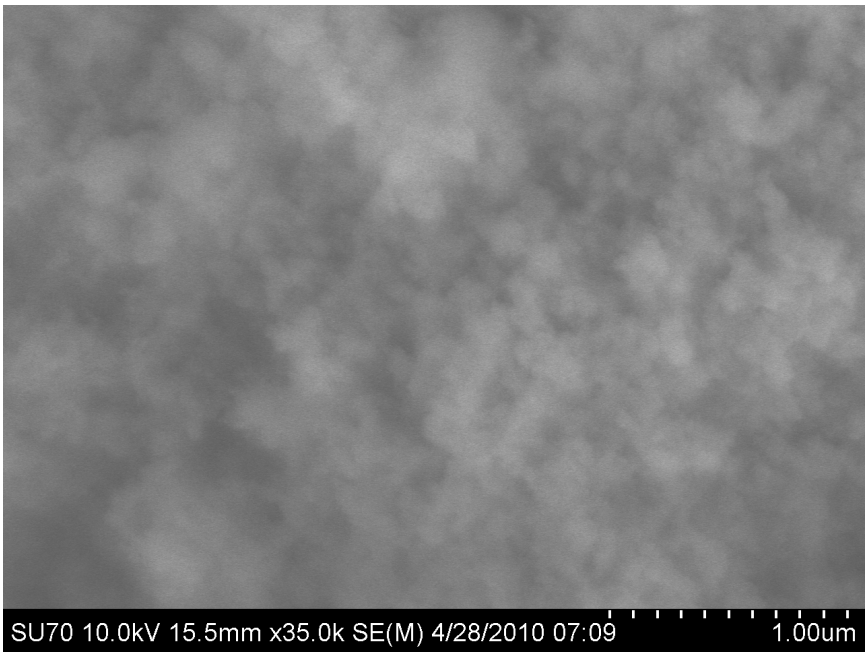

(a) Before

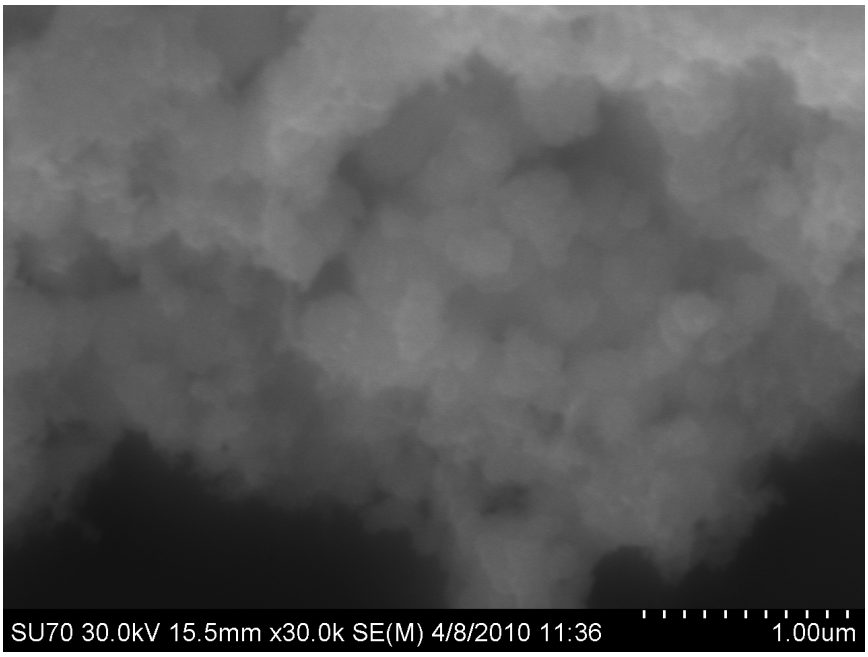

(b) After

Figure 5.13: SEM Images of Sample Sorbitol: Before and After Catalysis

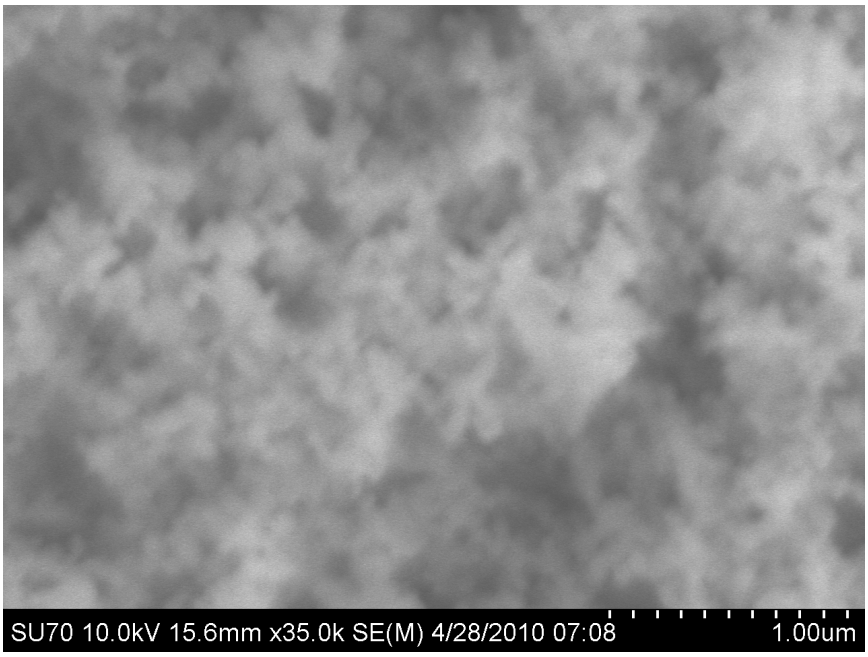

(a) Before

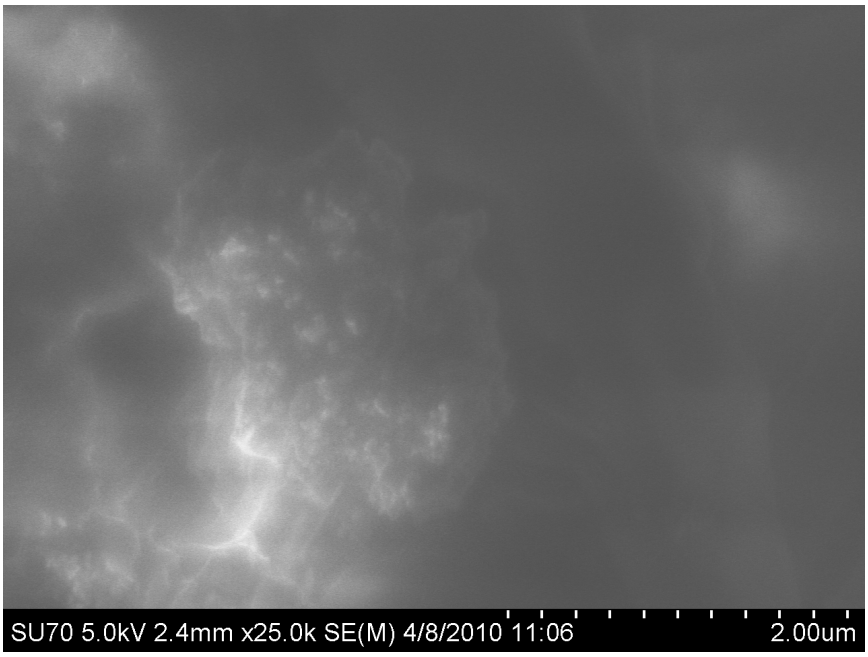

(b) After

Figure 5.14: SEM Images of Sample Citrate: Before and After Catalysis

5.3 Appendix C: XPS Spectra

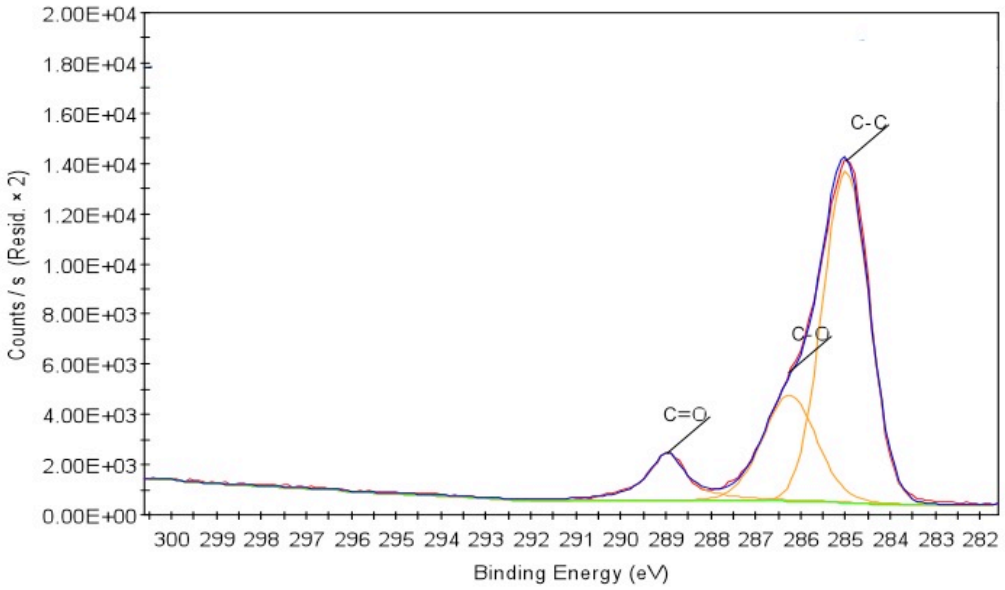

(a) Before

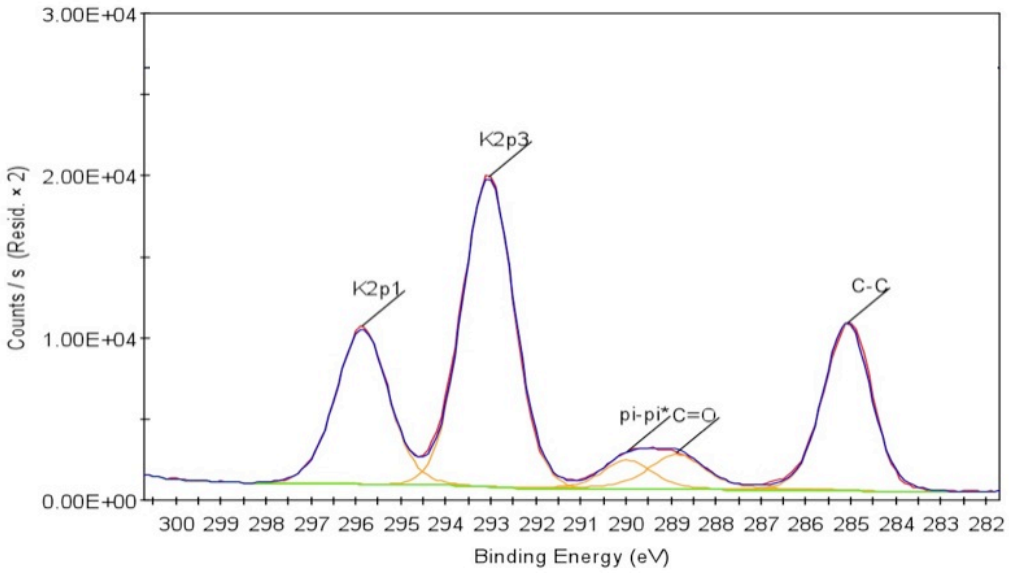

(b) After

Figure 5.15: XPS C1s Spectra for Sample Oleyl: Before and After Catalysis

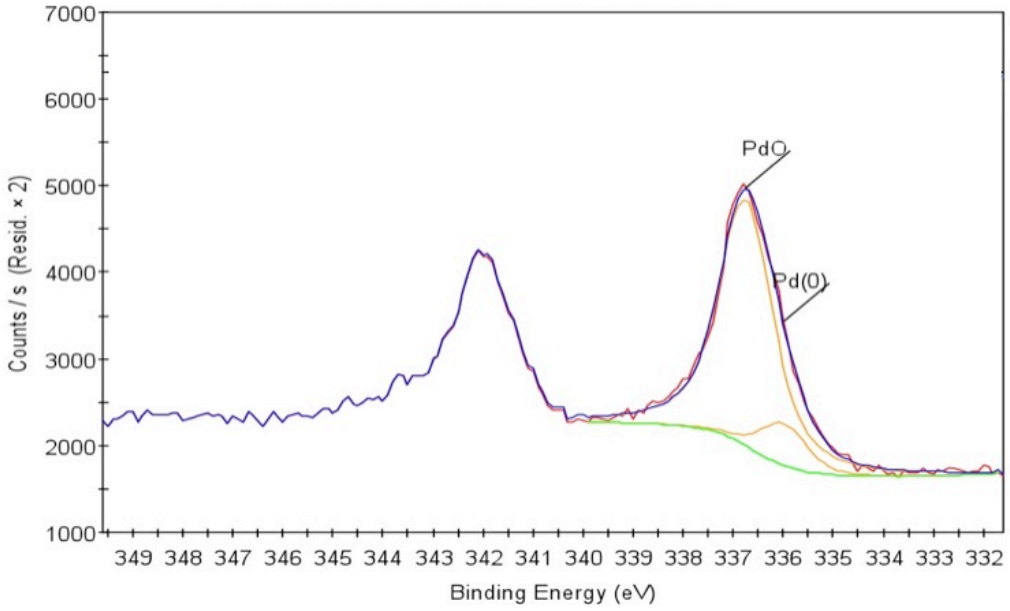

(a) Before

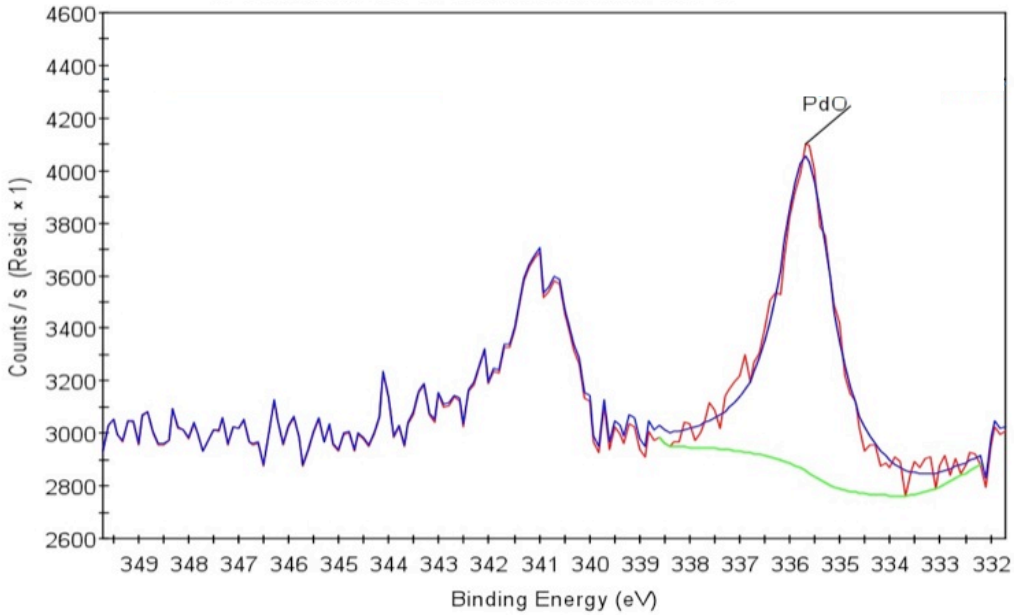

(b) After

Figure 5.16: XPS P3d Spectra for Sample Oleyl: Before and After Catalysis

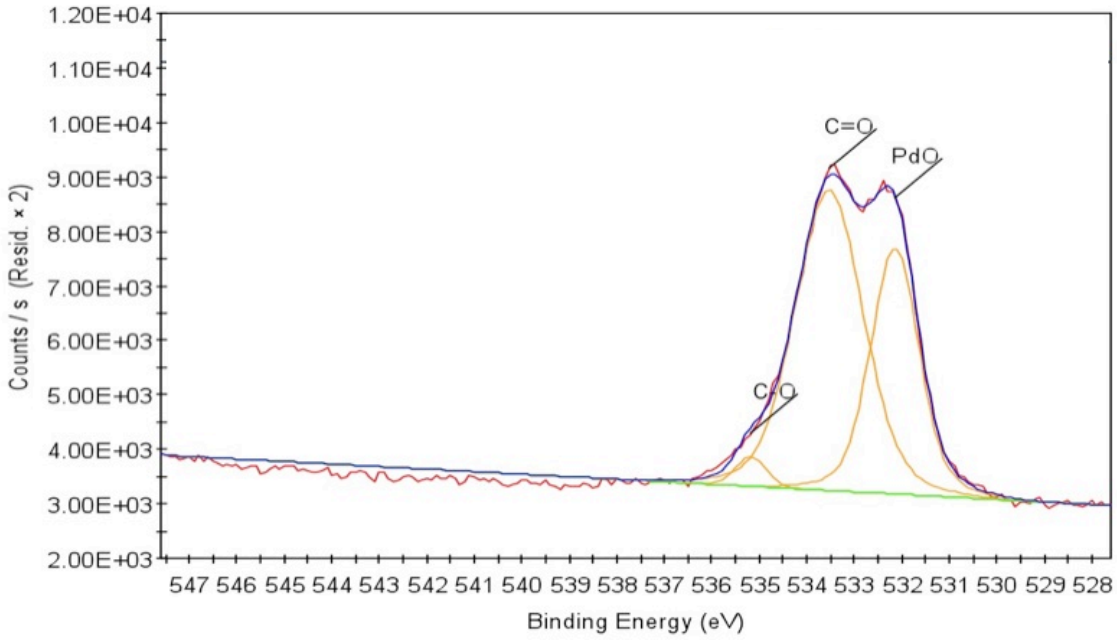

(a) Before

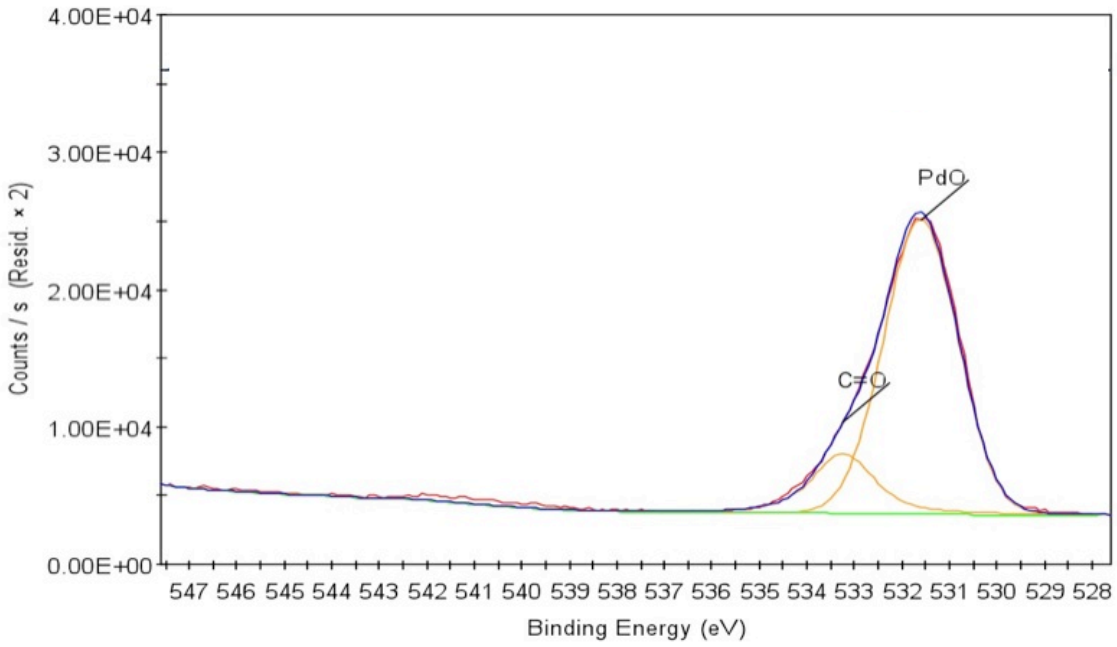

(b) After

Figure 5.17: XPS O1s Spectra for Sample Oleyl: Before and After Catalysis

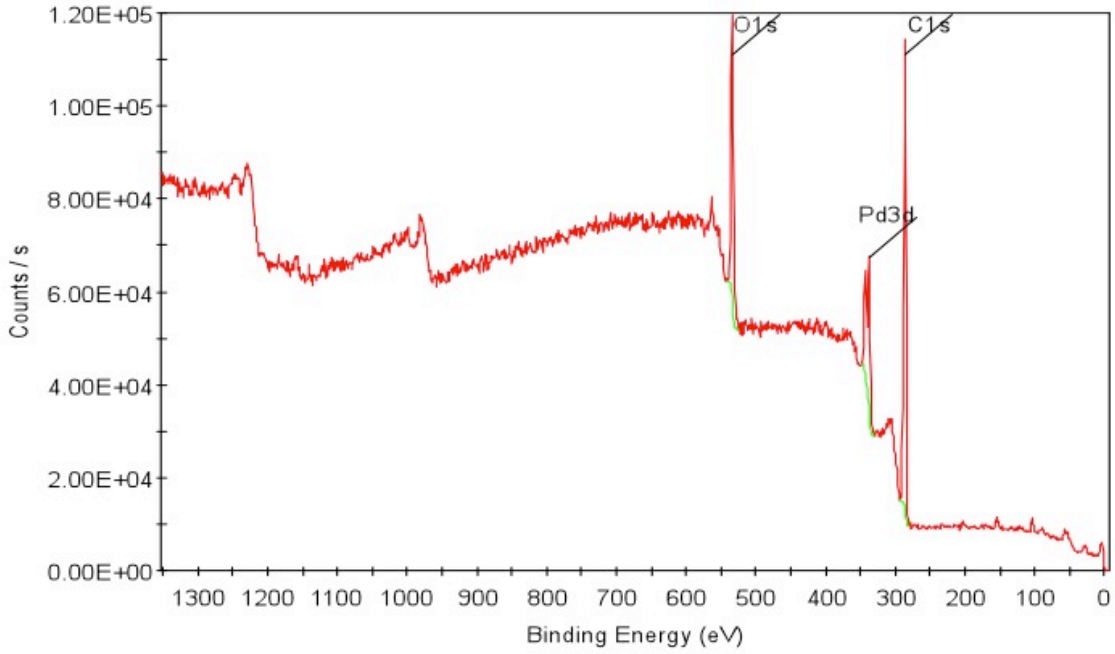

(a) Before

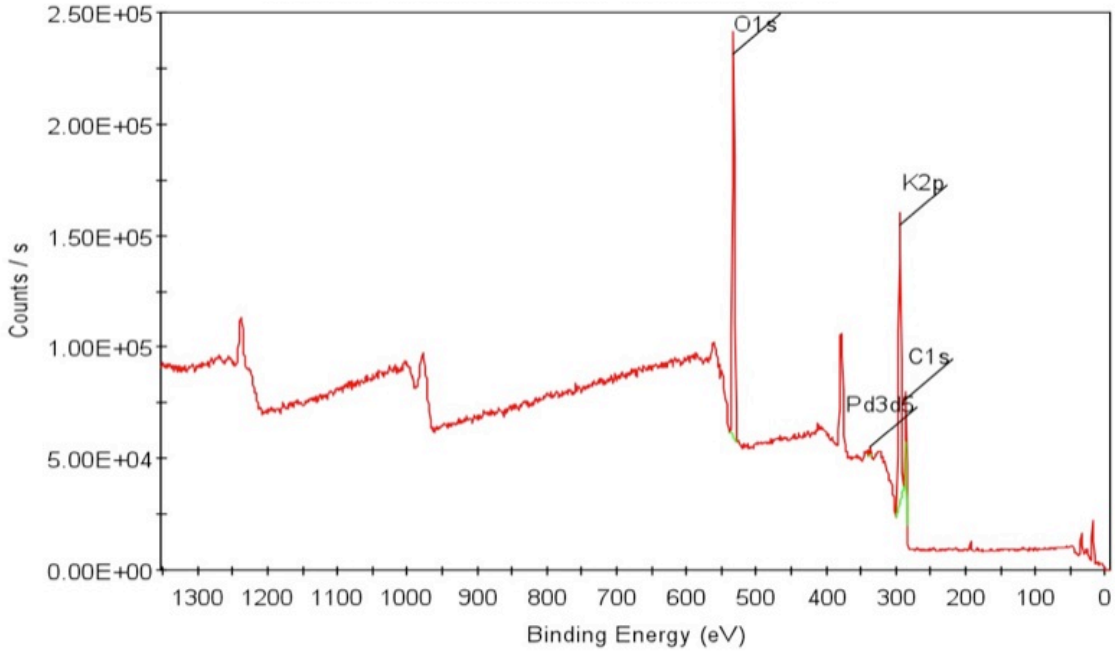

(b) After

Figure 5.18: XPS Survey Scan Spectra for Sample Oleyl: Before and After Catalysis

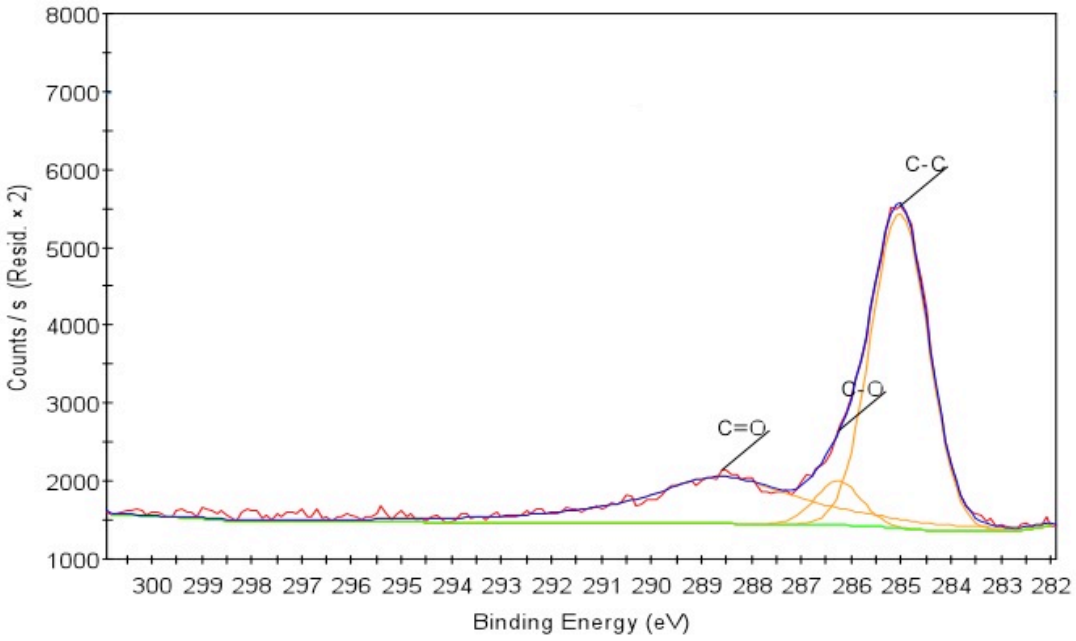

(a) Before

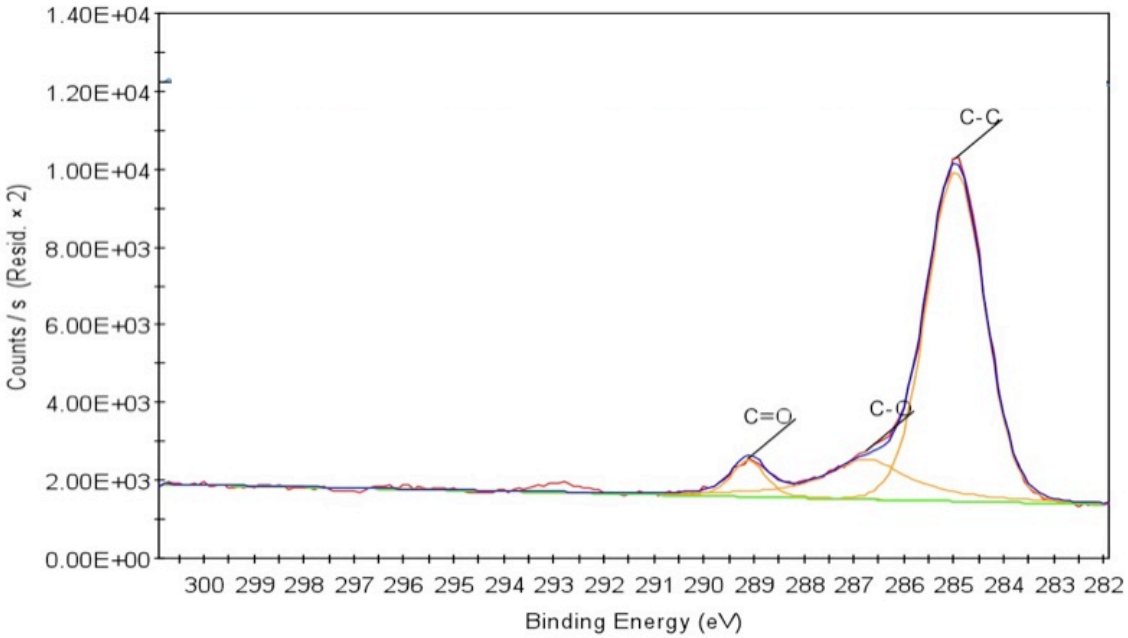

(b) After

Figure 5.19: XPS C1s Spectra for Sample HM: Before and After Catalysis

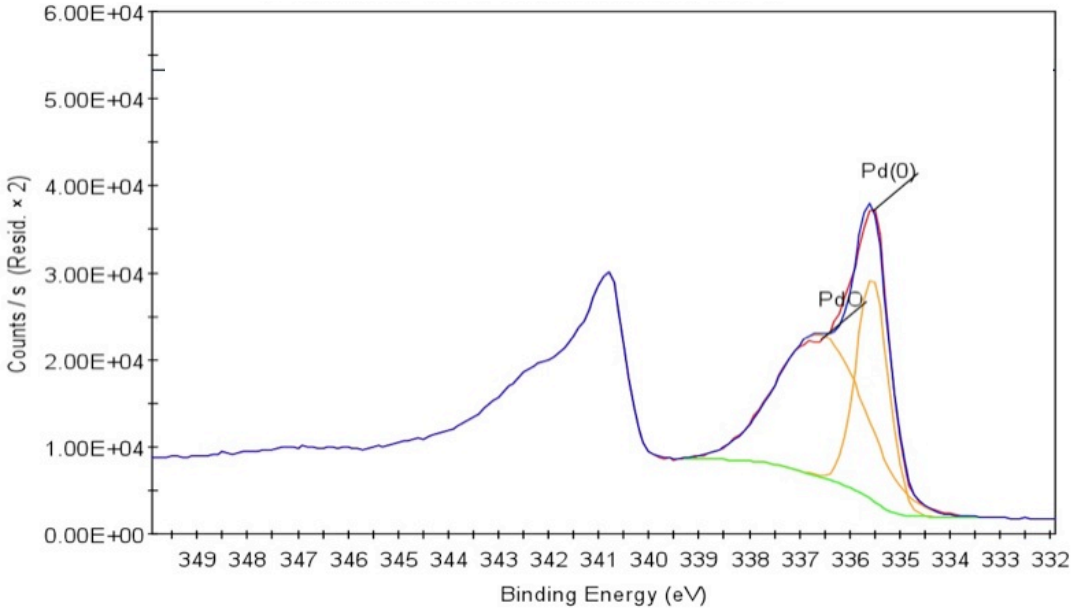

(a) Before

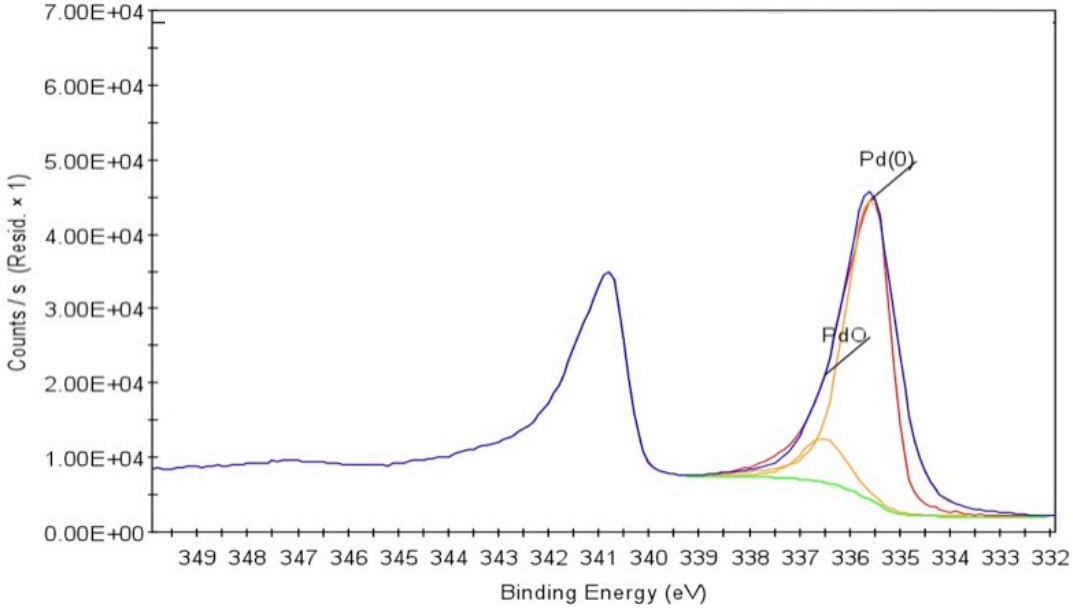

(b) After

Figure 5.20: XPS Pd3d Spectra for Sample HM: Before and After Catalysis

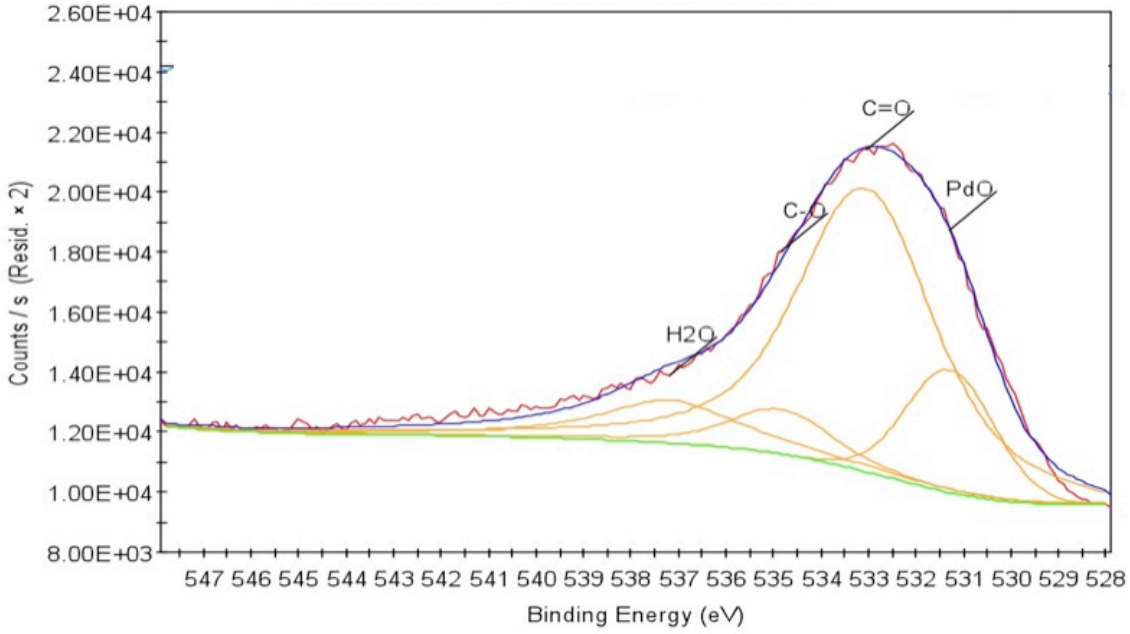

(a) Before

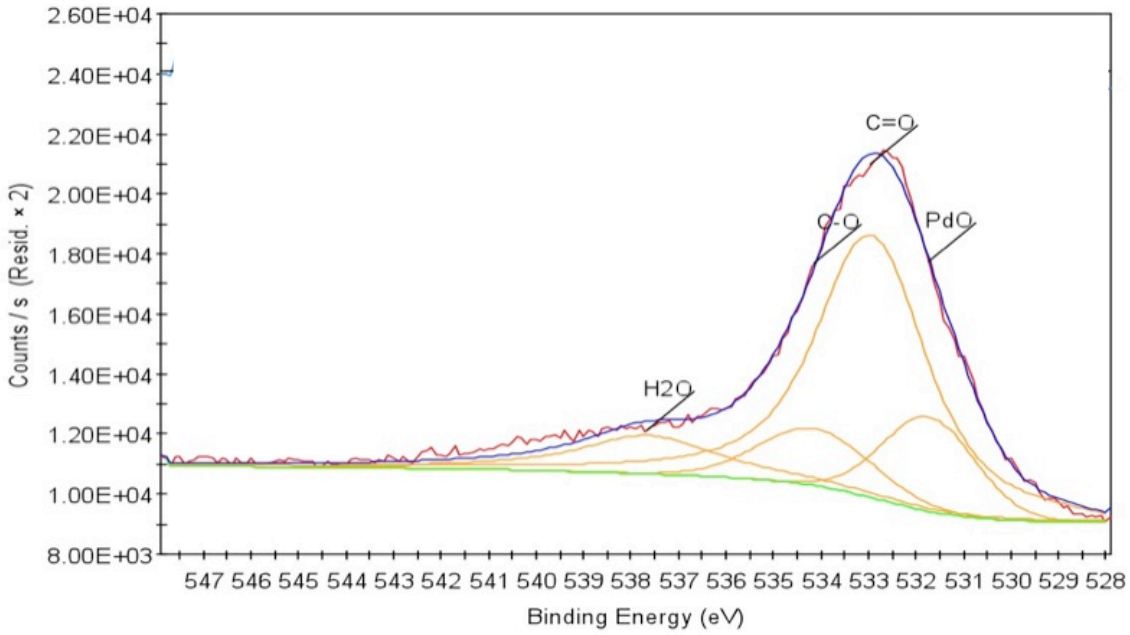

(b) After

Figure 5.21: XPS O1s Spectra for Sample HM: Before and After Catalysis

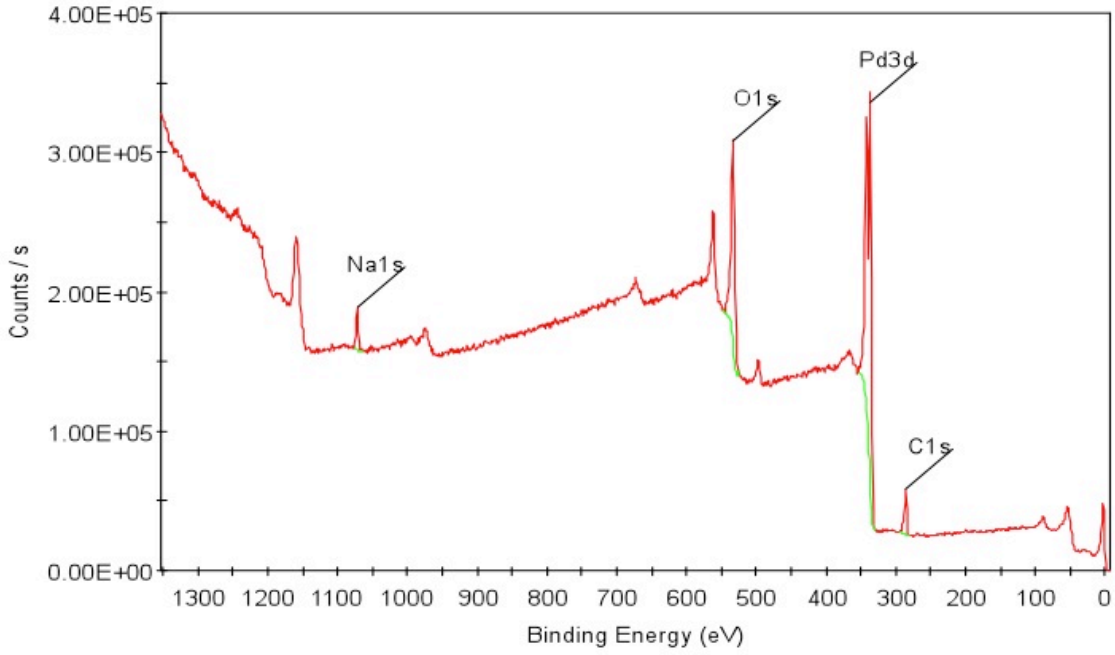

(a) Before

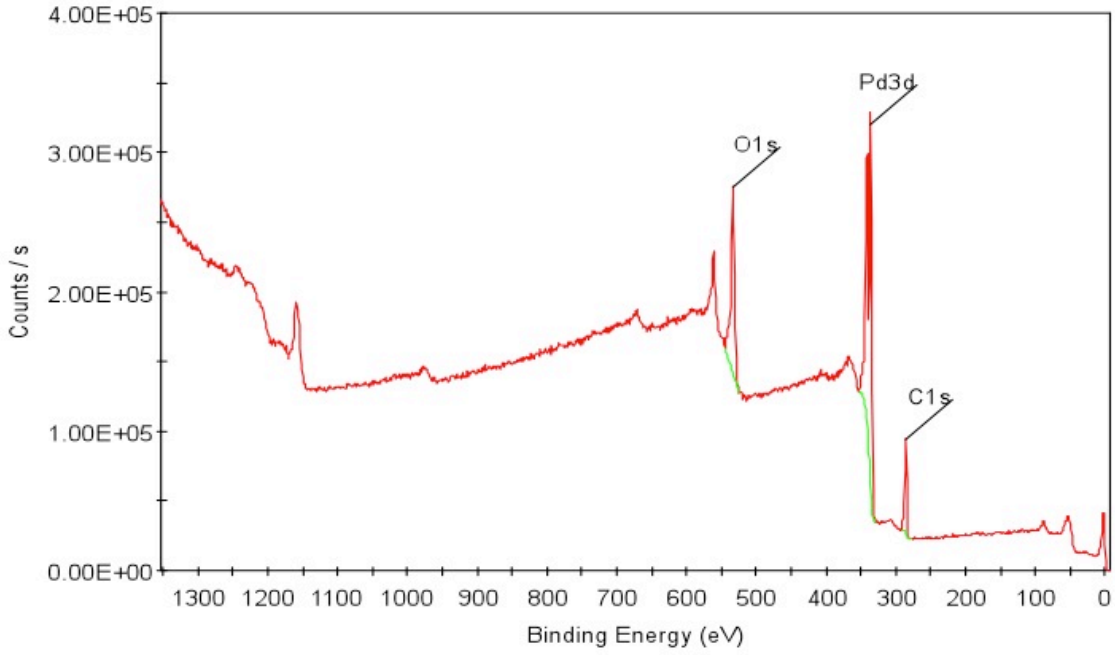

(b) After

Figure 5.22: XPS Survey Scan Spectra for Sample HM: Before and After Catalysis

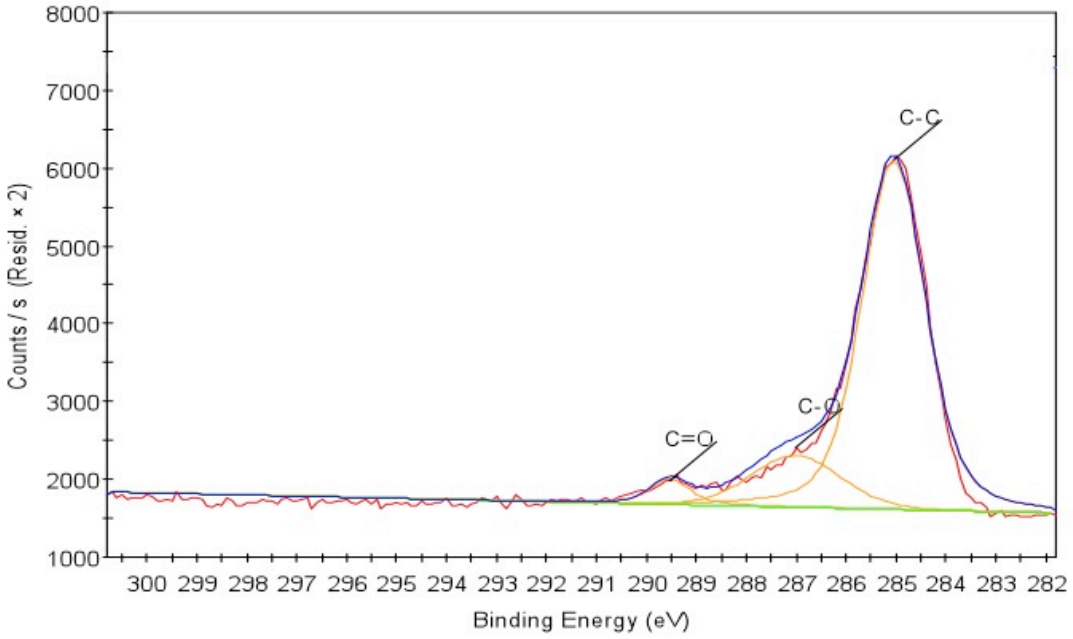

(a) Before

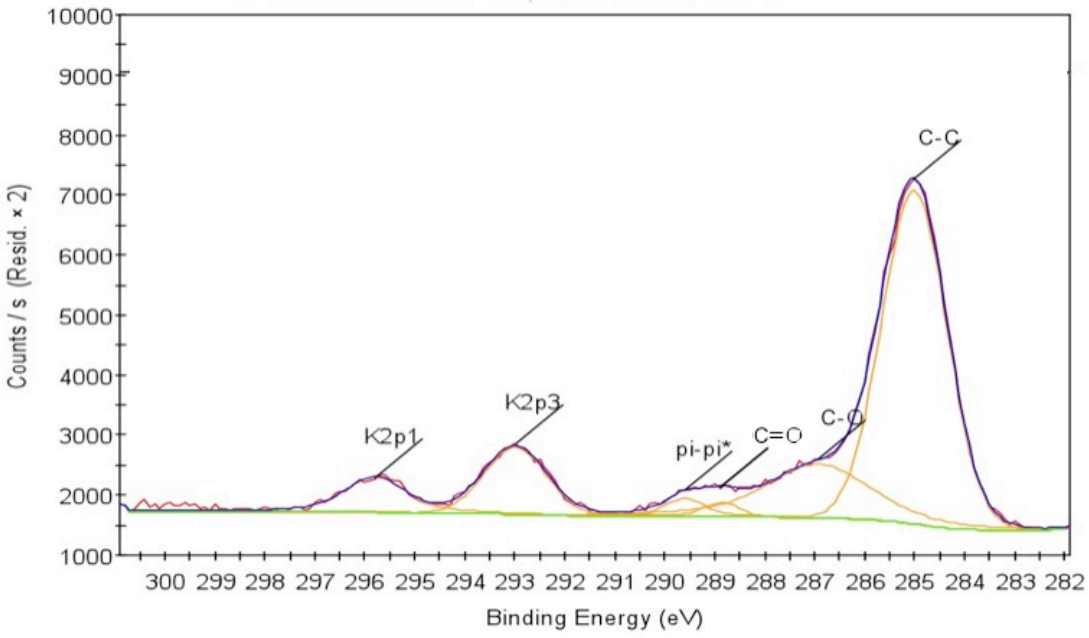

(b) After

Figure 5.23: XPS C1s Spectra for Sample MW: Before and After Catalysis

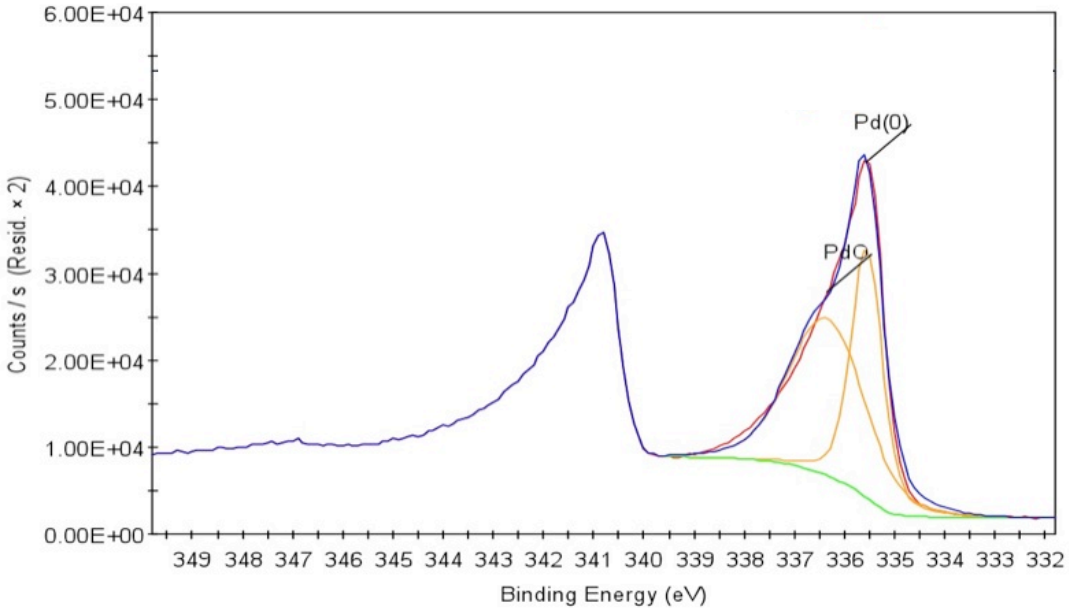

(a) Before

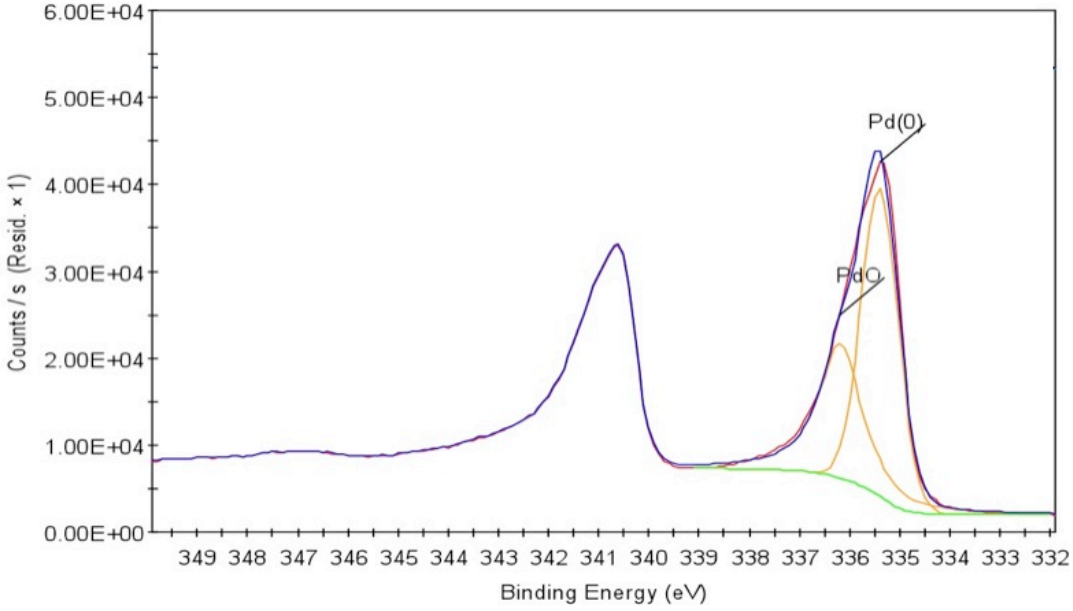

(b) After

Figure 5.24: XPS Pd3d Spectra for Sample MW: Before and After Catalysis

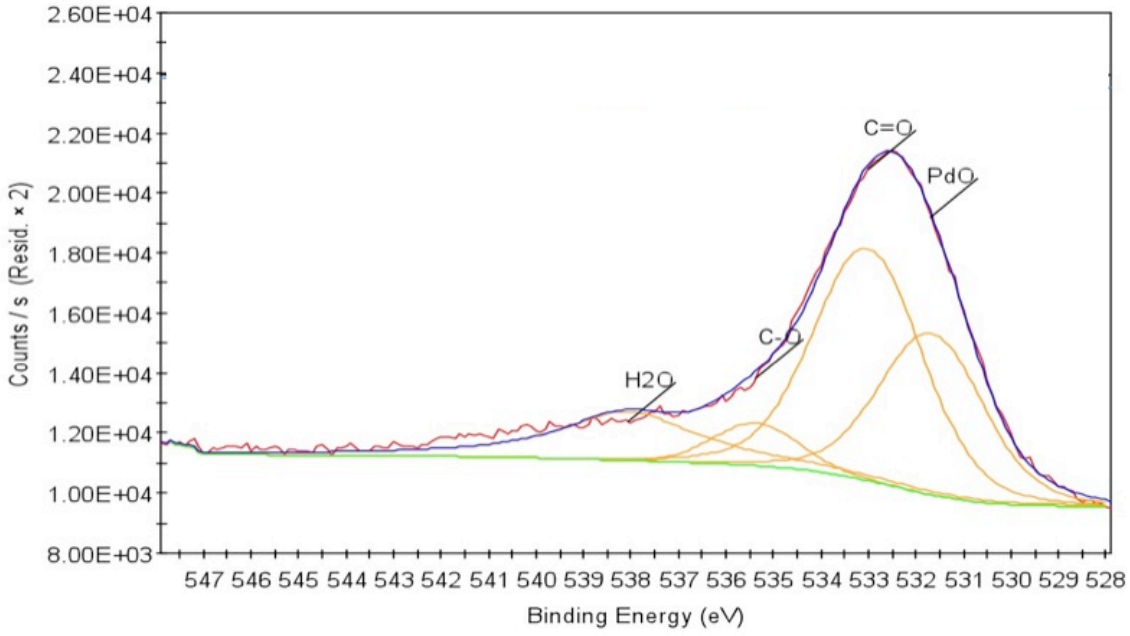

(a) Before

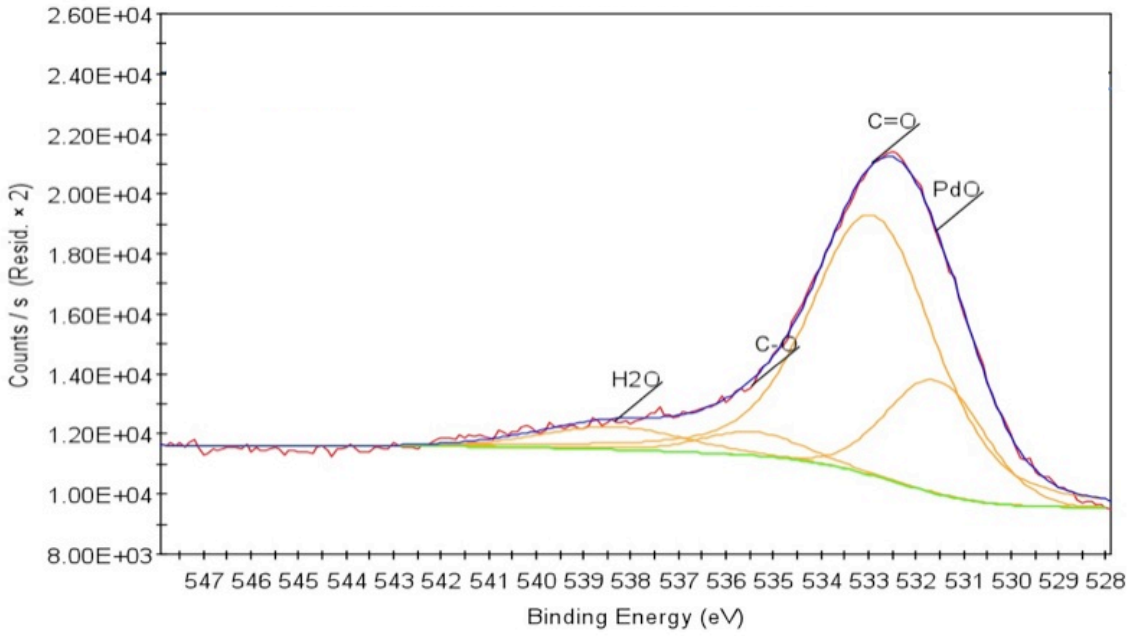

(b) After

Figure 5.25: XPS O1s Spectra for Sample MW: Before and After Catalysis

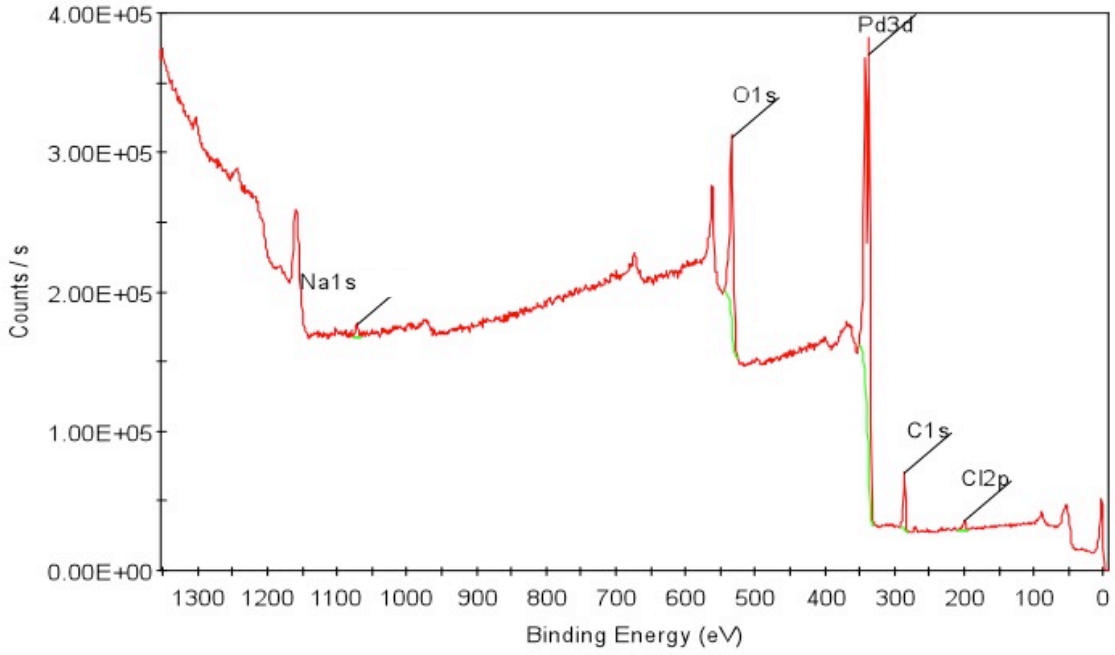

(a) Before

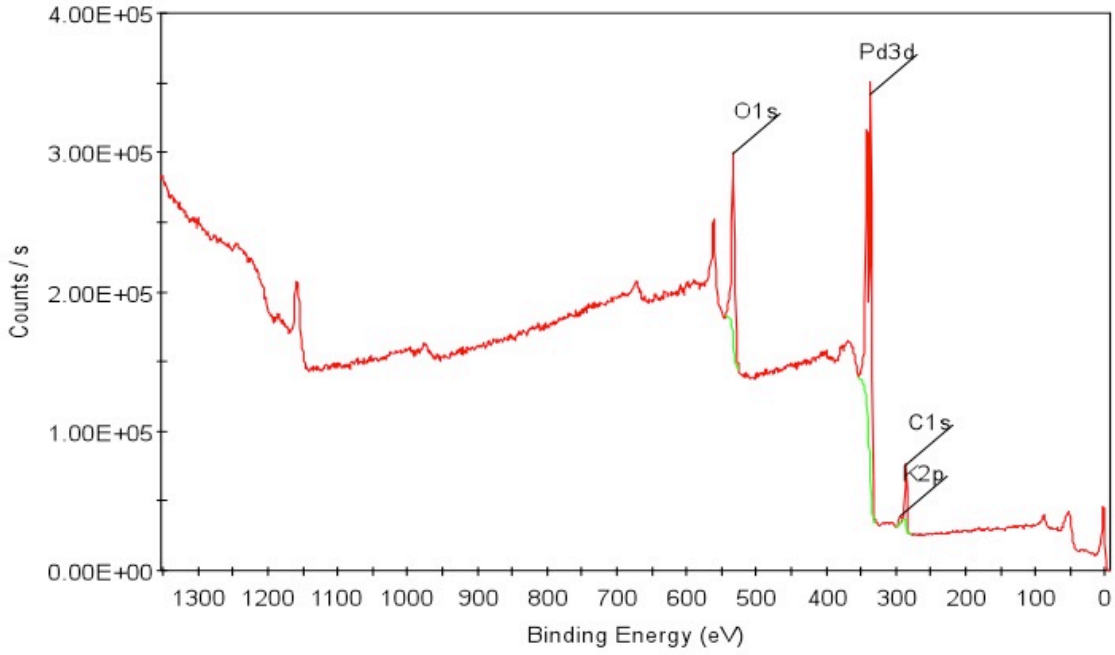

(b) After

Figure 5.26: XPS Survey Scan Spectra for Sample MW: Before and After Catalysis

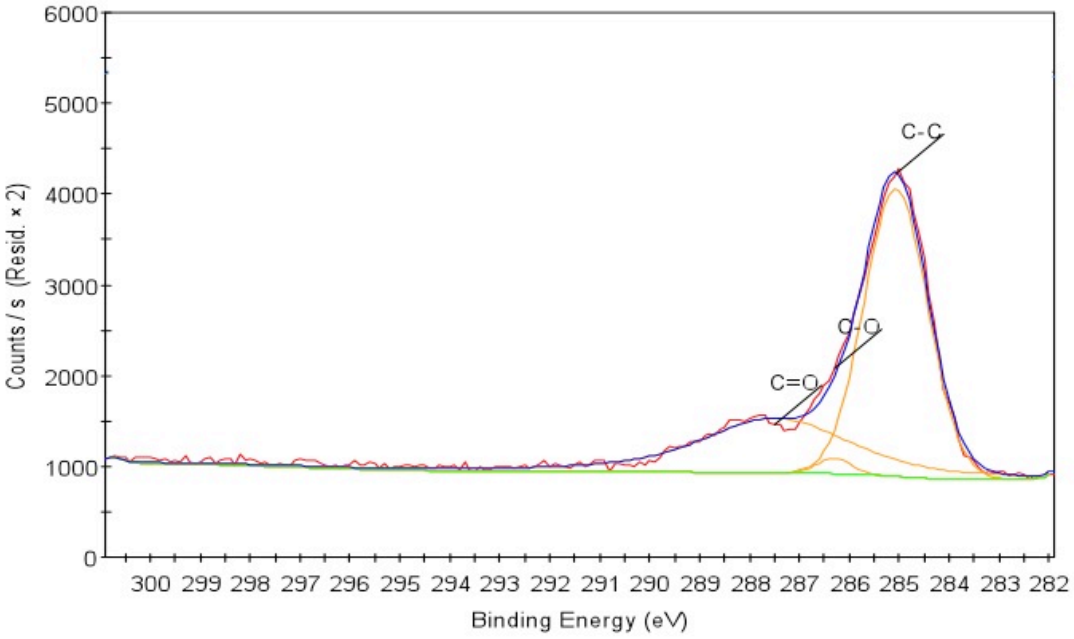

(a) Before

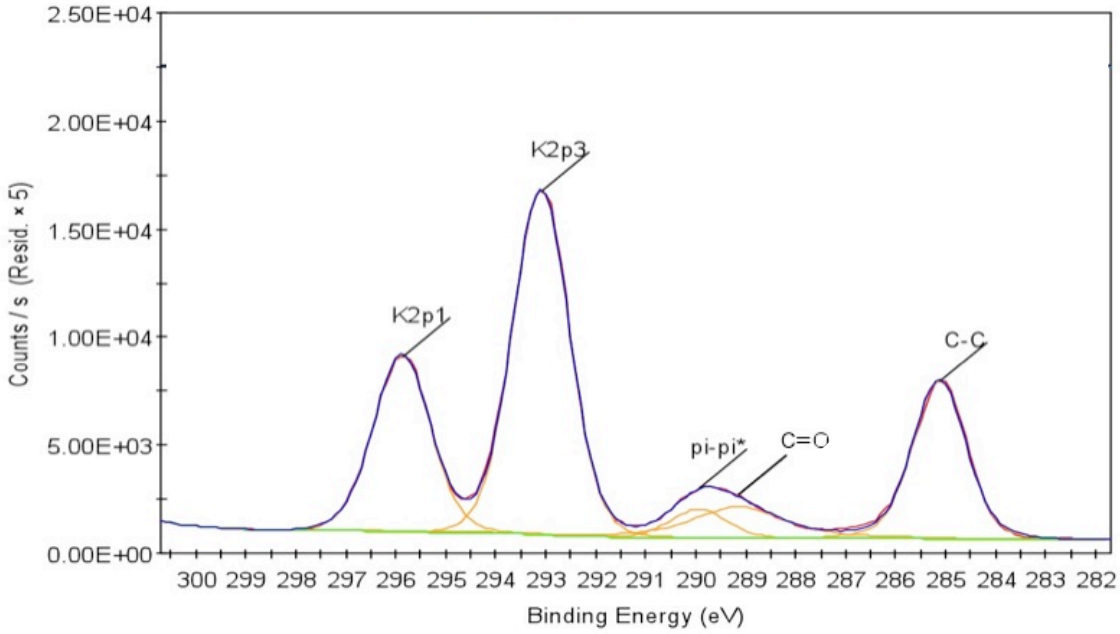

(b) After

Figure 5.27: XPS C1s Spectra for Sample PVP: Before and After Catalysis

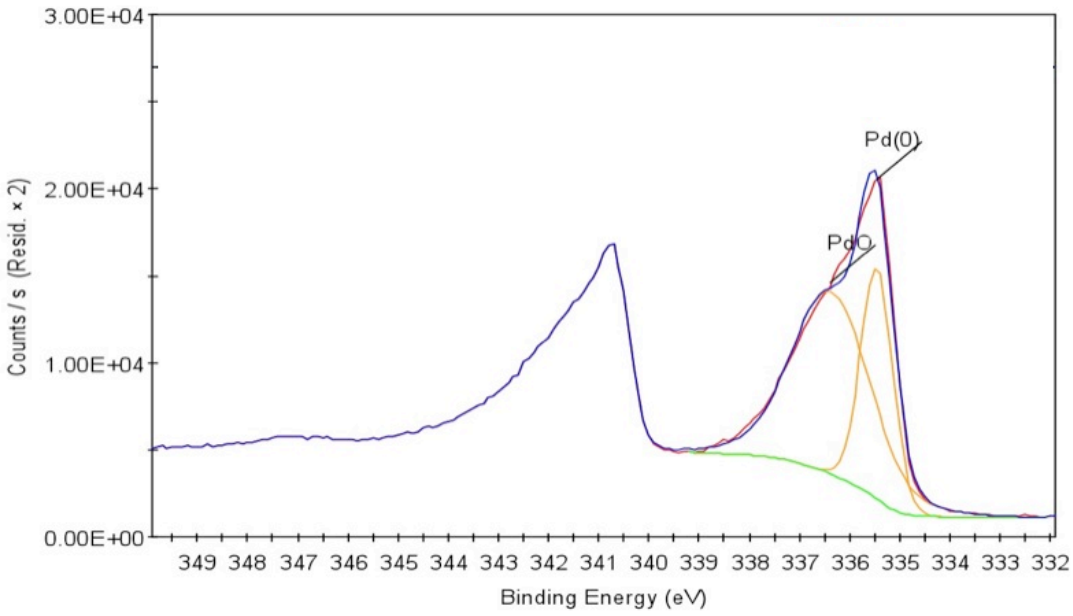

(a) Before

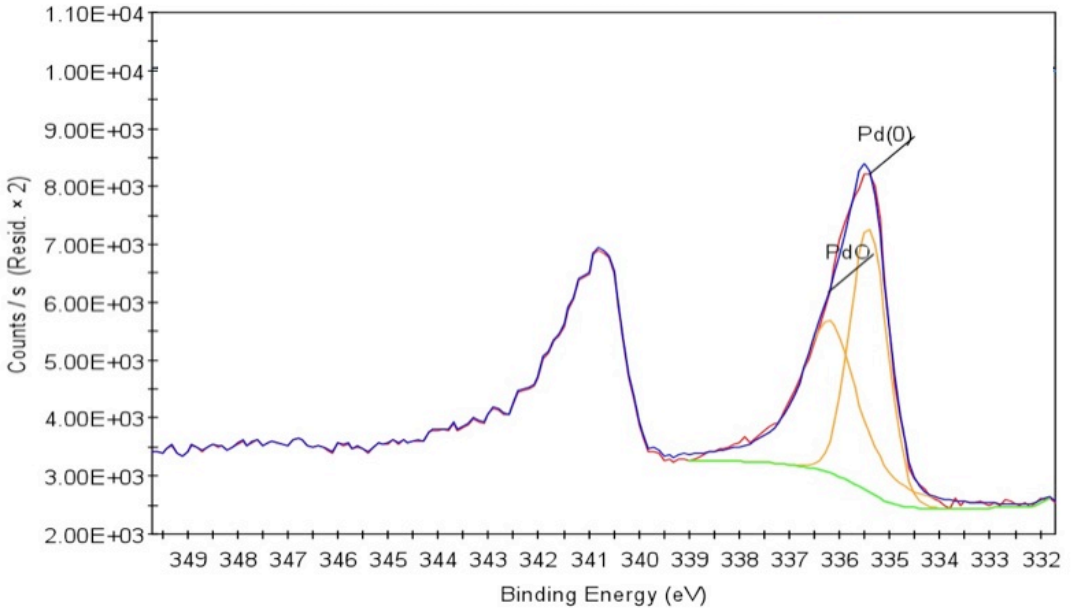

(b) After

Figure 5.28: XPS Pd3d Spectra for Sample PVP: Before and After Catalysis

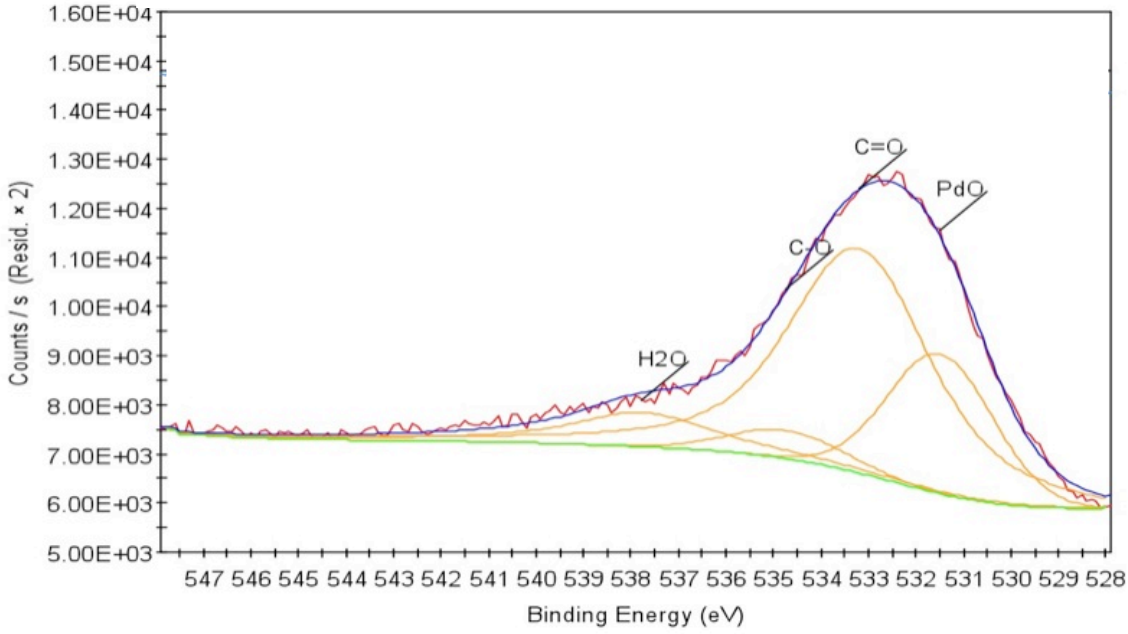

(a) Before

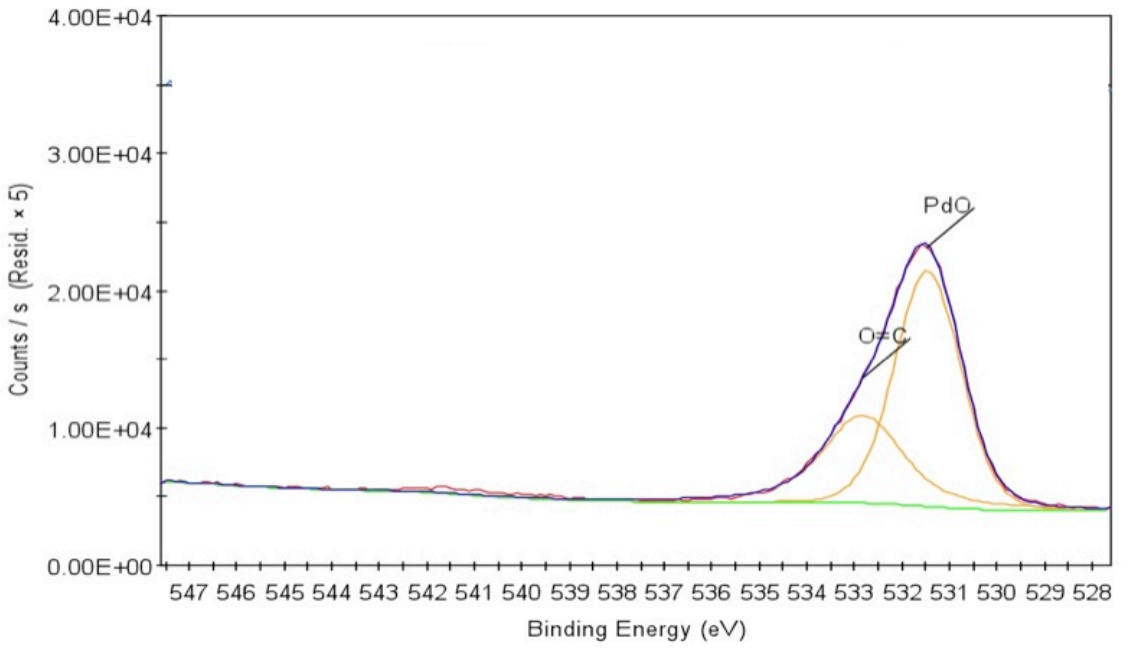

(b) After

Figure 5.29: XPS O1s Spectra for Sample PVP: Before and After Catalysis

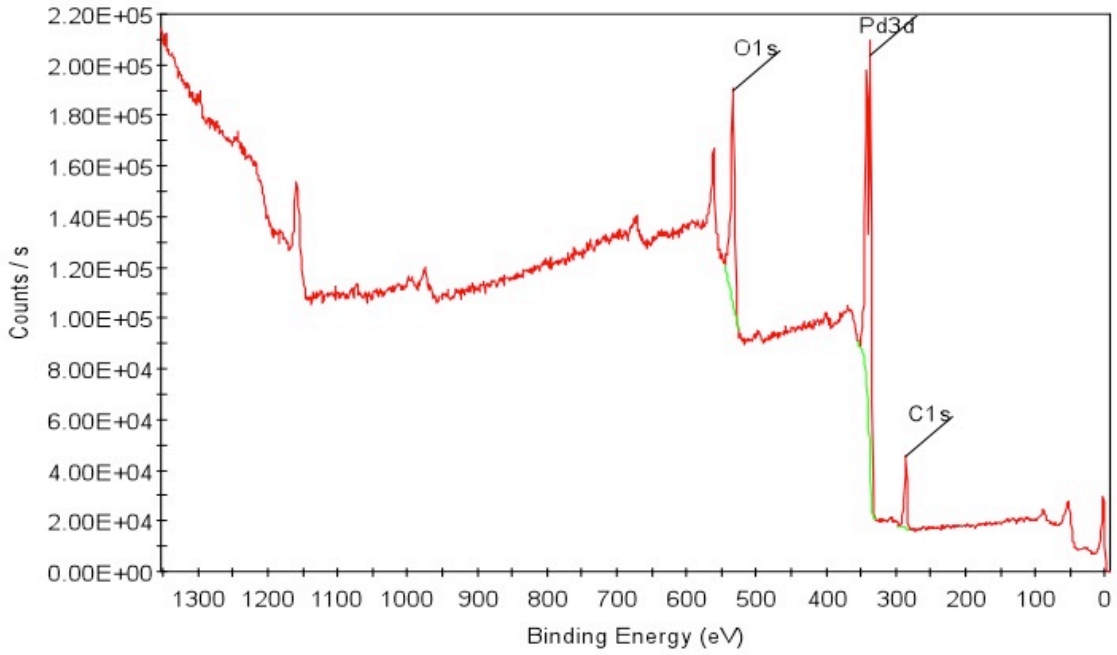

(a) Before

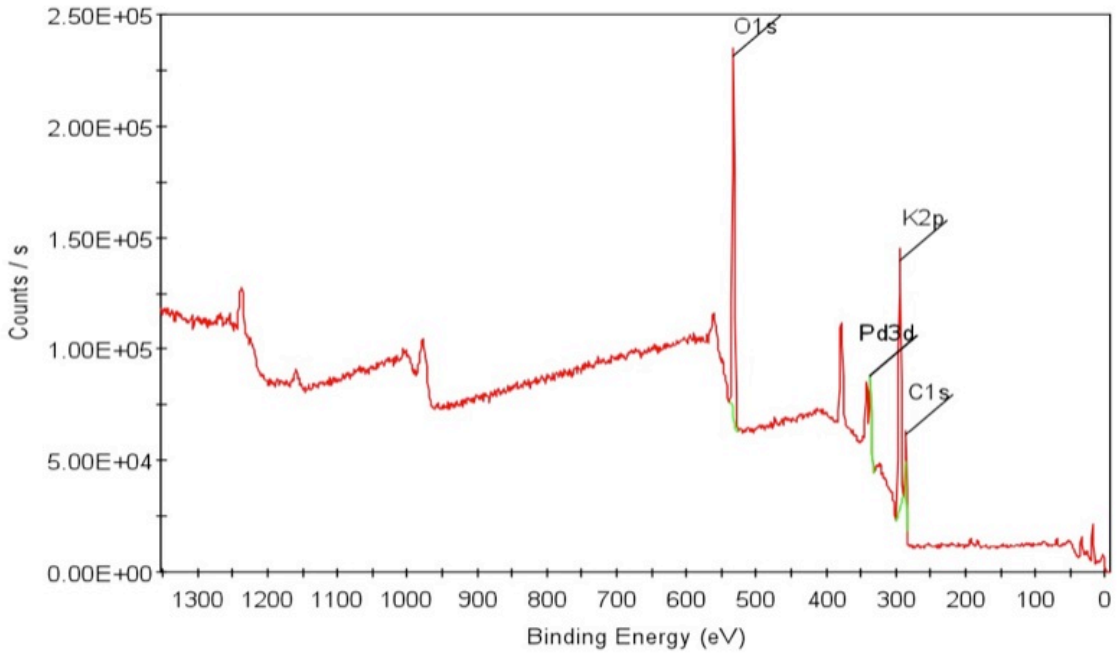

(b) After

Figure 5.30: XPS Survey Scan Spectra for Sample PVP: Before and After Catalysis

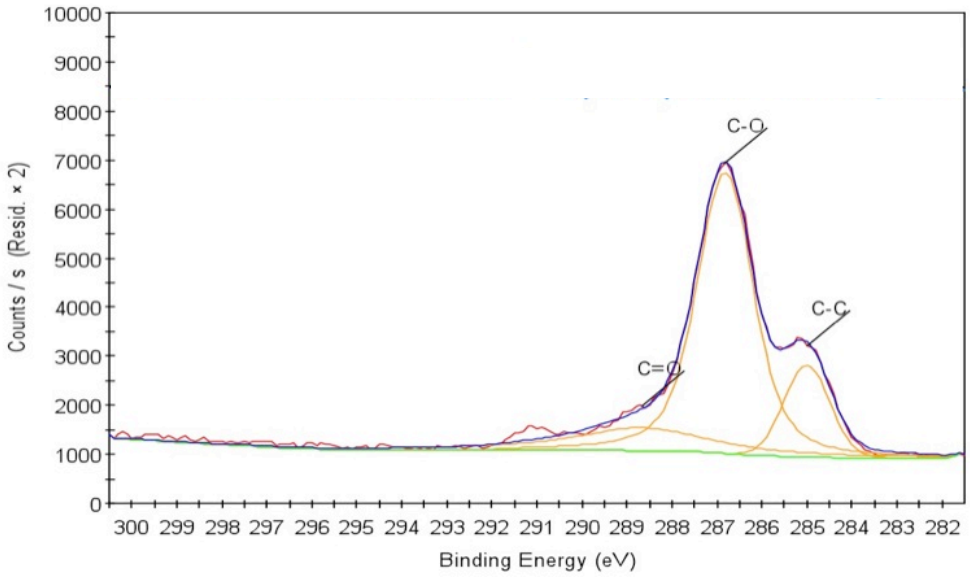

(a) Before

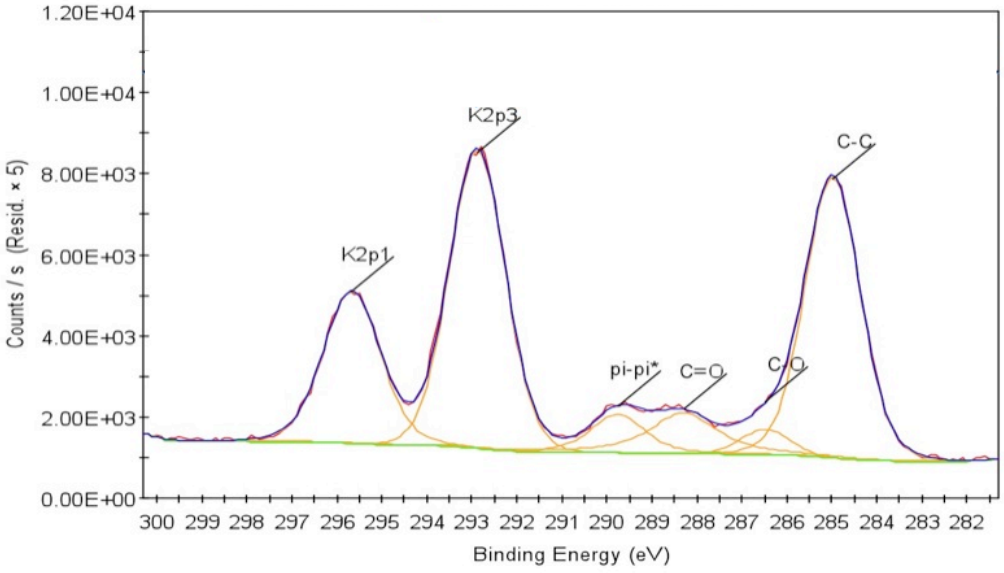

(b) After

Figure 5.31: XPS C1s Spectra for Sample PVA: Before and After Catalysis

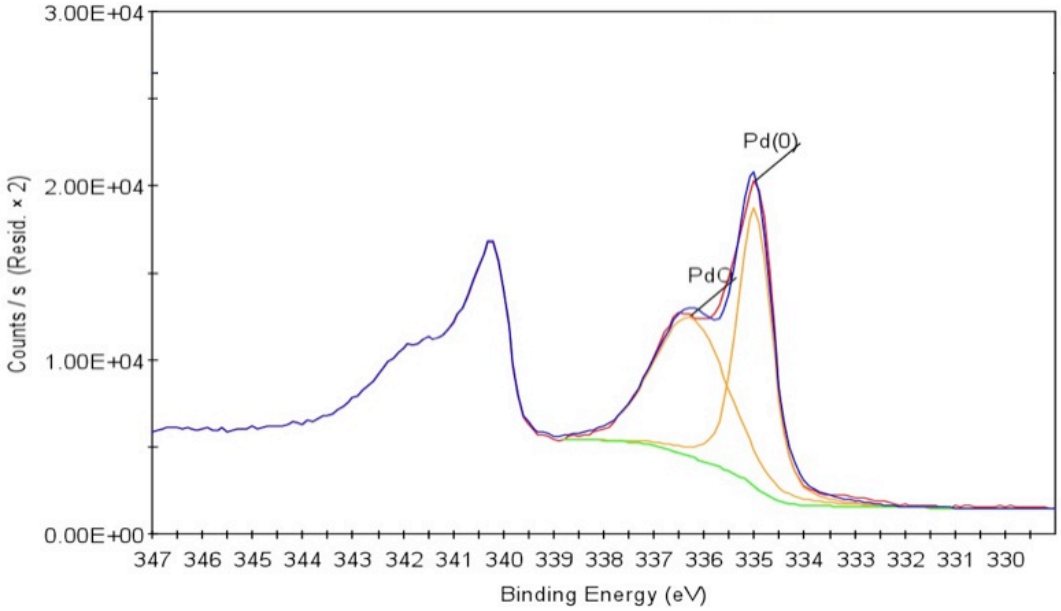

(a) Before

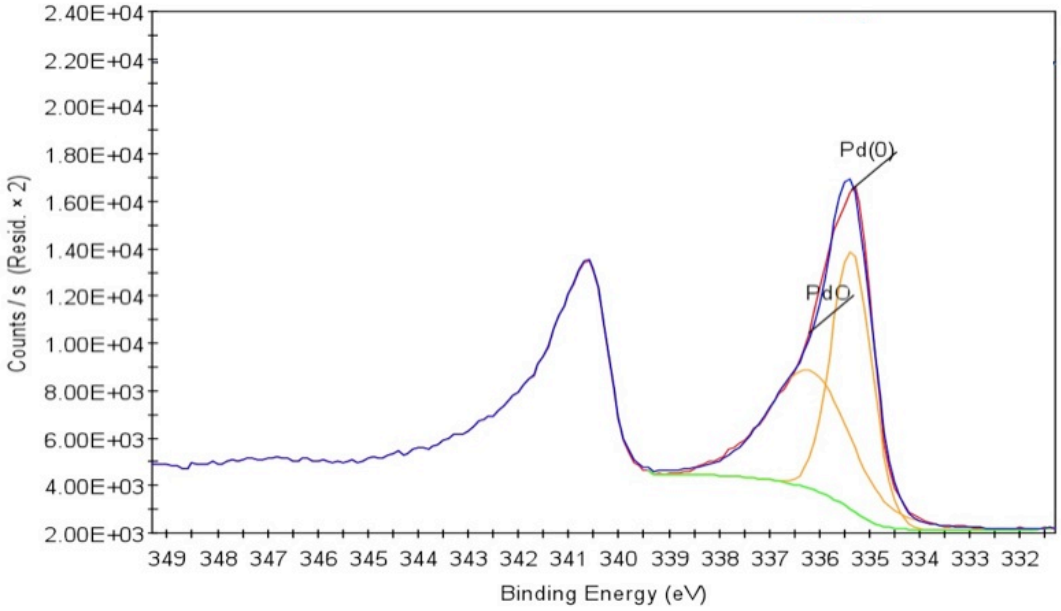

(b) After

Figure 5.32: XPS Pd3d Spectra for Sample PVA: Before and After Catalysis

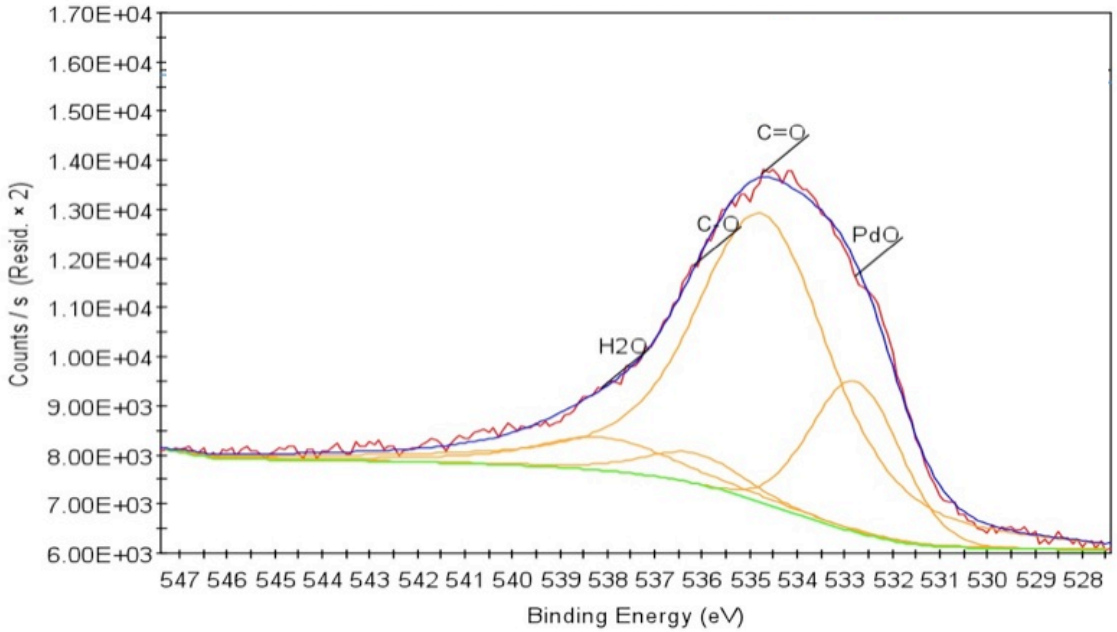

(a) Before

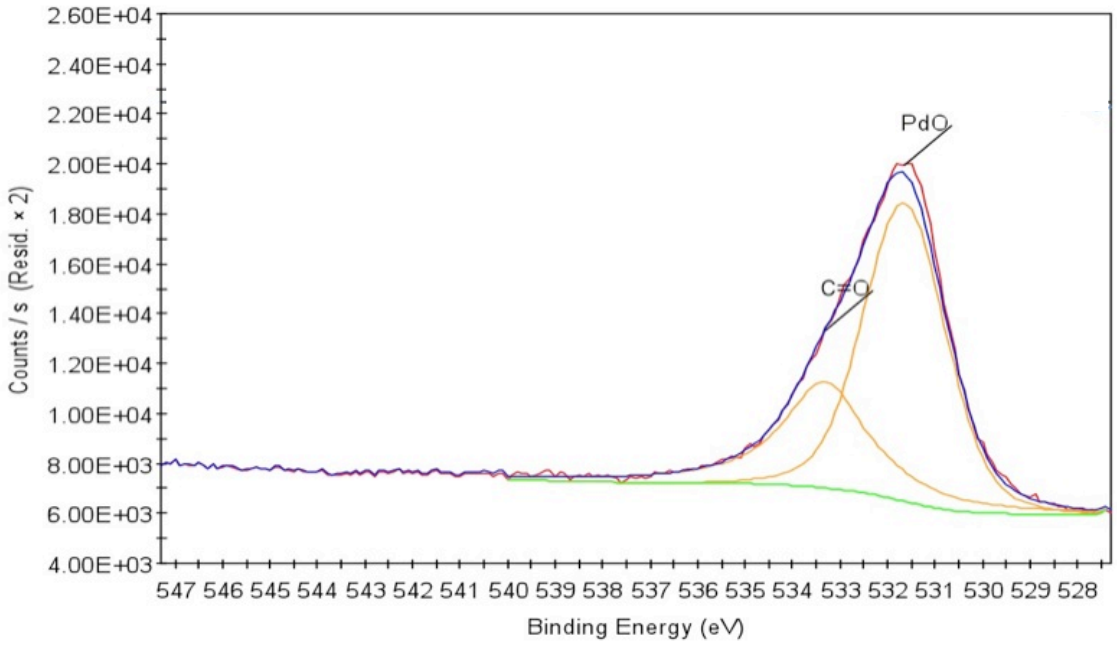

(b) After

Figure 5.33: XPS O1s Spectra for Sample PVA: Before and After Catalysis

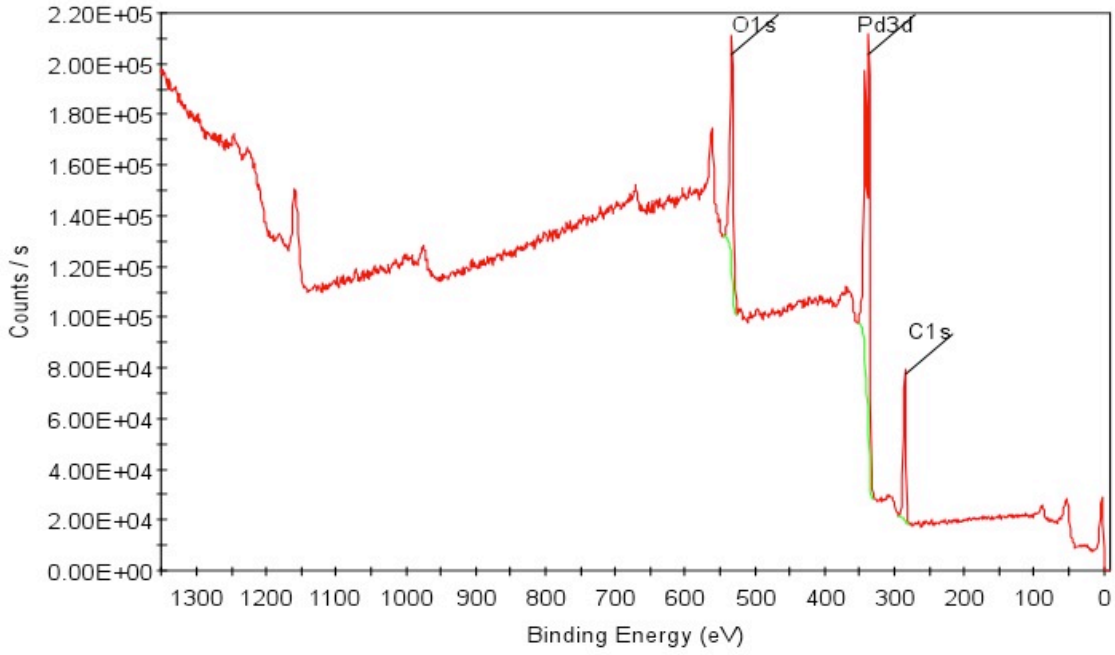

(a) Before

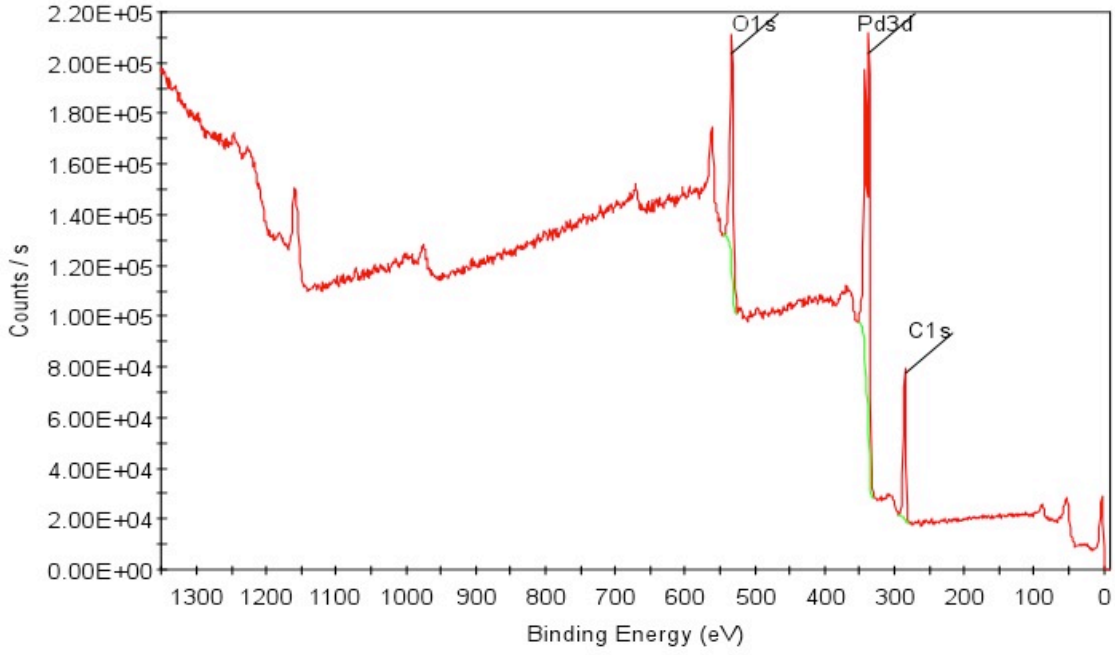

(b) After

Figure 5.34: XPS Survey Scan Spectra for Sample PVA: Before and After Catalysis

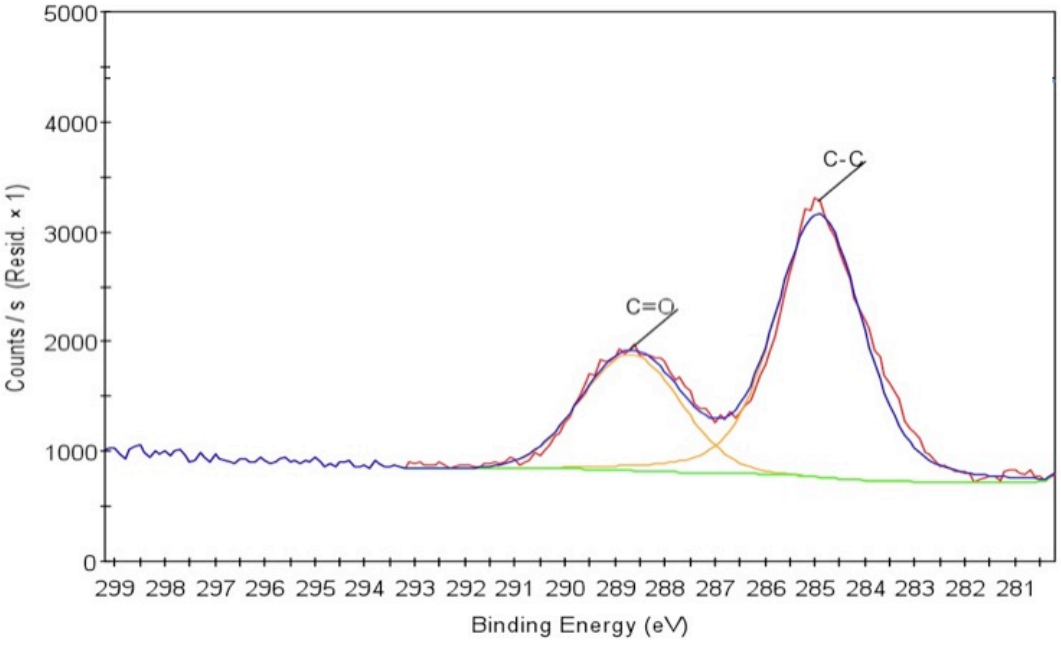

(a) Before

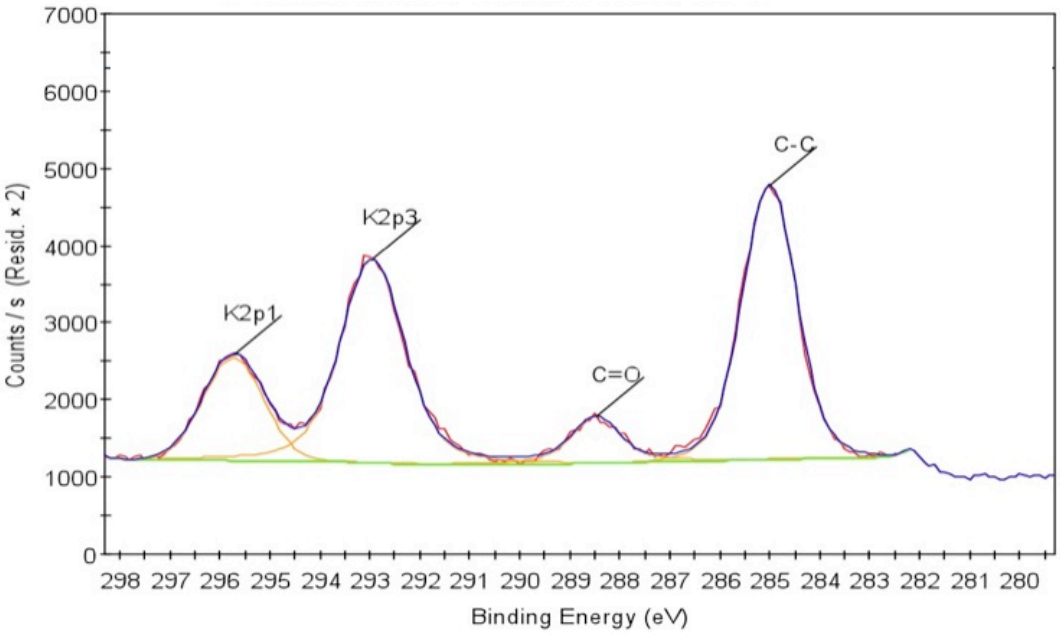

(b) After

Figure 5.35: XPS C1s Spectra for Sample Sorbitol: Before and After Catalysis

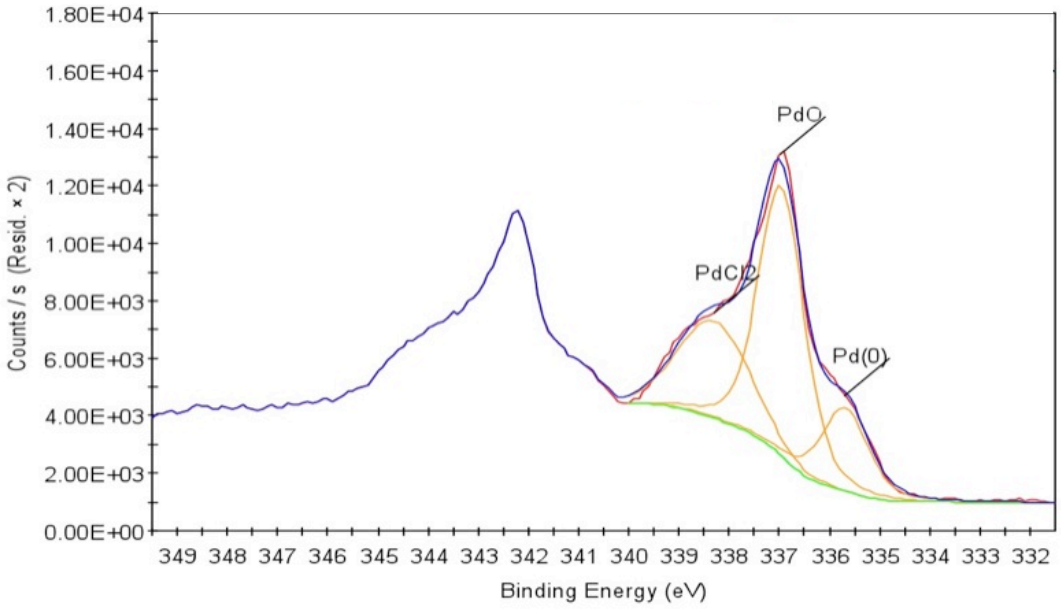

(a) Before

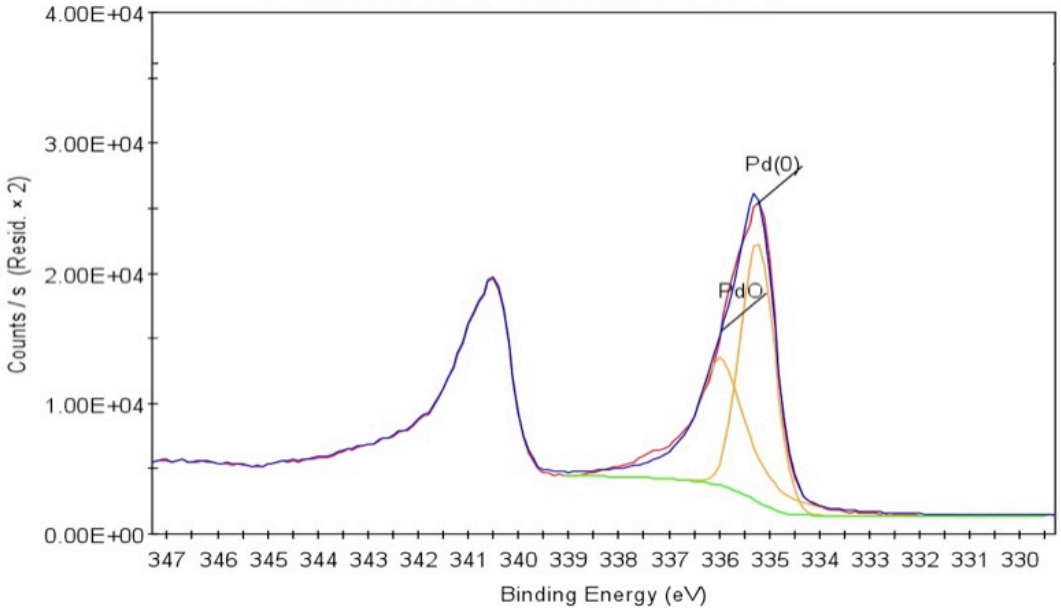

(b) After

Figure 5.36: XPS Pd3d Spectra for Sample Sorbitol: Before and After Catalysis

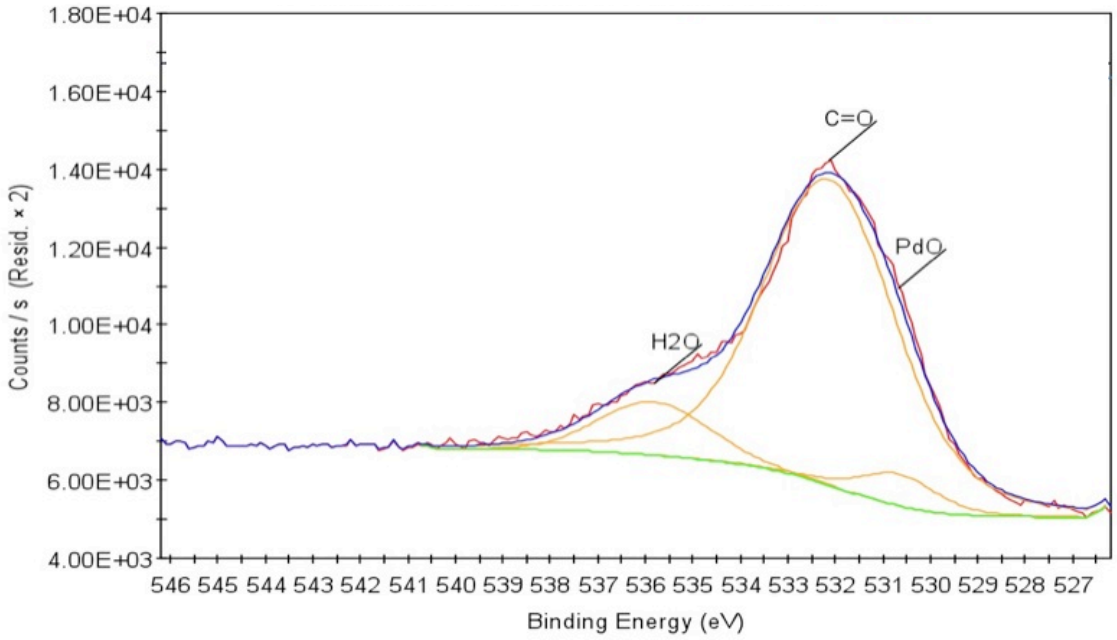

(a) Before

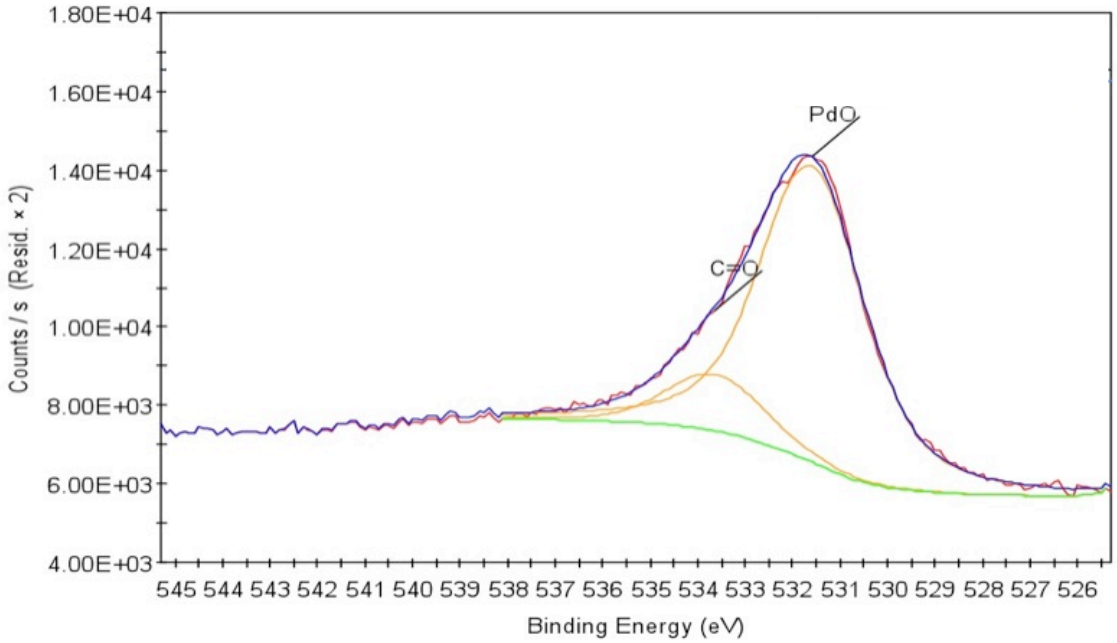

(b) After

Figure 5.37: XPS O1s Spectra for Sample Sorbitol: Before and After Catalysis

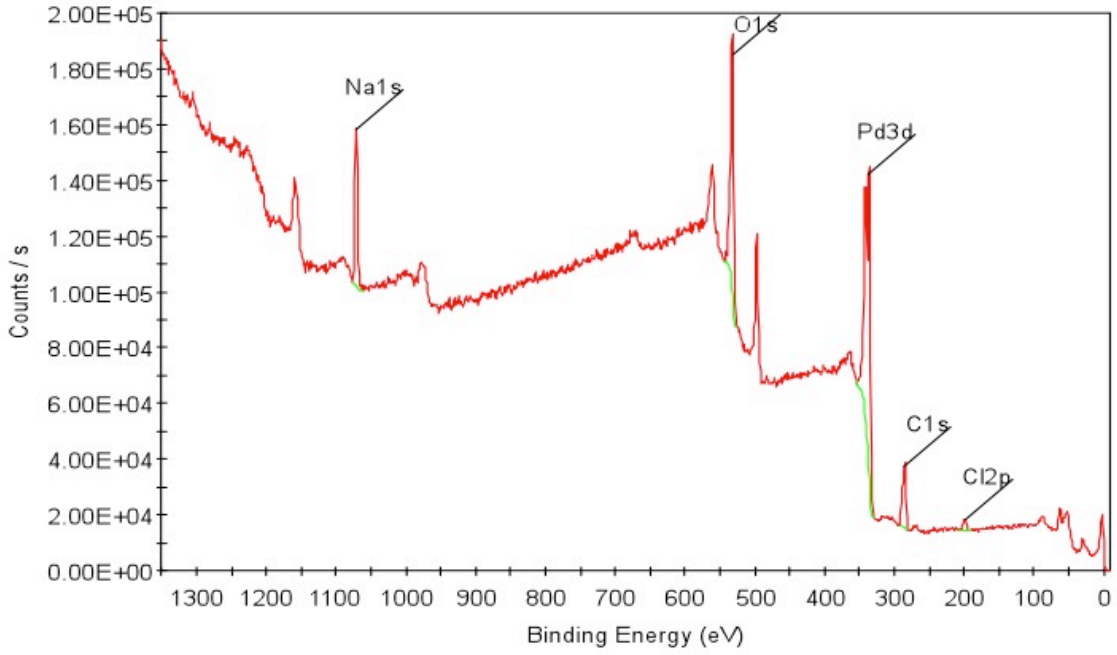

(a) Before

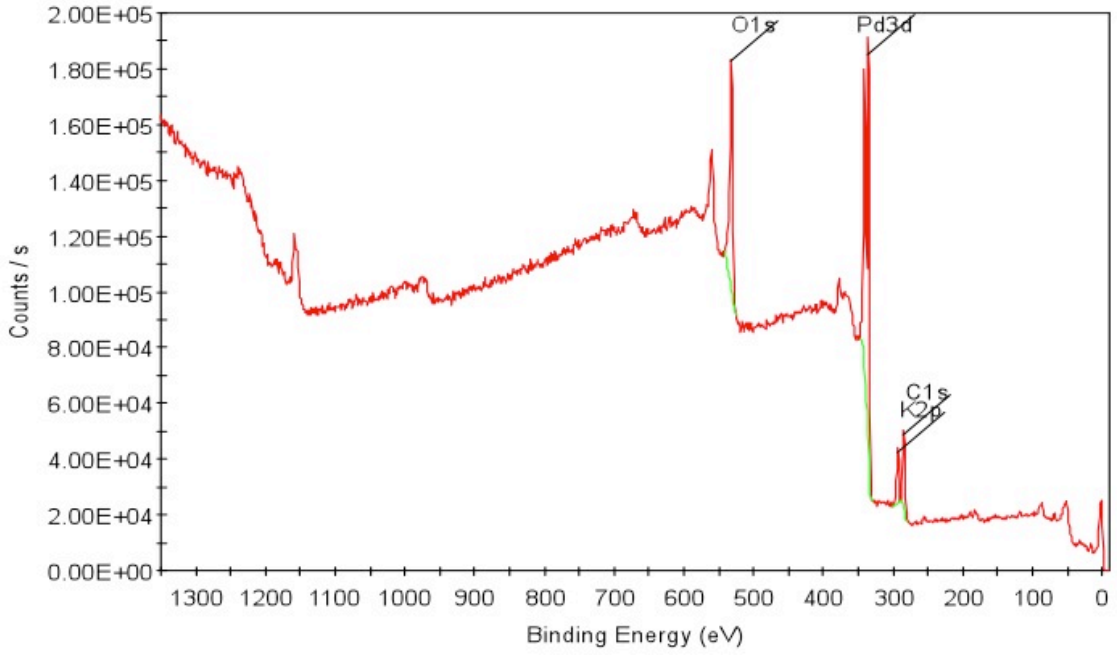

(b) After

Figure 5.38: XPS Survey Scan Spectra for Sample Sorbitol: Before and After Catalysis

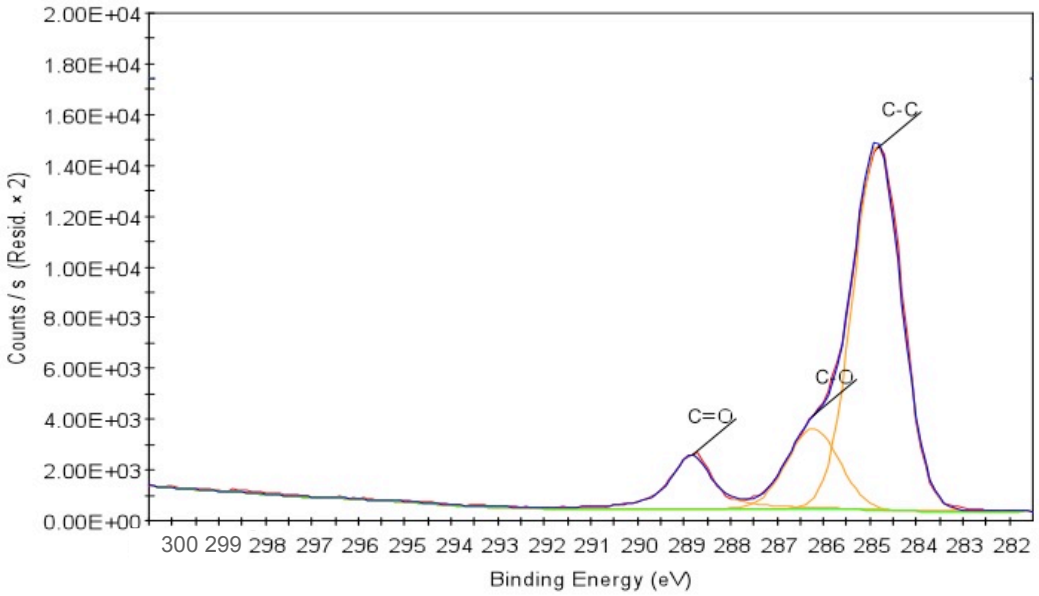

(a) Before

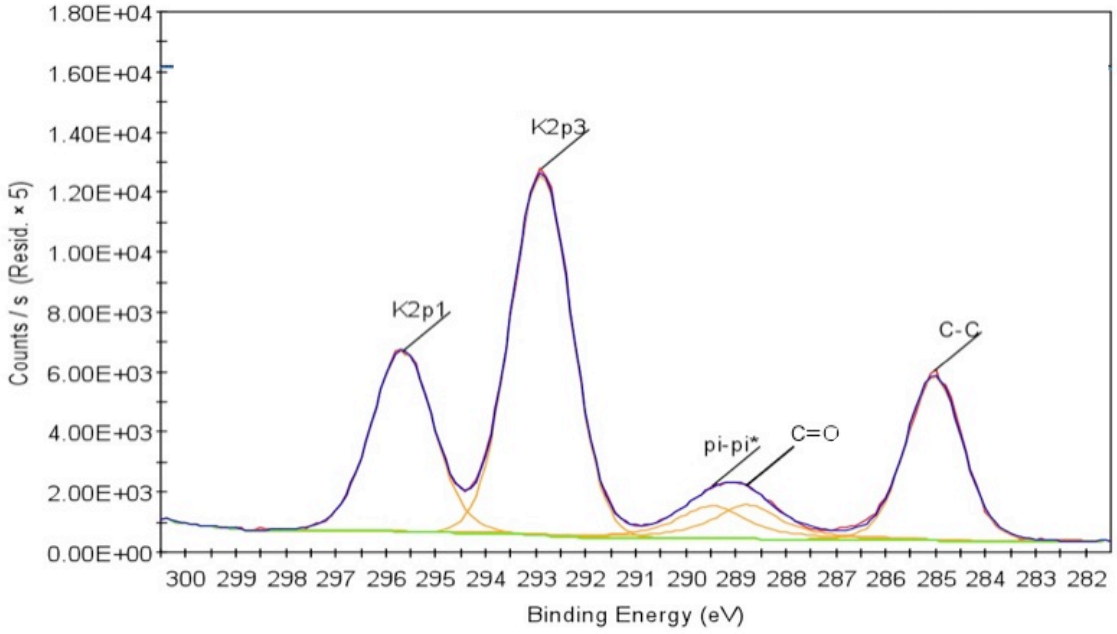

(b) After

Figure 5.39: XPS C1s Spectra for Sample Citrate: Before and After Catalysis

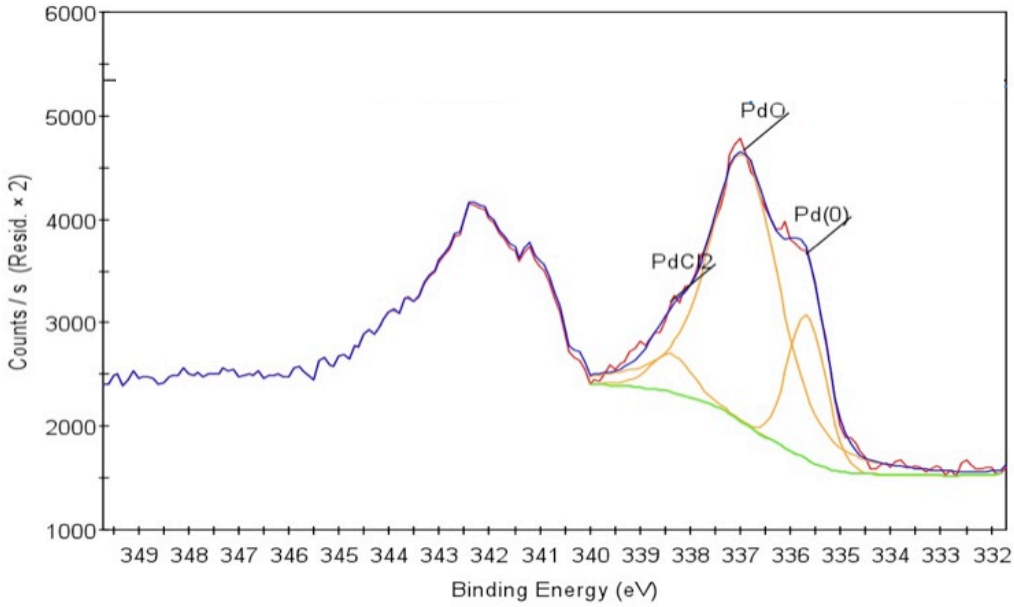

(a) Before

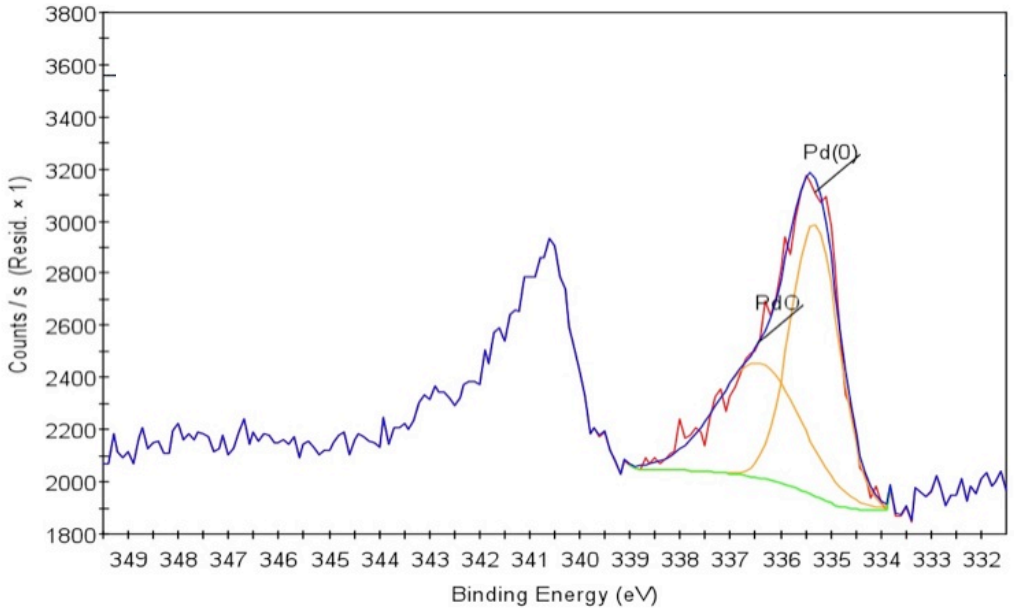

(b) After

Figure 5.40: XPS Pd3d Spectra for Sample Citrate: Before and After Catalysis

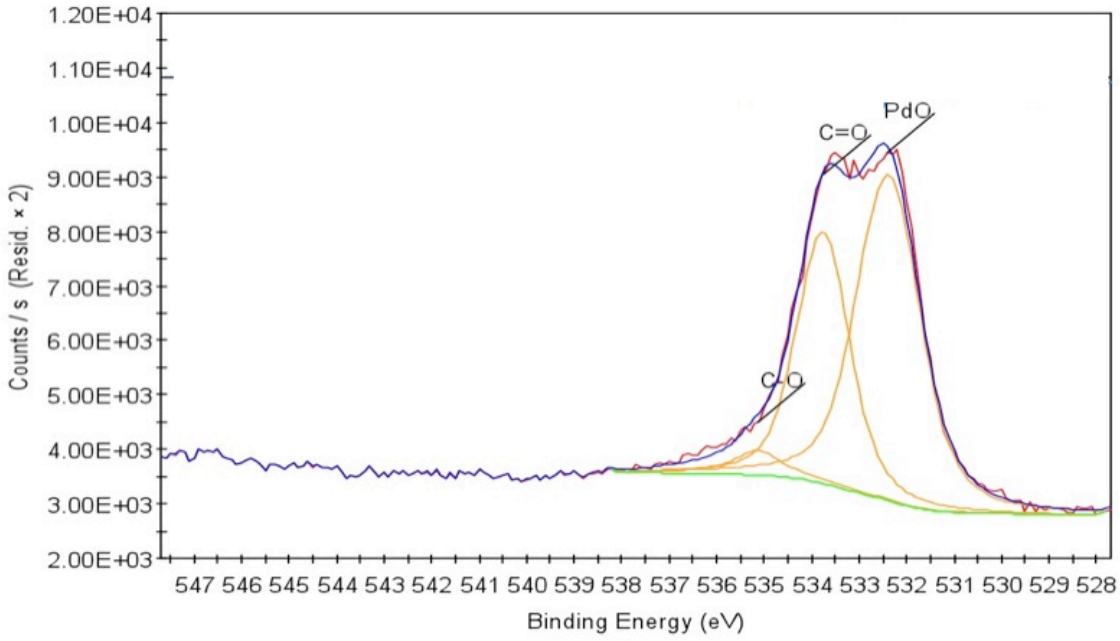

(a) Before

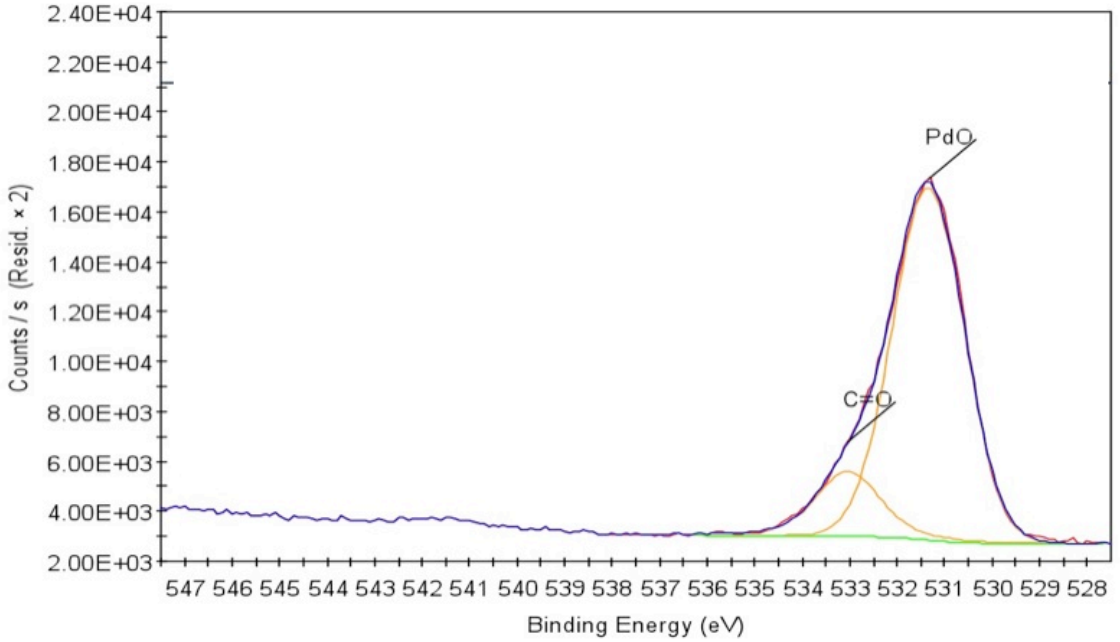

(b) After

Figure 5.41: XPS O1s Spectra for Sample Citrate: Before and After Catalysis

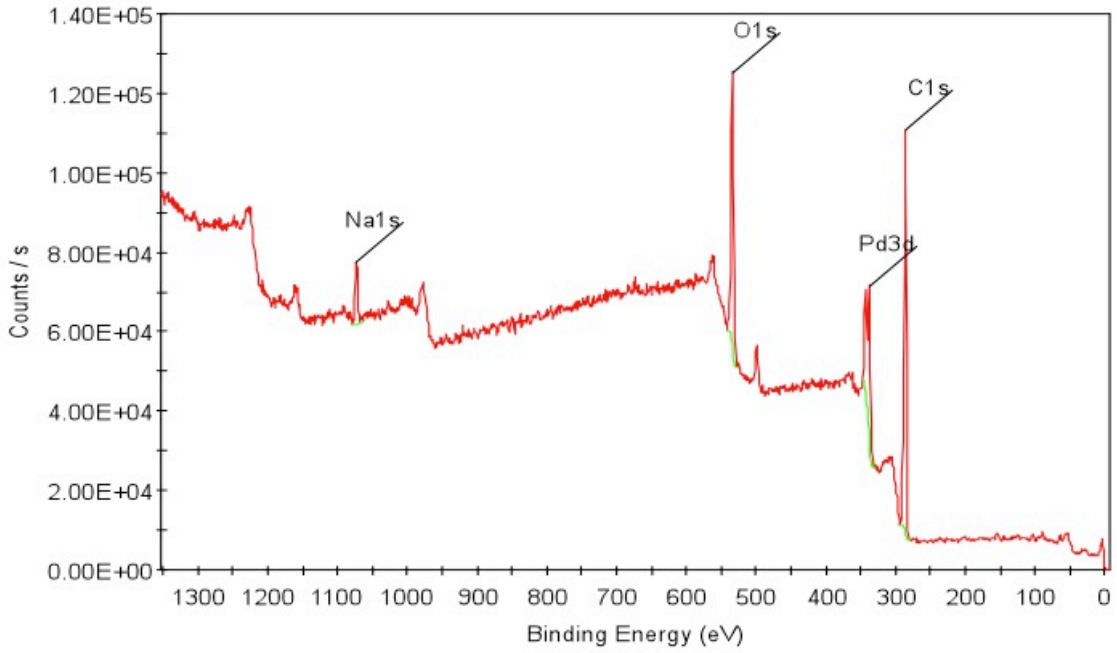

(a) Before

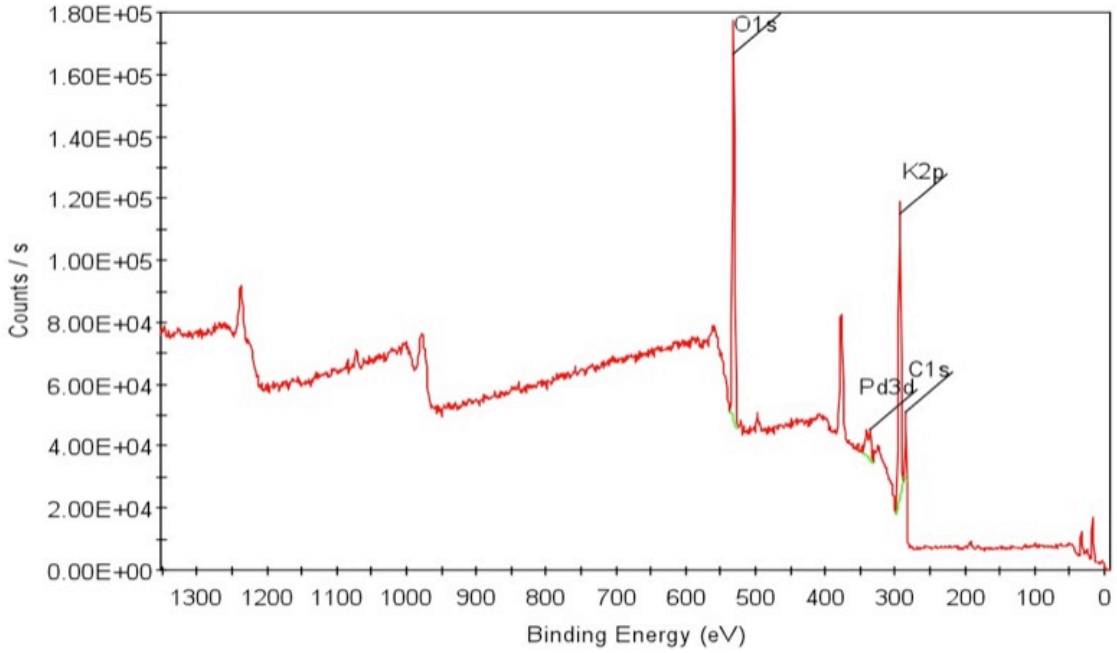

(b) After

Figure 5.42: XPS Survey Scan Spectra for Sample Citrate: Before and After Catalysis

5.4 Appendix D: EDS Data

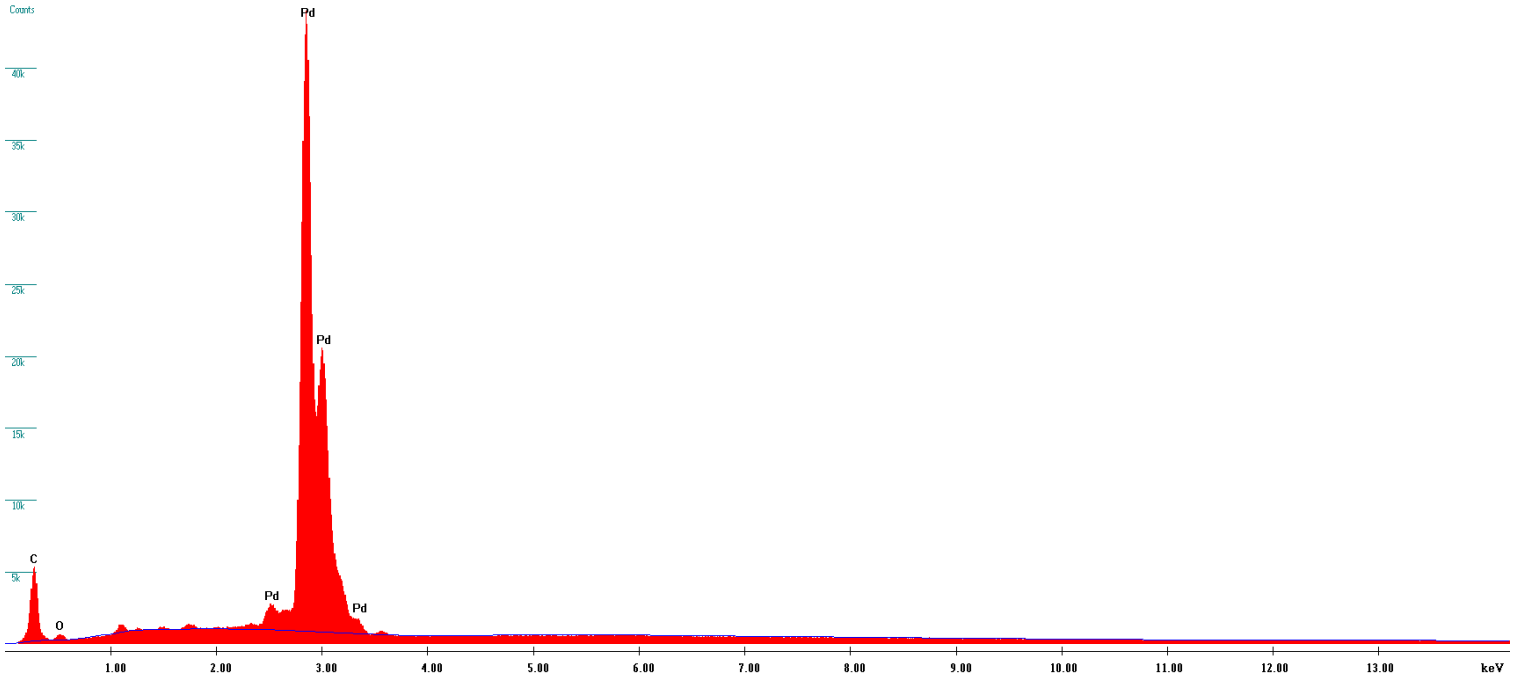

Figure 5.43: EDS Spectra for Sample Oleyl: Before Catalysis

Figure 5.44: EDS Spectra for Sample Oleyl: After Catalysis

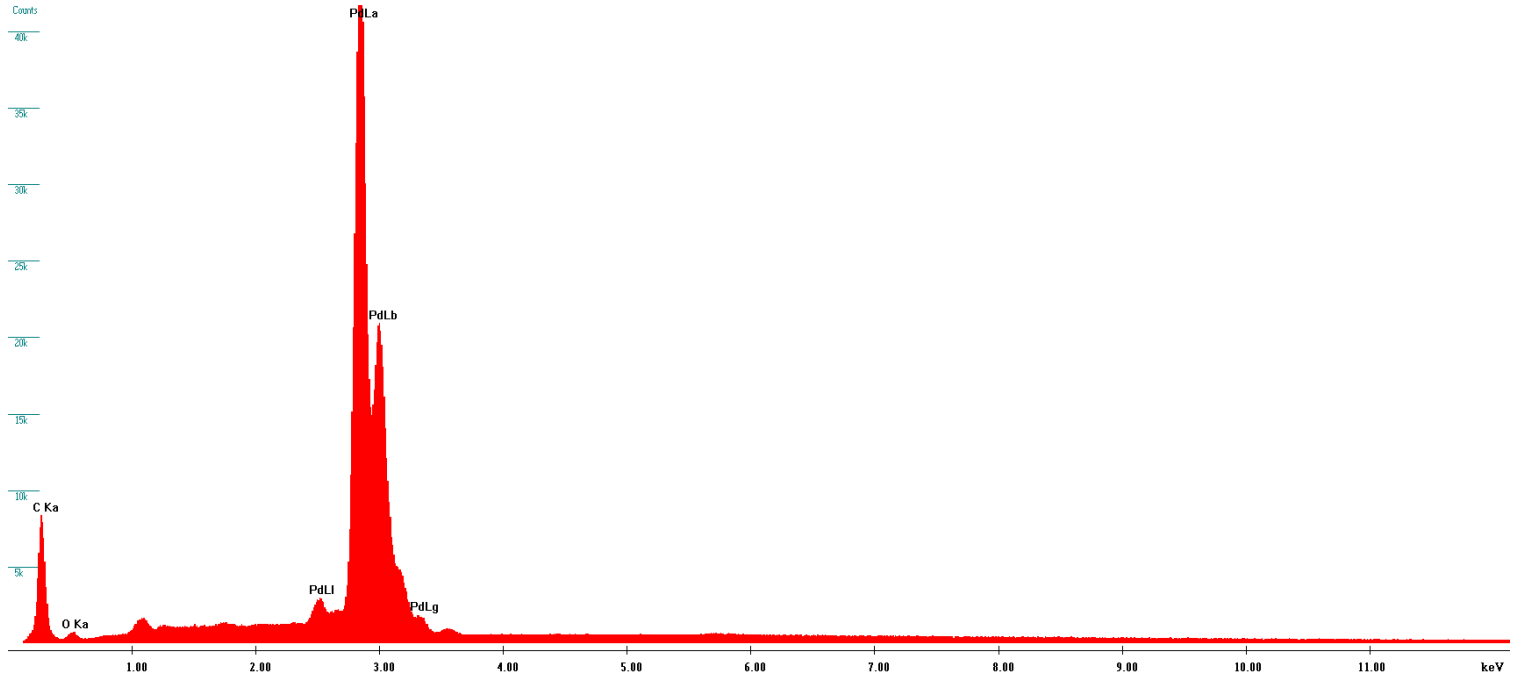

Figure 5.45: EDS Spectra for Sample HM: Before Catalysis

Figure 5.46: EDS Spectra for Sample HM: After Catalysis

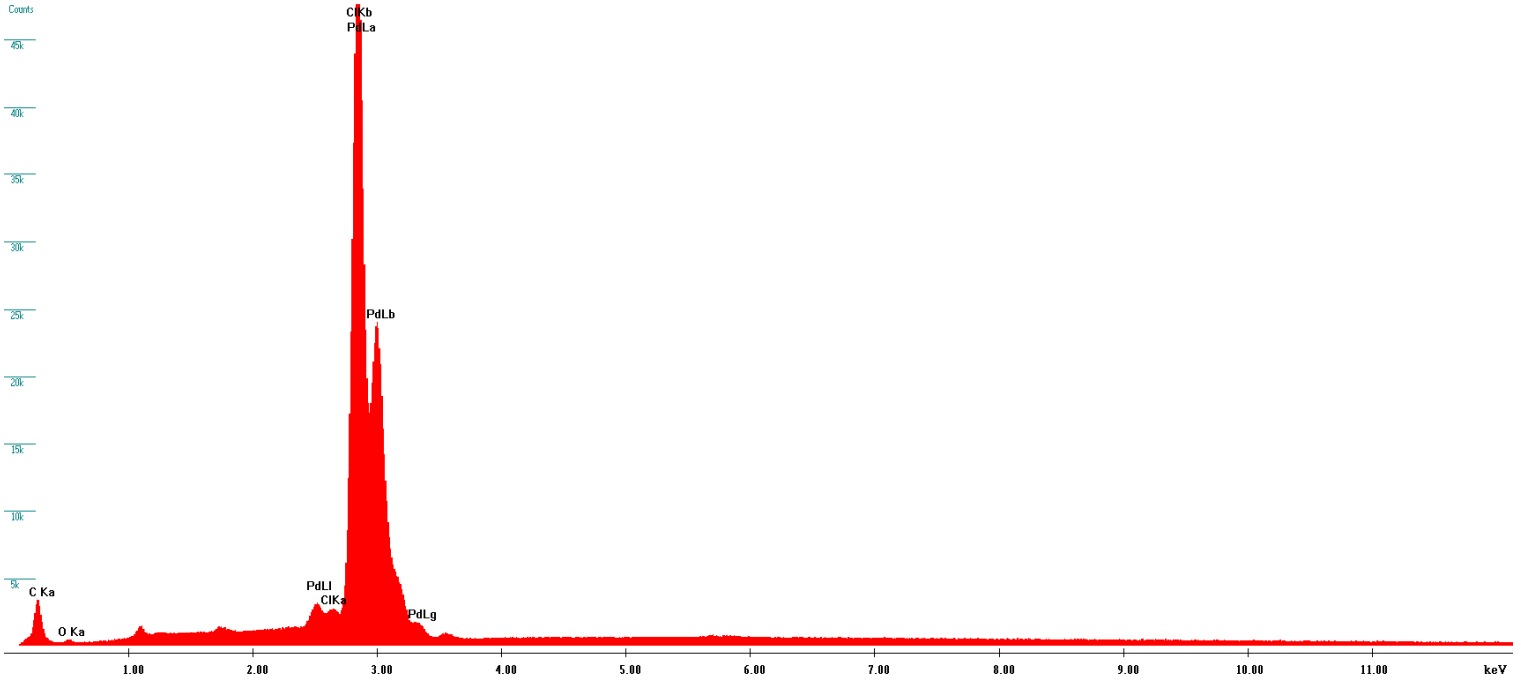

Figure 5.47: EDS Spectra for Sample MW: Before Catalysis

Figure 5.48: EDS Spectra for Sample MW: After Catalysis

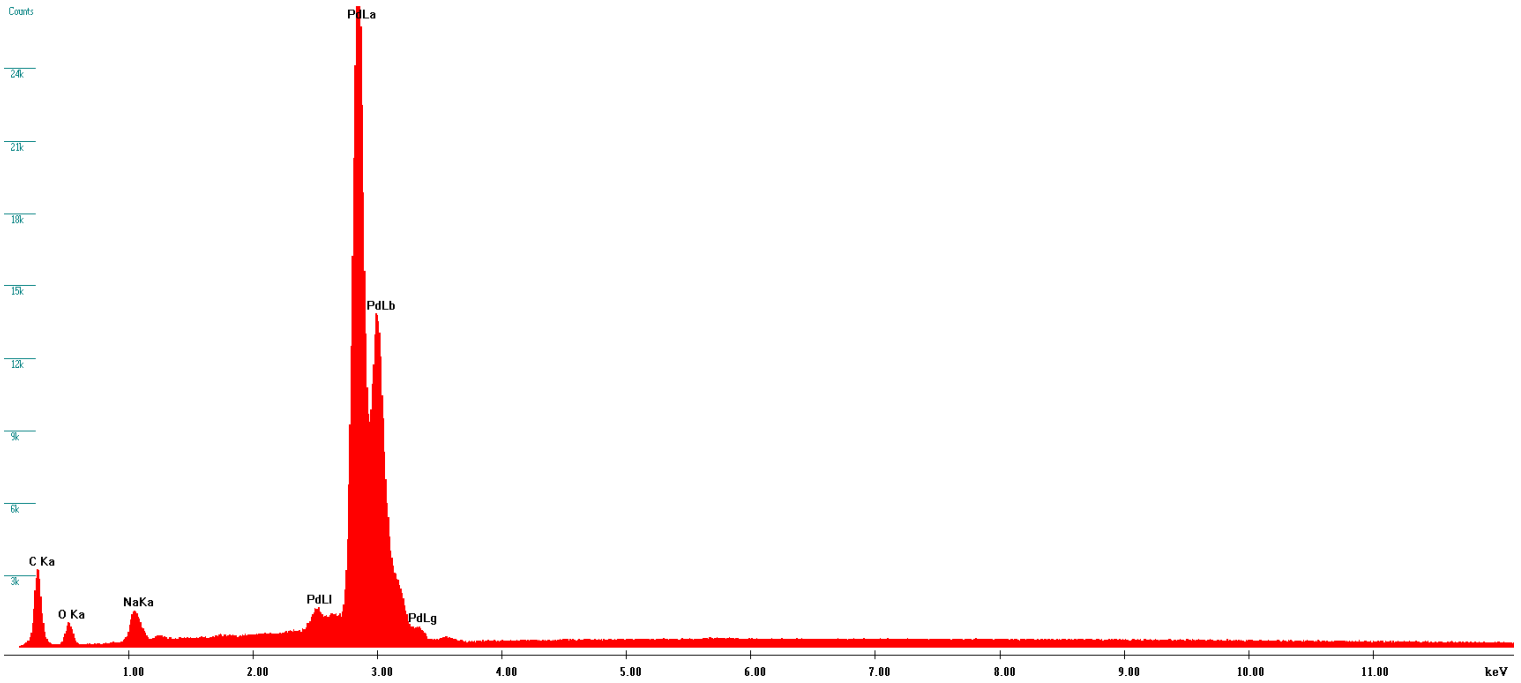

Figure 5.49: EDS Spectra for Sample PVP: Before Catalysis

Figure 5.50: EDS Spectra for Sample MW: After Catalysis

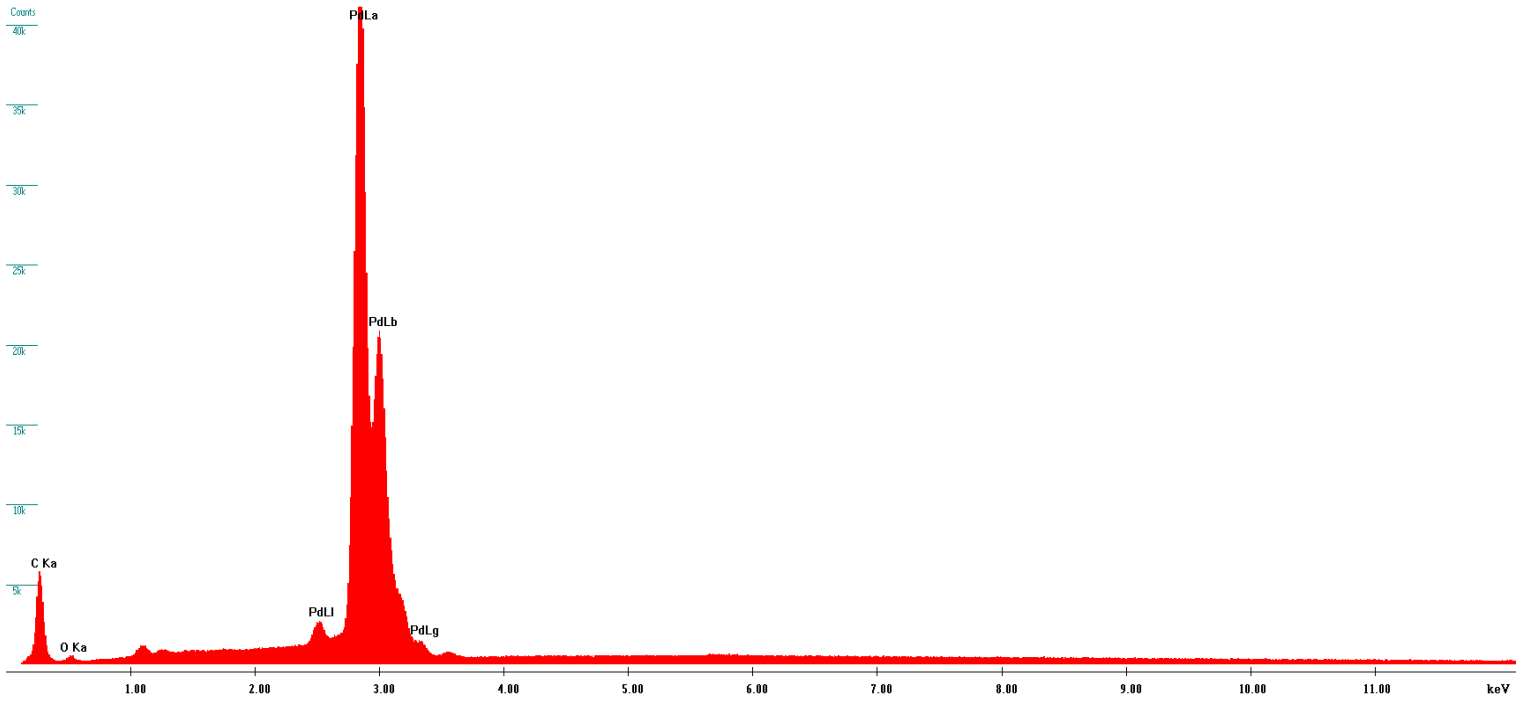

Figure 5.51: EDS Spectra for Sample PVA: Before Catalysis

Figure 5.52: EDS Spectra for Sample PVA: After Catalysis

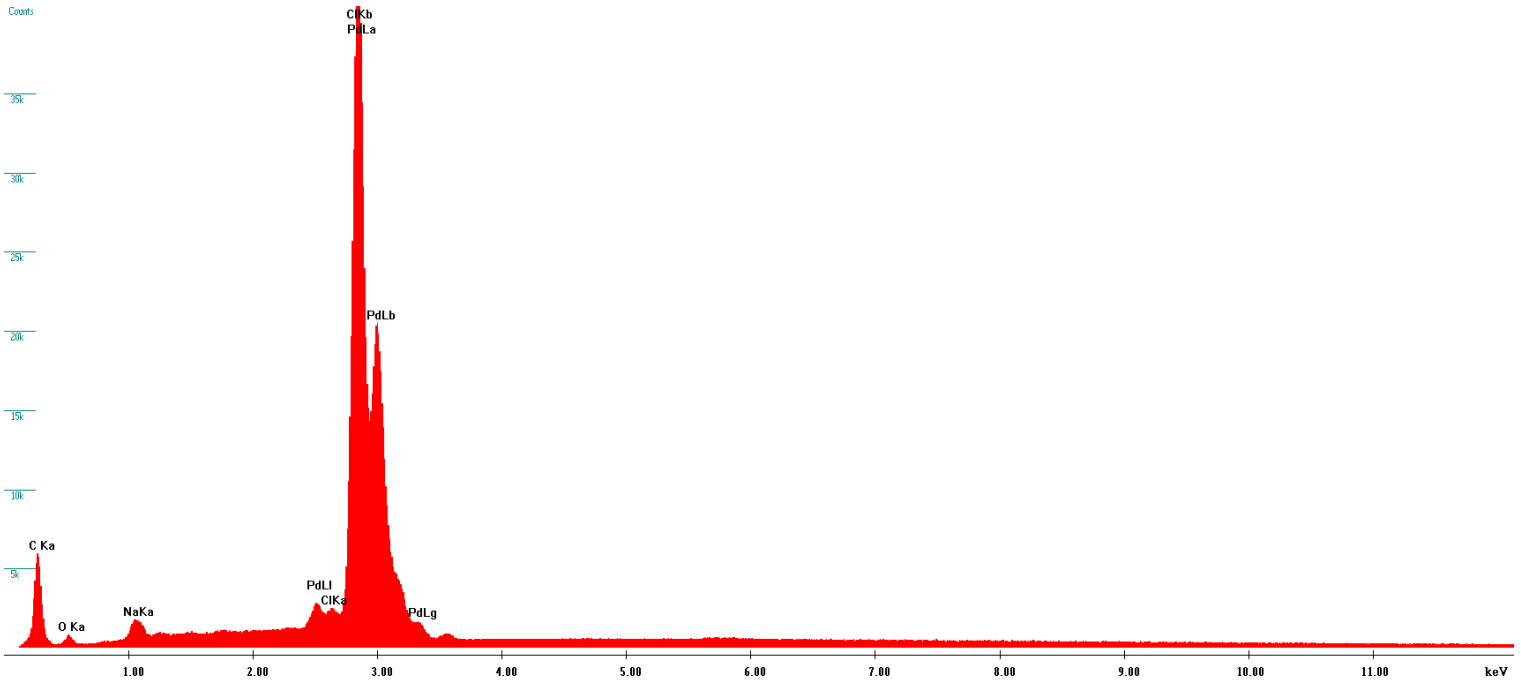

Figure 5.53: EDS Spectra for Sample Sorbitol: Before Catalysis

Figure 5.54: EDS Spectra for Sample Sorbitol: After Catalysis

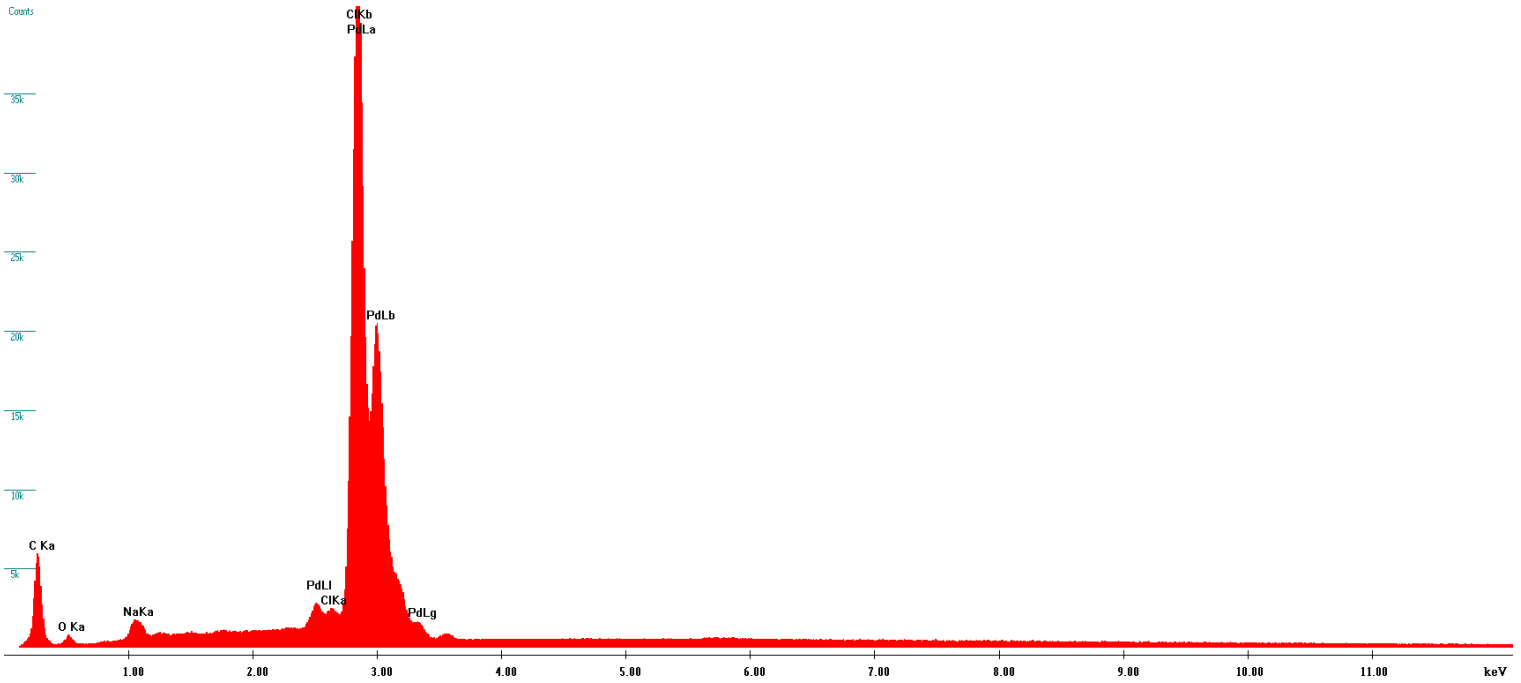

Figure 5.55: EDS Spectra for Sample Citrate: Before Catalysis

Figure 5.56: EDS Spectra for Sample Citrate: After Catalysis

Bibliography

[1] M. Lamblin, L. Nassar-Hardy, J. C. Hierso, E. Fouquet, and F. X. Felpin, Advanced Synthesis & Catalysis **352**, 33 (2010).

[2] B. M. Trost, Accounts of Chemical Research **35**, 695 (2002).

[3] J. M. Mayer and F. E. Michael, Inorganic Chemistry , 2 (2009).

[4] A. D. Curzons, D. J. C. Constable, D. N. Mortimer, and V. L. Cunningham, Green Chemistry **3**, 1 (2001).

[5] S. Sawoo, D. Srimani, P. Dutta, R. Lahiri, and A. Sarkar, Tetrahedron **65**, 4367 (2009).

[6] C. J. Li, Chemical Reviews **105**, 3095 (2005).

[7] S. Venkatraman, T. Huang, and C. J. Li, Advanced Synthesis & Catalysis **344**, 399 (2002).

[8] C.-J. Li, *Comprehensive Organic Reactions in Aqueous Media*, Second ed. (Wiley Interscience, 2007).

[9] H. Gulyas, A. Szollosy, B. E. Hanson, and J. Bakos, Tetrahedron Letters **43**, 2543 (2002).

[10] D. J. Brauer *et al.*, Journal of Organometallic Chemistry **645**, 14 (2002).

[11] J. tsuji, *Palladium Reagents and Catalysts- New Perspectives for the 21st Century*, First ed. (Wiley Interscience, 2004).

[12] Y. Tsuji and T. Fujihara, Inorganic Chemistry **46**, 1895 (2007).

[13] J. C. Hierso, M. Beauperin, and P. Meunierll, European Journal of Inorganic Chemistry , 3767 (2007).

[14] H. Hildebrand *et al.*, Environmental Pollution **158**, 65 (2010).

[15] R. Narayanan, C. Tabor, and M. A. El-Sayed, Topics in Catalysis **48**, 60 (2008).

[16] R. Narayanan and M. A. El-Sayed, Journal of the American Chemical Society **125**, 8340 (2003).

[17] D. Astruc, Inorganic Chemistry **46**, 1884 (2007).

[18] R. Klie, K. Sun, M. Disko, J. Liu, and N. Browning, *Dekker Encyclopedia of Nanoscience and Nanotechnology Volume 1* (Marcel Dekker, Inc. NY, 2004), pp. 179–191.

[19] J. A. Widegren and R. G. Finke, Journal of Molecular Catalysis a-Chemical **198**, 317 (2003).

[20] L. Z. Feng, Z. Y. Gan, X. P. Nie, P. P. Sun, and J. C. Bao, Catalysis Communications **11**, 555 (2010).

[21] G. Shore, S. Morin, D. Mallik, and M. G. Organ, Chemistry-a European Journal **14**, 1351 (2008).

[22] B. M. Choudary, S. Madhi, N. S. Chowdari, M. L. Kantam, and B. Sreedhar, Journal of the American Chemical Society **124**, 14127 (2002).

[23] N. T. S. Phan, M. V. D. Sluys, and C. W. Jones, Advanced Synthesis & Catalysis **348**, 609 (2006).

[24] J. S. Carey, D. Laffan, C. Thomson, and M. T. Williams, Organic & Biomolecular Chemistry **4**, 2337 (2006).

[25] T. N. Glasnov, S. Findenig, and C. O. Kappe, Chemistry-A European Journal **15**, 1001 (2009).

[26] V. F. Slagt, A. H. M. de Vries, J. G. de Vries, and R. M. Kellogg, Organic Process Research & Development **14**, 30 (2010).

[27] A. Spencer, Journal of Organometallic Chemistry **270**, 115 (1984).

[28] A. F. Littke and G. C. Fu, Angewandte Chemie-International Edition **41**, 4176 (2002).

[29] T. E. Barder, S. D. Walker, J. R. Martinelli, and S. L. Buchwald, Journal of the American Chemical Society **127**, 4685 (2005).

[30] A. Suzuki, Journal of Organometallic Chemistry **576**, 147 (1999).

[31] J. Hassan, M. Sevignon, C. Gozzi, E. Schulz, and M. Lemaire, Chemical Reviews **102**, 1359 (2002).

[32] B. K. Singh, N. Kaval, S. Tomar, E. V. der Eycken, and V. S. Parmar, Organic Process Research & Development **12**, 468 (2008).

[33] I. R. Baxendale, C. M. Griffiths-Jones, S. V. Ley, and G. K. Tranmer, Chemistry-a European Journal **12**, 4407 (2006).

[34] N. Miyaura and A. Suzuki, Chemical Reviews **95**, 2457 (1995).

[35] L. Djakovitch, M. Wagner, C. G. Hartung, A. Beller, and K. Koehler, Journal of Molecular Catalysis a-Chemical **219**, 121 (2004).

[36] A. R. Mirza *et al.*, Organic Process Research & Development **2**, 325 (1998).

[37] E. G. Kuntz, Chemtech **17**, 570 (1987).

[38] L. Huang, P. K. Wong, J. Tan, T. P. Ang, and Z. Wang, Journal of Physical Chemistry C **113**, 10120 (2009).

[39] K. Kohler, R. G. Heidenreich, S. S. Soomro, and S. S. Prockl, Advanced Synthesis & Catalysis **350**, 2930 (2008).

[40] R. K. Arvela *et al.*, Journal of Organic Chemistry **70**, 161 (2005).

[41] B. H. Lipshutz, S. Tasler, W. Chrisman, B. Spliethoff, and B. Tesche, Journal of Organic Chemistry **68**, 1177 (2003).

[42] A. Pal, S. Shah, D. Chakraborty, and S. Devi, Australian Journal of Chemistry **61**, 833 (2008).

[43] R. Narayanan and M. A. El-Sayed, Nano Letters **4**, 1343 (2004).

[44] N. Semagina, A. Renken, and L. Kiwi-Minsker, Journal of Physical Chemistry C **111**, 13933 (2007).

[45] D. Y. Liu, S. Ren, G. S. Wang, L. S. Wen, and J. Yu, Journal of Materials Science **44**, 108 (2009).

[46] B. Veisz and Z. Kiraly, Langmuir **19**, 4817 (2003).

[47] B. Baruwati, D. Guin, and S. V. Manorama, Organic Letters **9**, 5377 (2007).

[48] C. Burda, X. B. Chen, R. Narayanan, and M. A. El-Sayed, Chemical Reviews **105**, 1025 (2005).

[49] R. Narayanan and M. A. El-Sayed, Journal of Physical Chemistry B **109**, 12663 (2005).

[50] S. W. Kim, S. Kim, J. B. Tracy, A. Jasanoff, and M. G. Bawendi, Journal of the American Chemical Society **127**, 4556 (2005).

[51] M. T. Reetz, R. Breinbauer, and K. Wanninger, Tetrahedron Letters **37**, 4499 (1996).

[52] S. W. Kim *et al.*, Nano Letters **3**, 1289 (2003).

[53] R. Narayanan and M. A. El-Sayed, Topics in Catalysis **47**, 15 (2008).

[54] A. Howard, C. E. J. Mitchell, and R. G. Egdell, Surface Science **515**, L504 (2002).

[55] R. Narayanan and M. A. El-Sayed, Journal of the American Chemical Society **126**, 7194 (2004).

[56] R. Narayanan and M. A. El-Sayed, Journal of Catalysis **234**, 348 (2005).

[57] R. Narayanan and M. A. El-Sayed, Journal of Physical Chemistry B **108**, 8572 (2004).

[58] R. Narayanan and M. A. El-Sayed, Langmuir **21**, 2027 (2005).

[59] M. Simoes, S. Baranton, and C. Coutanceau, Applied Catalysis B-Environmental **93**, 354 (2010).

[60] F. Fievet, *Surfactant Science Series Volume 92* (Marcel Dekker, Inc. NY, 2000), pp. 460–495.

[61] V. Muralidharan and A. Subramania, *Nanoscience & Technology* (CRC Press Taylor & Francis Group, 2009).

[62] F. F. Abraham, *Homogeneous Nucleation Theory* (Academic Press, NY, 1974).

[63] I. V. Markov, *Crystal Growth for Beginners: Fundamentals of Nucleation, Crystal Growth and Epitaxy*, Second ed. (World Scientific, 2003).

[64] I. H. Leubner, *Precision Crystallization: Theory and Practice of Controlling Crystal Size* (CRC Press Taylor & Francis Group, 2010).

[65] A. N. Grace and K. Pandian, Materials Chemistry and Physics **104**, 191 (2007).

[66] D. S. Li and S. Komarneni, Journal of Nanoscience and Nanotechnology **8**, 3930 (2008).

[67] M. H. Huang, L. R. Li, and Y. L. Guo, Electrochimica Acta **54**, 3303 (2009).

[68] C. O. Kappe, Angewandte Chemie-International Edition **43**, 6250 (2004).

[69] R. Abargues *et al.*, New Journal of Chemistry **33**, 913 (2009).

[70] W. X. Tu and H. F. Liu, Journal of Materials Chemistry **10**, 2207 (2000).

[71] N. N. Mallikarjuna and R. S. Varma, Crystal Growth & Design **7**, 686 (2007).

[72] X. Tong, Y. X. Zhao, T. Huang, H. F. Liu, and K. Y. Liew, Applied Surface Science **255**, 9463 (2009).

[73] W. X. Tu, S. J. Cao, L. P. Yang, and W. C. Wang, Chemical Engineering Journal **143**, 244 (2008).

[74] Y. T. Jeon and G. H. Lee, Journal of Applied Physics **103**, 094313/1 (2008).

[75] A. R. Katritzky, D. A. Nichols, M. Siskin, R. Murugan, and M. Balasubramanian, Chemical Reviews **101**, 837 (2001).

[76] V. Baudel, F. Cazier, P. Woisel, and G. Surpateanu, European Polymer Journal **38**, 615 (2002).

[77] J. Y. An, L. Bagnell, T. Cablewski, C. R. Strauss, and R. W. Trainor, Journal of Organic Chemistry **62**, 2505 (1997).

[78] M. Larhed, C. Moberg, and A. Hallberg, Accounts of Chemical Research **35**, 717 (2002).

[79] G. L. Miessler and D. A. Tarr, *Inorganic Chemistry*, Third ed. (Pierson Education Inc., 2004).

[80] R. H. Crabtree, *The Organometallic Chemistry of Transition Metals*, Fourth ed. (John Wiley & Sons, Inc., 2005).

[81] V. Percharsky, *Fundamentals of Powder Diffraction and Structural Characterization of Materials*, Second ed. (Springer, 2009).

[82] W. H. Qi, M. P. Wang, and Y. C. Su, Journal of Materials Science Letters **21**, 877 (2002).

[83] P. Jiang, F. Jona, and P. M. Marcus, Physical Review B **36**, 6336 (1987).

[84] K. Heinemann and H. Poppa, Surface Science **156**, 265 (1985).

[85] B. C. Gates, *Impact of Surface Science on Catalysis* (Academic Press, 2000).

[86] R. V. Bucur and D. Lupu, Journal of Physics and Chemistry of Solids **43**, 697 (1982).

[87] P. Bergonzo, R. Barrett, O. Hainaut, D. Tromson, and C. Mer, Nuclear Instruments & Methods in Physics Research Section a-Accelerators Spectrometers Detectors and Associated Equipment **514**, 100 (2003).

[88] S. R. Kelemen, K. D. Rose, and P. J. Kwiatek, Applied Surface Science **64**, 167 (1993).

[89] I. Minkov *et al.*, Journal of Physical Chemistry A **109**, 1330 (2005).

[90] R. M. Dey, M. Pandey, D. Bhattacharyya, D. S. Patil, and S. K. Kulkarni, Bulletin of Materials Science **30**, 541 (2007).

[91] R. Morent, N. D. Geyter, C. Leys, L. Gengernbre, and E. Payen, Surface and Interface Analysis **40**, 597 (2008).

[92] P. Parhi, J. Kramer, and V. Manivannan, Journal of Materials Science **43**, 5540 (2008).

[93] H. Pulm *et al.*, Journal of the Less-Common Metals **115**, 127 (1986).

[94] R. Dey, B. Sreedhar, and B. C. Ranu, Tetrahedron **66**, 2301 (2010).

[95] B. M. Choudary, K. R. Kumar, Z. Jamil, and G. Thyagarajan, Journal of the Chemical Society-Chemical Communications , 931 (1985).

[96] A. R. Phani, S. Manorama, and V. J. Rao, Journal of Physics and Chemistry of Solids **61**, 985 (2000).

[97] D. Lennon, D. T. Lundie, S. D. Jackson, G. J. Kelly, and S. F. Parker, Langmuir **18**, 4667 (2002).

[98] J. L. Figueiredo, M. F. R. Pereira, M. M. A. Freitas, and J. J. M. Orfao, Carbon **37**, 1379 (1999).

Vita

Meghann Elizabeth Broderick was born on August 9, 1984, in Salt Lake City, Utah, and is an American citizen. She graduated form Allegan High School, Allegan, Michigan in 2002. She received her Bachelor's of Science in chemistry and French from Aquinas College, Grand Rapids, Michigan in 2007.